$NPSH_r$ scaling in centrifugal pumps

Investigation of the influence of impeller speed and diameter on $NPSH_r$ properties of centrifugal pumps

J.M. in't Veld

$NPSH_r$ scaling in centrifugal pumps

Investigation of the influence of impeller speed and diameter on $NPSH_r$ properties of centrifugal pumps

by

J.M. in't Veld

to obtain the degree of Master of Science

at the Delft University of Technology,

Student number:	1270079	
Thesis committee:	Dr. ir. A.M. Talmon,	TU Delft, supervisor
	Prof. dr. ir. C. van Rhee,	TU Delft
	Dr. ir. C.H. Thill,	TU Delft
	ir. C.F. Hofstra,	Royal IHC

An electronic version of this thesis is available at http://repository.tudelft.nl/.

TU Delft

IHC

Abstract

In this MSc study the Net Positive Suction Head required ($NPSH_r$) of centrifugal pumps is investigated, specifically for those pumps used in the dredging industry. The $NPSH_r$ defines the inlet conditions at which a pump loses a given percentage of available manometric head due to cavitation.
This knowledge is relevant in order to be able to predict whether or not the pump can operate under given conditions. In this research the cavitation behavior of a centrifugal dredging pump is investigated at lab scale, the pump has an inlet diameter of 100 mm. For this scale a broad range of shaft speeds and flows is investigated as well, also available field measurements are used to compare the data with and to distinguish scaling laws. This is done with the following research question in mind:

How does the $NPSH_r$ change with changing shaft speed and pump diameter?

In the investigation several known scaling methods are used and compared with the acquired data. A distinction is also made between the operating conditions expressed in $NPSH_r$ and the inlet pressure at a given flow.

The experiment and subsequent analysis showed a quadratic relation between $NPSH_r$ and the impeller diameter as well as the shaft speed.
Scaling only the inlet pressure showed a similar condition, however the relative error increased due to the fact that the $NPSH_r$ contains a velocity component which influences the results positively.

Preface

This report describes the research into the scaling of $NPSH_r$ properties in centrifugal pumps as carried out at Royal IHC in order to obtain the MSc degree in offshore and engineering studies at TU Delft with dredging engineering as the specialisation. The experiments have been carried out at the Royal IHC research lab in Kinderdijk.

First of all I would like thank former IHC-MTI director Robert van de Ketterij who gave me the opportunity to work at IHC and combine this with my master studies. Likewise my thanks goes his successor Léon Seijbel who continued to facilitate this work-study combination. Special thanks to dr. Talmon from TU Delft whose feedback and thorough reading was much appreciated

Many colleagues have been involved in one way or another in this research. Some of those colleagues I would like to name specifically:
I'm very grateful to my supervisor Frits Hofstra for the energetic discussions and his invaluable insights. Many thanks to Jazzie Hoebe for providing his technical drawing skills and continued help in building and adapting the setup. To Yarno Keting I owe my thanks for giving help where needed and for providing a great workplace. The input from Edwin de Hoog regarding sensors and electronics as well as the joyful collaboration was much appreciated. Also I'm grateful to Jort van Wijk for the conversations we had, both technical and non-technical.

Finally I would like to remember my father and thank my mother, for their support.
And to Merel, just thanks.

J.M. in't Veld
Puttershoek, Januari 4, 2021

Contents

introduction 3

I Literature review 5

1 Centrifugal Pump 7
1.1 General principle . . . 7
1.1.1 Velocity triangles . . . 8
1.1.2 Pre-rotation . . . 11
1.1.3 Conservation of angular momentum . . . 12
1.1.4 Bernoulli . . . 12
1.2 Head . . . 13
1.3 Net Positive Suction Head available . . . 14
1.4 Net Positive Suction Head required ($NPSH_r$) . . . 15
1.5 Scaling . . . 16
1.6 Affinity laws . . . 16
1.7 Dimensionless numbers . . . 17
1.8 Additional dimensionless numbers . . . 18
1.8.1 Euler number . . . 18
1.8.2 Suction specific speed . . . 19
1.8.3 Cavitation number . . . 19
1.8.4 $NPSH_r$ over $\vec{v}$ squared . . . 19
1.8.5 Thoma cavitation number . . . 19
1.8.6 Type number . . . 20
1.9 Discussion of pump theory . . . 20

2 Cavitation 21
2.1 Phase changes . . . 21
2.2 Cavitation definition . . . 22
2.2.1 Head loss . . . 23
2.2.2 Cavitation damage . . . 24
2.2.3 Cavitation development . . . 24
2.2.4 Water conditions . . . 26
2.3 Cavitation modelling . . . 28
2.3.1 Homogenous nucleation theory . . . 28
2.3.2 Heterogeneous nucleation theory . . . 30
2.3.3 Bubble development . . . 30
2.3.4 Bubble collapse . . . 31
2.3.5 Cavitation types . . . 31
2.3.6 Roughness . . . 32
2.4 Cavitation prediction . . . 33
2.4.1 $NPSH_r$ scaling . . . 33
2.4.2 Tenot scaling . . . 36
2.4.3 Variable suction specific speed . . . 37
2.4.4 Extrapolating flow rate at constant speed . . . 38
2.4.5 Cavitation scaling on a hemispherical body . . . 38
2.4.6 CFD . . . 39
2.4.7 Conclusion . . . 39
2.5 Cavitation measurement . . . 40
2.5.1 Non scalable efficiency drop . . . 41
2.6 Cavitation noise . . . 42

2.7 Discussion of cavitation theory . . . 44
2.7.1 Scaling models . . . 44
2.7.2 Approach . . . 44
2.8 Conclusions . . . 45

II Experiments **47**

3 Experimental design **49**
3.1 Flow loop . . . 49
3.1.1 Basic measurement and sensors . . . 50
3.1.2 First $NPSH_r$ experiments . . . 51
3.1.3 Testing the setup . . . 52
3.2 Pump . . . 53
3.2.1 Electric motor and shaft . . . 53
3.2.2 Pump casing . . . 54
3.2.3 Impeller . . . 54
3.2.4 Clearance . . . 56
3.3 Pump sensors . . . 57
3.4 $NPSH_r$ measurement . . . 60
3.4.1 Measurement procedure . . . 61
3.4.2 Acoustic emission measurements . . . 62
3.5 Valve . . . 65
3.5.1 Choked flow . . . 68
3.5.2 Globe valve . . . 68
3.5.3 Measurement preparation . . . 68

4 $NPSH_r$ Measurements **71**
4.1 Analysis . . . 72
4.1.1 scaling . . . 73
4.1.2 linearisation . . . 73
4.2 Test plan . . . 73
4.2.1 HRMD3 pump properties . . . 73
4.2.2 HRMD4B-curve test matrix . . . 74
4.3 Influence of centripetal force of pre-rotation . . . 75
4.4 Results HRMD3B . . . 76
4.4.1 $NPSH_r$ vs inlet pressure . . . 76
4.4.2 Comparing different parameters . . . 77
4.4.3 Comparison with true size data . . . 81
4.4.4 True $NPSH_r$ scaling . . . 83
4.4.5 Linear regression . . . 84
4.4.6 Inlet pressure vs velocity and speed . . . 84
4.4.7 Specific capacity and specific inlet pressure . . . 85
4.4.8 Reciprocal of the cavitation number vs specific capacity . . . 86
4.4.9 Pin vs $\omega\vec{v}D_{imp}$ . . . 86
4.5 Results HRMD4B-curve . . . 87
4.5.1 Specific pressure vs specific capacity . . . 87
4.5.2 Pin vs specific capacity . . . 88
4.6 Conclusions of Measurements . . . 89
4.6.1 Scaling . . . 89
4.6.2 Linearisation . . . 89

5 Conclusions and recommendations **91**
5.1 Conclusions . . . 91
5.1.1 Scaling . . . 91
5.1.2 Linearisation . . . 91
5.1.3 Acoustic emission . . . 92
5.2 Recommendations . . . 92

A Appendix **93**
A.1 Linear regression 93
A.2 Measurement data 95

Bibliography **99**

Introduction

Each river, sea or ocean has either soil or some other material at the bottom of it. Dredging is the industry that works on excavating this material and its subsequent transport, be it for deepening of a river or providing material for land-reclamation.
This is done a multitude of ways, ranging from a bucket dredger to a Trailing Suction Hopper Dredge (TSHD) as shown in Figure 1. In this figure three components are pointed out, the draghead where the excavation takes place, the discharge pipe to transport the soil to the desired location and, of course, the centrifugal pump.

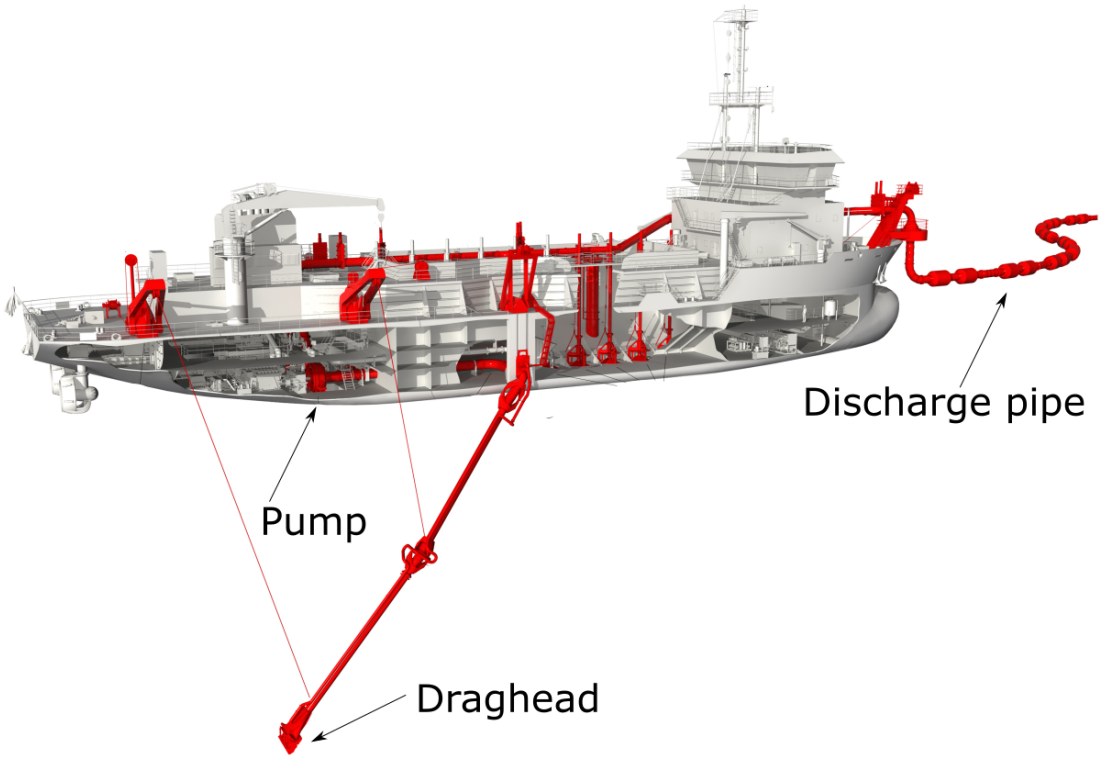

Figure 1: Trailing Suction Hopper Dredge

The pump is used not only to create a flow to move the soil into the draghead, but also pumping it along the discharge pipe toward the desired location. For a good operation one chooses a pump that can operate at a desired flow velocity and also provide a sufficient pressure difference required for the layout and anticipated production. Here 1 pump is used as an example, but it is not unusual that multiple pumps are used.

Here the formulation *pressure difference over the pump* is used. An other way to express this is the *head*, the relation between the two will also be given later on in Equation 1.10. Since the head can be linearly expressed in terms of the pressure differential over the pump the two can often be used used interchangeably, which is also done in this thesis.

One problem a pump in operation can encounter is *cavitation*. This term (later more precisely defined) refers to the forming vapour. This vapour can cause the centrifugal pump to be unable to build up a pressure difference, diminishing production. The following conditions influence the occurrence of this phenomenon:

- water temperature
- flow velocity
- pump speed
- inlet pressure

If the speed and flow velocity are known the conditions under which a drop in head, due to cavitation, occurs can be given by the Net Positive Suction Head required ($NPSH_r$).The difficulty lies not only in the occurrence of cavitation, but foremost in predicting the $NPSH_r$.

Under ideal conditions one would test this for all pumps under a wide variety of conditions, this is not always possible. Therefore the use of small scale experiments would be a great solution, leading to the main research question:

How does $NPSH_r$ change with changing shaft speed and pump diameter?

In order to do this a small scale pump setup will be used (inlet pump diameter 100mm). The influence of pump speed will initially be investigated after which the results will be compared with available field data i.e. a larger pump size.

This thesis is structured as follows:

- literature review studying the working of a centrifugal pump in general and cavitation in particular
- the experimental design and validation of the setup
- the cavitation measurements and its results
- the analysis and comparison with field data

I

Literature review

1

Centrifugal Pump

1.1. General principle

In its essence a centrifugal pump is a simple device to move liquids or mixtures. To achieve this there are two main components: an impeller and a volute (casing) see also Figure 1.1.
The impeller rotates and transfers momentum to the liquid creating an outward flow. This flow is then redirected by the volute, which leads it to the discharge.

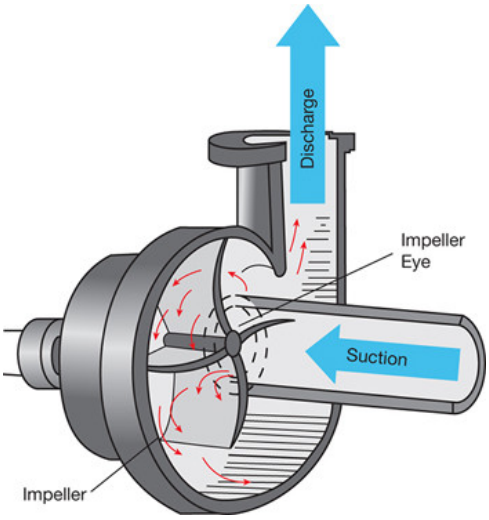

Figure 1.1: flow through centrifugal pump, source: *https://www.pumpfundamentals.com*

For centrifugal pumps there are many designs possible, one way to differentiate between pumps is the distinction between radial and axial outflow as is shown in Figure 1.2.

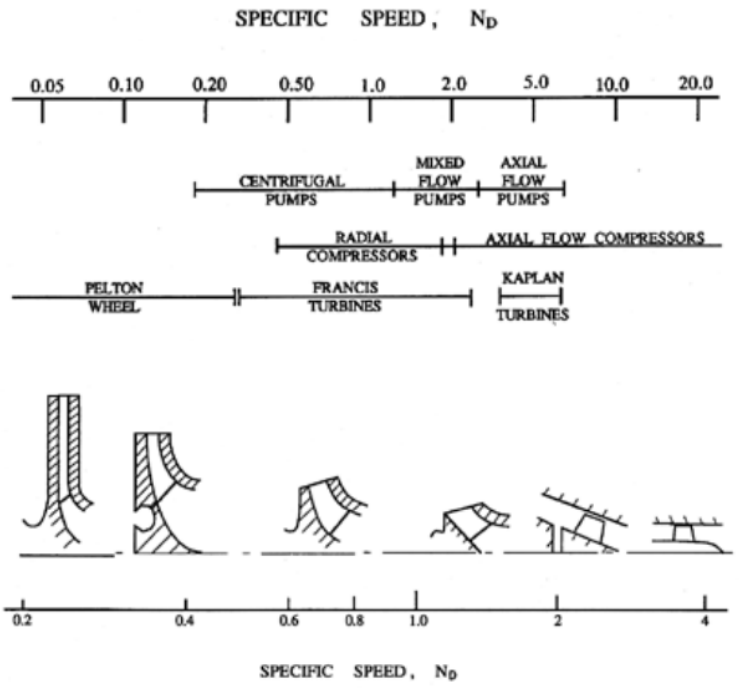

Figure 1.2: Pump design specific speed after Brennen (1994)

In Figure 1.2 the parameter design specific speed (n_d) is used, this is defined in section 1.7. For now, one can see that a high n_d indicates an axial pump whereas a low n_s is typical for a radial pump. In axial flow the pump operates at a relatively high flow but generates limited amount of pressure, for radial flow the reverse is true.
The pumps used in the dredging industry, and under consideration here, are centrifugal pumps with a typical n_s around 0.3.

An important notion with respect to a centrifugal pump is that it does not suck water in. It expels water by means of the impeller, creating a high pressure at the outlet and a low pressure at the inlet (suction side). As a result of this low pressure water naturally flows in (or by other mechanical means) after which it is pumped away, in a pump this typically is a continuous process.

1.1.1. Velocity triangles

A fluid flows into the impeller which not only adds energy to the fluid, but also changes its direction. This happens optimally if the flow velocity and the impeller speed have a specific ratio. To model this the velocity triangle is often used (Stepanoff 1948).
This model simplifies the flow behaviour through an impeller in the sense that it assumes a uniform flow with continuous stream lines. Despite those simplifications the model provides relevant insight with regards to the flow profile in the pump, but also at the suction side. In the velocity triangle the absolute velocity ($\vec{v}$) is related to the peripheral velocity of the impeller (u) and the velocity relative to the impeller blade (w). In Figure 1.3 the outlet velocity triangle is shown in relation to a schematic impeller. In Figure 1.4 those triangles are shown for the inlet of the impeller blades and the outlet.

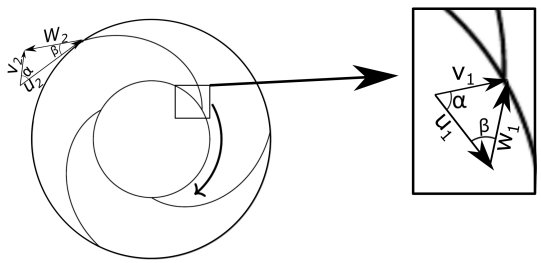

Figure 1.3: Velocity triangles in 2d impeller representation

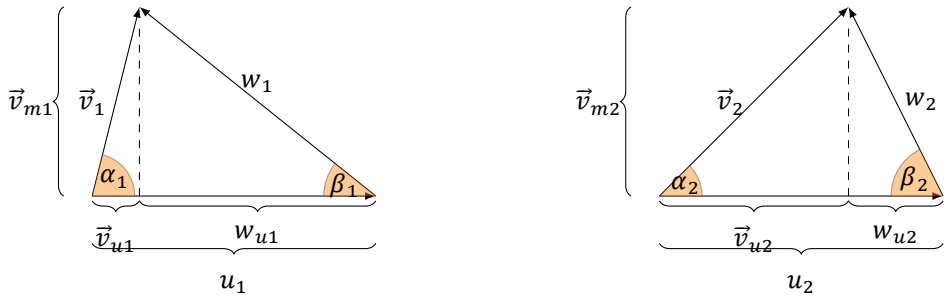

Figure 1.4: Velocity trangles; inlet (left), exit (right)

The angle β gives the blade angle relative to the tangent of the impeller circumference.

Best Efficiency Point
If angle α_1 equals 90 degree the flow resistance will be minimal, in this case one speaks of shock-less flow or Best Efficiency Point (BEP).

Flow profile
The flow profile is often discussed relative to the pump blades, below some terminology and examples of flow profile will be discussed. The focus lies on the inlet properties since here the pressure is typically lowest and most prone to cavitation.
In Figure 1.5 the blade edges and sides are shown.

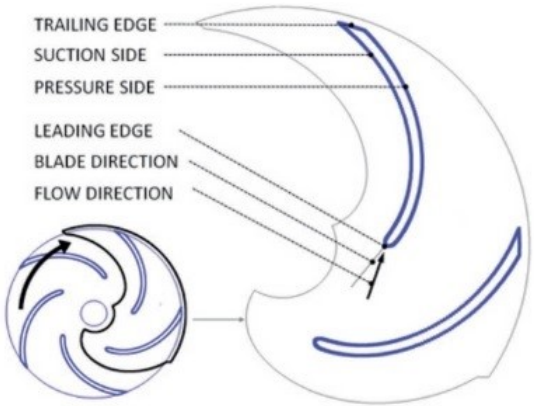

Figure 1.5: identifying pressure side, suction side, leading and trailing (Went 2018)

Changes in flow profile can be represented by changes in the velocity triangles. If $\alpha \neq 90°$, recirculation will occur and influence the pressure distribution in the pump. This recirculation is minimal at BEP flow, a visualization of which is shown in Figure 1.6. It can be seen that the flow direction is parallel to the impeller blades (vanes) resulting in an optimal energy transfer.

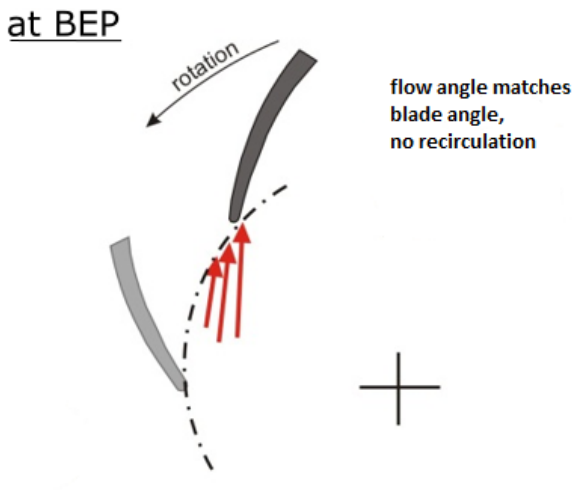

Figure 1.6: Flow profile in centrifugal pump at BEP

For flows below BEP (partial capacity) the flow ”hits” the pressure side and vortices (recirculation) occur at the suction of the blade as is shown in Figure 1.7.

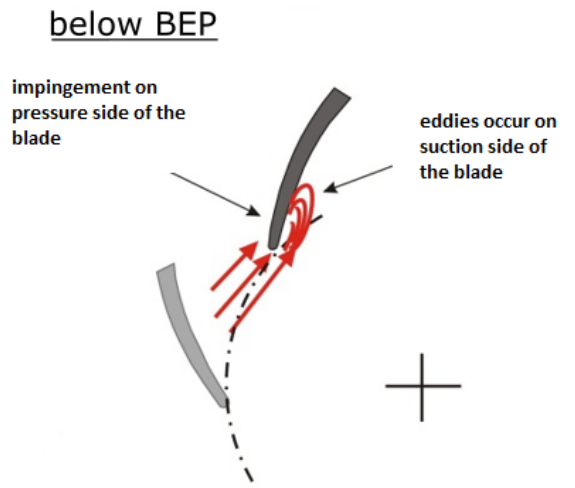

Figure 1.7: Flow profile in centrifugal pump below BEP

If the flow exceeds BEP (over capacity) the vortices occur at the pressure side and the flow ”hits” the suction side, see also Figure 1.8.

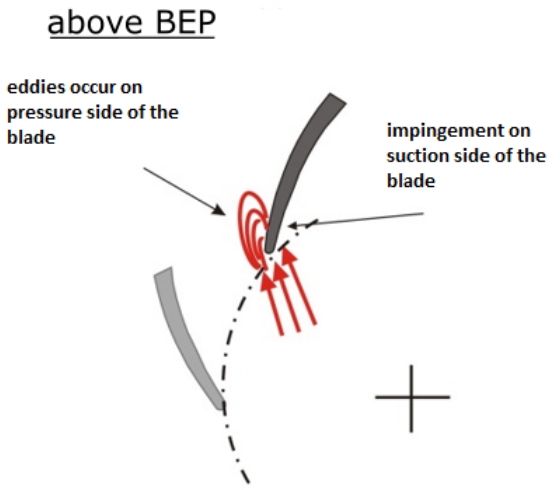

Figure 1.8: Flow profile in centrifugal pump above BEP

The illustrations above are not complete, the size of the vortex region can differ, also local minima can occur at the trailing edge instead of the leading edge.

1.1.2. Pre-rotation

A well known effect in pump flow is pre-rotation, this effect occurs if a pump operates outside of BEP, if this occurs the flow gets a rotational component in addition to the axial component, this can be explained with the velocity triangles:
If β does not match the blade angle the blades will exert a radial force on the medium, resulting in a secondary flow moving through the casing with the speed of the impeller, causing pre-rotation resulting in β approaching the vane angle of the impeller (Predin and Biluš 2003).

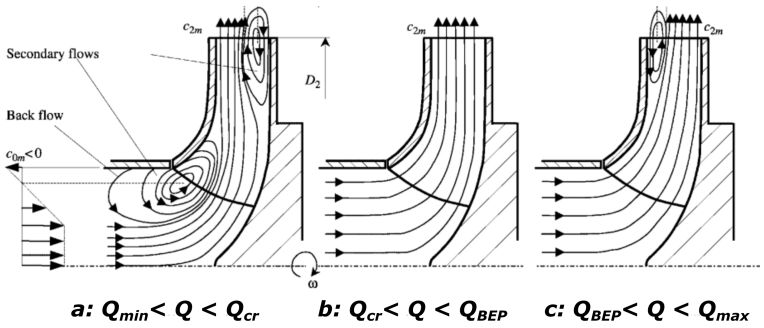

Figure 1.9: secondary flow in impeller, causing pre-rotation (Predin and Biluš 2003)

This pre-rotation can cause an overestimation of the inlet pressure measured at the pipe wall, this is caused by the centrifugal force exerted by the flow, one could also call this the dynamic pressure due to the radial component of the pre-rotation.

In order to compare identical pumps under different conditions one criterion is that the flow pattern is comparable. As will also be discussed in Chapter1.7. For comparable flow patterns the velocity triangles need to have the same shape, i.e. α and β need to be identical. This is also the case if the so called flow coefficient is identical:

$$\phi = \frac{\vec{v}_{m1}}{u_1} \tag{1.1}$$

In Chapter 1.7 the specific capacity (Q_s) will be introduced, which serves the same purpose.

1.1.3. Conservation of angular momentum

A centrifugal pump adds energy to the fluid via the impeller, considering the rotational movement of the impeller it adds angular momentum to the fluid. This fact is exploited in deriving the amount of work done on the fluid.
The first step is to use the relation between the torque and the derivative of the angular momentum of the fluid:

$$M = \frac{d\,(m \cdot \vec{v}_u \cdot r)}{dt} \tag{1.2}$$

Considering the entire impeller as a whole the equation can be specified as follows:

$$M = \frac{dm}{dt}\,(r_2\vec{v}_{u2} - r_1\vec{v}_{u1}) \tag{1.3}$$

The mass flow (dm/dt) can be expressed as follows $Q_V\rho$. Noting that multiplying the torque with the angular speed (ω) gives the power of the impeller, and that multiplying the radius with the angular velocity gives the peripheral velocity results in the following equation:

$$M\omega = P = Q_V\rho\,(u_2\vec{v}_{u2} - u_1\vec{v}_{u1}) \tag{1.4}$$

The power converted to flow can be expressed by the hydraulic power as in Equation 1.5 (Stepanoff 1948).

$$P = Q_V\Delta p \tag{1.5}$$

1.1.4. Bernoulli

A pump adds energy to a flowing liquid, mostly expressed as pressure, in thinking about pressure in a flow system the Bernoulli equation is essential (Stepanoff 1948).
The Bernoulli Equation (1.6) can be derived by considering the conservation of energy in a flow system. If one considers the path along a streamline the energy along this path gets transformed between three states: pressure, flow velocity and potential energy. For example, if the path increases in height the potential energy increases while the pressure energy decreases. If, at a constant height, the diameter increases, the flow velocity will decrease while the pressure increases.

$$\rho g h + p + \frac{\rho\vec{v}^2}{2} = constant \tag{1.6}$$

With p reference is made to the gauge pressure, meaning the pressure with respect to the ambient pressure. If the absolute pressure is used the subscript abs will be added.

The Bernoulli equation describes conservation of energy for idealized fluids, along a streamline, although this does not apply to the flow in (or the measurements performed on) a centrifugal pump it is still a good measure for the added energy to the system.
Naturally the constant in the Bernoulli equation will hold, in the first instance there will always be energy losses due to friction and turbulence, also a pump is specifically intended to add energy.

1.2. Head

In dividing by $\rho_{medium}g$ the constant in Bernoulli's equation is expressed in length, and called head (H):

$$h + \frac{p}{\rho g} + \frac{\vec{v}^2}{2g} = H \tag{1.7}$$

To quantify the energy added to the system by a pump the concept of head is often used; therefore the change in head between the suction and the discharge side is used, this is referred to as the manometric head:

$$h_{suc} - h_d + \frac{p_d - p_{suc}}{\rho g} + \frac{\vec{v}_d^2 - \vec{v}_{suc}^2}{2g} = H_{man} \tag{1.8}$$

The head is often interpreted as the maximum height a pump can add to a liquid system. Note that H is expressed in length but can easily be converted to pressure:

$$p = H * \rho * g \tag{1.9}$$

The head of a pump gives an indication of the energy added to the system. This also allows for the definition of the manometric pressure p_{man}, which is the pressure difference over a pump, and thus linearly related to manometric head.

$$pressureoverpump = p_{man} = H_{man} * \rho * g \tag{1.10}$$

This added energy is a combination of flow velocity and pressure. Which of the two dominates depends on the pump type and working point.

1.3. Net Positive Suction Head available

The pressure at the inlet of the pump gives information about the flow conditions at the inlet of the pump (Paugh 1996). The pressure alone however is not sufficient, in the head only the gauge pressure is taken into account, so the ambient pressure is needed to acquire the absolute pressure.

$$p_{suc,abs} = p_{suc} + p_{amb} \tag{1.11}$$

Knowing the absolute pressure, geodetic height and flow velocity are not enough. This is due to the vapour pressure i.e. the pressure at which the liquid starts to vaporize. If this happens the fluid is no longer incompressible due to a phase change and the continuity equation no longer holds, see also Chapter 2. These considerations are taken into account in the Net Positive Suction Head available, the height component is relative to the datum of the inlet of the pump and can therefore be ignored:

$$NPSH_a = \frac{p_{suc} + p_{amb} - p_{vap}}{\rho g} + \frac{\vec{v}_s^2}{2g} \tag{1.12}$$

Figure 1.10 illustrates the different pressure terms relating to inlet pressure. The value of p_{suc} can be either positive or negative, in this example it is negative (i.e. the absolute pressure is below the ambient pressure)

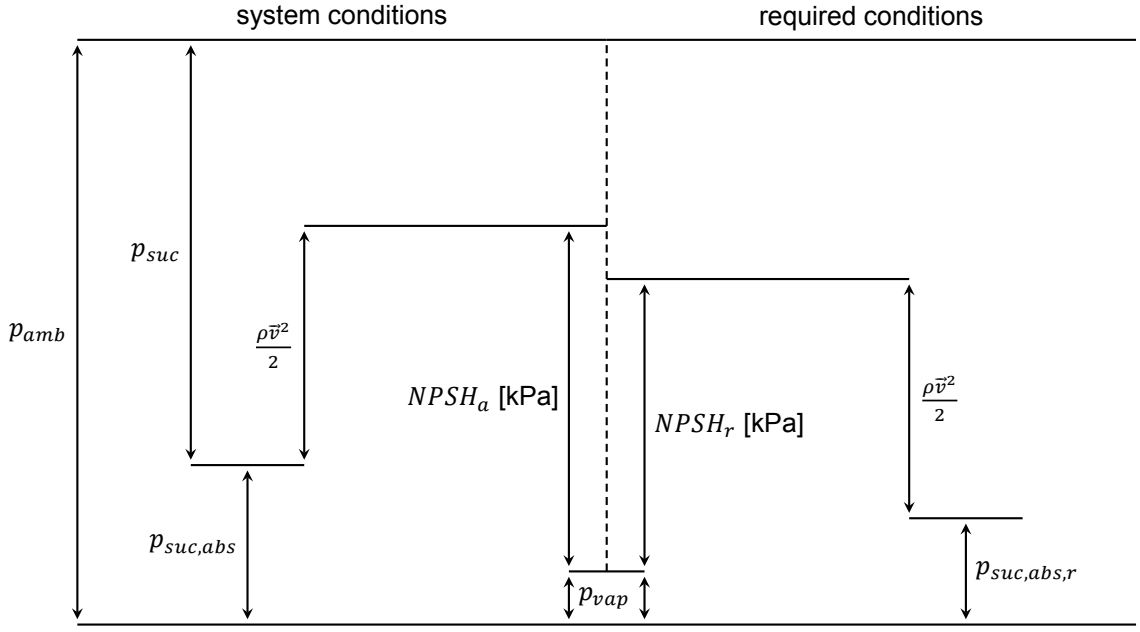

Figure 1.10: Schematic view of parameters relating to inlet pressure, after Berg (2013)

Note that atmospheric pressure is shown but not limiting. A pump under water for example can have a $NPSH_a$ well above p_{atm}. It is also essential to realize that the flow velocity $\vec{v}$ on both sides of the diagram is equal, as is the impeller speed. Changing one of those also means a change in the required p_{suc}.

1.4. Net Positive Suction Head required ($NPSH_r$)

The $NPSH_r$ is essential in this thesis and will be discussed in Chapter 2. However a short definition will be given here. The $NPSH_r$ is strongly associated with cavitation but is defined by a symptom resulting from cavitation. This symptom is simply a drop in head. A centrifugal pump typically is insensitive for changes in inlet pressure. However, if for a given flow velocity the inlet pressure drops below a certain threshold the pump head will start to drop. This drop is easily determined and defined below:

- $NPSH_{rx}$, this is the $NPSH_a$ for which the drop in H_{pump} drops below a certain percentage x of the maximum head. This percentage is often 97% but can also be set at 95%. The x indicates the chosen percentage.

A typical measurement to determine this is shown in Figure 1.4.
In this measurement the inlet pressure is slowly lowered, whilst the flow velocity and speed are kept constant. The green line indicates the 100% head, i.e. the head when there is sufficient inlet pressure. The red line indicates the point where the head has dropped to 97%. With the corresponding inlet pressure the $NPSH_r$ can be calculated.

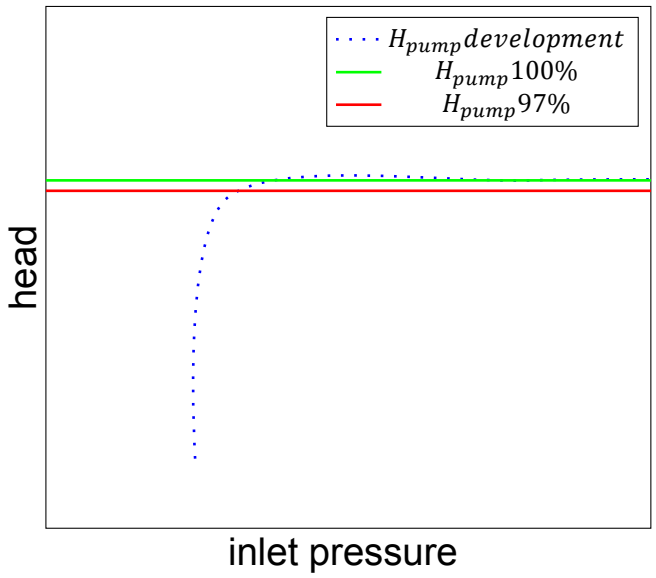

The percentage drop can be chosen according to requirements. Though if the value is too low, say below 90%, there is no distinction between even lower values.
If the specifications of a pump are given, the $NPSH_r$ is often based on measurements and provided by a graph representing the results of a range of $NPSH_r$ measurements for multiple flow velocity at a given speed. As shown in Figure 1.11:

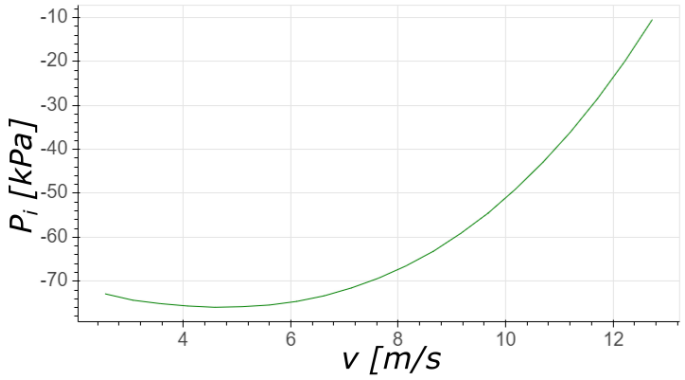

Figure 1.11: $NPSH_r$ specifications example

1.5. Scaling

Scaling is an important factor in researching the pump properties of a pump. This is interesting to predict what happens if the operating conditions change, for example if the impeller speed or the flow velocity is changed. Fluid properties can also be subject to change, the kinematic viscosity or the density change, in practice however those are often constant because most pumps are designed for a specific liquid (mostly water) at a narrow temperature range.
In dredging there can be changes due to the salinity of the water or the high temperatures. And, of course, in dredging a multiphase flow with changing density is daily practice. In this research however the experiments are conducted with fresh water in a narrow temperature range.

The size of the pump can also be subject to scaling, if one wants to relate two pumps with different sizes it is essential that the geometry is identical. If the geometry changes, the pump also changes and can therefore not be compared.

To analyse the influence of scaling pump properties or conditions it is important to identify all contributing variables relevant for the pump properties. The relevant variables are listed in table 1.1.

Table 1.1: relevant pump variables

Symbol	Description	Unit
ν	kinematic viscosity	$\frac{m^2}{s}$
ρ	density	$\frac{kg}{m^3}$
gH	energy per unit of mass	$\frac{m^2}{s^2}$
D_{imp}	impeller diameter	m
Q_V	volumetric flow rate	$\frac{m^3}{s}$
ω	angular speed	$\frac{rad}{s}$

The choice for D_{imp} and not D_{pipe} is arbitrary since they scale in the same way. However later the tip velocity will also be used making the use of D_{imp} logical.

1.6. Affinity laws

Those dimensionless parameters are used in the so called ”affinity laws” (Güllich 2010), those laws describe how the relevant parameters, head, flow and power, behave under scaling.

$$Q_{V1} = Q_{V2}\frac{\omega_1}{\omega_2}\left(\frac{D_{imp_1}}{D_{imp_2}}\right)^3 \tag{1.13}$$

$$H_1 = H_2\left(\frac{\omega_1}{\omega_2}\right)^2\left(\frac{D_{imp_1}}{D_{imp_2}}\right)^2 \tag{1.14}$$

From Equation 1.13, 1.14 and the notion that the head can be converted to pressure as in Equation 1.9 the equation for the power follows:

$$P_1 = P_2\left(\frac{\omega_1}{\omega_2}\right)^3\left(\frac{D_{imp_1}}{D_{imp_2}}\right)^5\frac{\rho_1}{\rho_2} \tag{1.15}$$

The density is often omitted since the same medium is often assumed.

It is important to note that the affinity laws assume an idealized situation,Güllich (2010) suggests taking the efficiency into account:

$$Q_{V1} = Q_{V2}\frac{\omega_1}{\omega_2}\left(\frac{D_{imp_1}}{D_{imp_2}}\right)^3\frac{\eta_{V1}}{\eta_{V2}} \tag{1.16}$$

$$H_1 = H_2\left(\frac{\omega_1}{\omega_2}\right)^2\left(\frac{D_{imp_1}}{D_{imp_2}}\right)^2\frac{\eta_{h1}}{\eta_{h2}} \tag{1.17}$$

$$P_1 = P_2\left(\frac{\omega_1}{\omega_2}\right)^3\left(\frac{D_{imp_1}}{D_{imp_2}}\right)^5\frac{\rho_1}{\rho_2}\frac{\eta_1}{\eta_2} \tag{1.18}$$

In a multistage pump, a pump with multiple impellers, the number of stages (impellers) can also be taken into account in the scaling. Since those are always one in this research this factor is omitted here.

1.7. Dimensionless numbers

The affinity laws can be used to derive certain dimensionless parameters which are important to express the pump properties. Equation 1.13 can be used te derive the specific capacity (Q_s)

$$Q_{V1} = Q_{V2}\frac{\omega_1}{\omega_2}\left(\frac{D_{imp_1}}{D_{imp_2}}\right)^3 \rightarrow \frac{Q_{V1}}{\omega_1 {D_{imp_1}}^3} = \frac{Q_{V2}}{\omega_2 {D_{imp_2}}^3} \rightarrow Q_s = \frac{Q_V}{\omega {D_{imp}}^3} \tag{1.19}$$

In the same way other dimensionless numbers can be derived. If one applies the Buckinham Pi theorem

(Stepanoff 1948) on the parameters from Table 1.1 more parameters can be derived:

- **Specific Capacity** gives a relation between flow en impeller speed. Stepanoff (1948) gives this as the dominant parameter to derive the affinity law regarding the volume flow, see Equation 1.13.

$$Q_s = \frac{Q_V}{\omega D_{imp}^3} \tag{1.20}$$

If one looks at the velocity triangles in Figure 1.4 it is reasonable to assume those to have the same shape for equal Q_s. This because an increase in Q_V scales linearly with flow velocity, so in order to have a constant α and β, ω needs to scale linearly with Q_V.
If the assumption is made that changes in efficiency are dominated by the flow behavior (and thus the velocity triangles) it can be assumed that efficiency is constant at constant Q_s.

- **Specific Head** provides no additional information since it can be derived by rewriting a combination of the specific speed and specific capacity. Resulting in the equation below:

$$h_s = \frac{gH}{\left(\omega D_{imp}\right)^2} \tag{1.21}$$

The specific head is very useful in combination with the Q_s, since the one represents the head and the other the flow profile. Also all dominating parameters are used i.e. speed and diameter.

- **1: Reynolds**, Equation 1.22 is a form of the Reynolds number. This Reynolds number does not describe the actual flow in the pump but the relation between the flow through the entire pump, its impeller diameter and the kinematic viscosity.

$$Re_{pump} = \frac{Q_V}{\nu D_{imp}} \tag{1.22}$$

- **2:Specific speed**

$$n_s = \frac{\omega {Q_V}^{1/2}}{(gH)^{3/4}} \tag{1.23}$$

The specific speed as a generic parameter is rarely used, the specific speed at the design conditions of the pump (optimal efficiency) is used to compare pumps.

  - **3:Design specific speed** is the value of the specific speed at optimal efficiency (i.e. design conditions). The main interpretation here is to provide the ratio between head and flow. These conditions are closely related to the pump geometry as was shown in Figure 1.2

$$n_d = n_s(\eta\text{=max}) \tag{1.24}$$

This parameter is also used as a type number to classify a pump, see also 1.8.6. For a specific pump the design specific speed is given for one value of the specific capacity, see below.

1.8. Additional dimensionless numbers

1.8.1. Euler number

The Euler number describes the relation between pressure and flow velocity as a dimensionless number.

$$Eu = \frac{p}{\rho \vec{v}^2} \tag{1.25}$$

The reciprocal of Equation 1.25 is known as the Ruark number (Ru).
Often a pressure differential is used, an example of which can be seen in Equation 1.27.

1.8.2. Suction specific speed

Some additional parameters are used in order to facilitate comparing different pumps. One of those is the suction specific speed, a quick calculation will show that this is not a truly dimensionless number. It's application however is important since it endeavours to scale the $NPSH_r$ properties of a pump. Also making it dimensionless could be easily achieved by adding the gravitational acceleration before $NPSH_r$. Making it almost identical to specific speed without changing the scaling effects of the equation.

$$n_{ss} = \omega \frac{\sqrt{Q_V}}{NPSH_r{}^{0.75}} \tag{1.26}$$

The suction specific speed is associated with re-circulation of water (Hirschberger and James 2009). Or, more generic, pump conditions that exacerbate the onset of cavitation. This effect is due to the increased local velocity caused by re-circulation.
Especially for pumps with identical n_s the n_{ss} is a useful comparison for $NPSH_r$ properties. Although it also needs to be mentioned that the numbers are typically given for BEP conditions. One of the possible causes of a low specific speed is too large an impeller eye causing even at BEP re-circulation.

1.8.3. Cavitation number

One of the most used parameters to predict cavitation behaviour is the cavitation number σ. It describes the ratio between the static pressure (actually the difference with the vapour pressure) and the dynamic pressure. Since the static pressure counteracts the onset of cavitation and the dynamic pressure enables it, it follows that the lower σ the more likely cavitation is.

$$\sigma = \frac{p_{inlet} - p_{vap}}{\frac{1}{2}\rho\vec{v}^2} \tag{1.27}$$

An earlier version of the σ is given by Wislecenus (1942) and derived as an extension of the affinity laws. It's reasoning is as follows: the ratio between the tip velocity and the flow velocity must be constant (i.e. the specific capacity must be constant) in order to have comparable flow profiles.

1.8.4. $NPSH_r$ over $\vec{v}$ squared

A derivation similar to the affinity laws can be applied where it is assumed that the Net Positive Suction Head required can be used in scaling interchangeably with the head (whether this assumption is applicable remains a subject of discussion). The resulting equation is:

$$\frac{2 * g * NPSH_r}{\vec{v}^2} = \text{constant} \tag{1.28}$$

1.8.5. Thoma cavitation number

Similar to the cavitation number is the Thoma cavitation number (σ_T). This parameter however is not that useful for it is the $NPSH_a$ over the head of the pump. Change in the head however is a symptom of developed cavitation but is less useful for the prediction.
Also the $NPSH$ contains the sum of a flow velocity component and static pressure component, while the flow velocity promotes cavitation the pressure counteracts it. See the items below:

- $\frac{\vec{v}_s^2}{2g}$: increased flow velocity lowers local pressure, thus inducing cavitation.
- $\frac{p_{suc}+p_{amb}-p_{vap}}{\rho g}$: an increased value of this pressure component reduces the risk of cavitation.

Since the head scales with flow velocity and speed, as the $NPSH_r$ is expected to be, this parameter can have some use in scaling. Unfortunately it obscures the point that the minimum required inlet pressure is mainly influenced by the flow velocity and speed. As is also discussed by Wislecenus (1942).

$$\sigma_T = \frac{NPSH_a}{H_{man}} \tag{1.29}$$

1.8.6. Type number

As mentioned in section 1.7 the design specific speed is used as type number, below Equation 1.23 is shown again.

$$n_s = \frac{\omega {Q_V}^{1/2}}{(gH)^{3/4}} \text{at BEP}$$

Unfortunately there are multiple definitions of specific speed and type number not all of which are dimensionless (Brennen 1995), in fact the gravitational acceleration is quite often omitted as in Equation 1.30. Though it might not be as elegant it does not influence the relative results since this parameter can be considered as a constant.

$${n_s}^* = \frac{\omega {Q_V}^{1/2}}{H^{3/4}} \tag{1.30}$$

This type number needs to be considered carefully, often design values are suggested but the exact definition can differ eg. the angular speed (ω) can be replaced by the number of rotations per second (N), the result for either parameter is dimensionless and the physical interpretation is the same, only the one is a factor of 2π larger than the other.
The definition used here is equal to the one used by Brennen (1994) who provides a classification by Equation 1.23 see Figure 1.2.
The specific speed is closely related to pump geometry (Porwall 2015). Equation 1.23 shows that a high n_s is typical for a high flow-head ratio and that a low n_s is typical for a low flow-head ratio.

1.9. Discussion of pump theory

In comparing pump measurements and in trying to make predictions the affinity laws are the obvious starting point. The specific capacity is perfect for comparing pump behaviour under comparable flow profiles. Using comparable flow profiles means that a range of different specific capacity are to be investigated for a range of different impeller speeds. The specific capacities will be chosen relative to the Best Efficiency Point.

In investigating the way $NPSH_r$ changes, and the mathematical relation between the relevant parameters it will be a good start to compare the results with the cavitation number and the Thoma cavitation number.

2

Cavitation

2.1. Phase changes

In Section 1.3 the onset of cavitation is mentioned. To understand this the comparison with boiling is often used. Boiling, as is well known, is the moment that water starts to vaporize due to added heat. Once the boiling temperature is reached a small amount of heat (the latent heat) needs to be added for the liquid to vaporize. There are however other conditions creating a phase change.

These conditions are visualized in the phase diagram as shown in Figure 2.1. In this diagram it can be seen that the phase of water (or any other substance for that matter) depends on the pressure and the temperature (Predel et al. 2004). The crossing between vapour and liquid, the red line, is called the binodal and can be described by the Clausius-Clapeyron relation (Velasco et al. 2009).
In principle the medium in a centrifugal pump operates in the liquid phase (grey area), that is also one of the assumptions for the affinity laws, see Section 1.6. However one can see that if the pressure of the medium starts to drop (which it does in a pump system) it can drop to the point that the medium gets in the vapour phase. In this phase one is no longer pumping an in-compressible medium which can reduce the efficiency of the pump significantly. One way of moving from liquid to vapour is via cavitation and discussed in Section 2.2.
The diagram shows the three most common states of matter, if the graph were extended, especially to extreme pressures (well above the MPa range), several other states of matter would appear. This is such an exotic case however that it will not be discussed here. If both the pressure and the temperature increase above the corresponding values in the critical point the medium becomes supercritical which is where the line separating liquid from vapour ends.

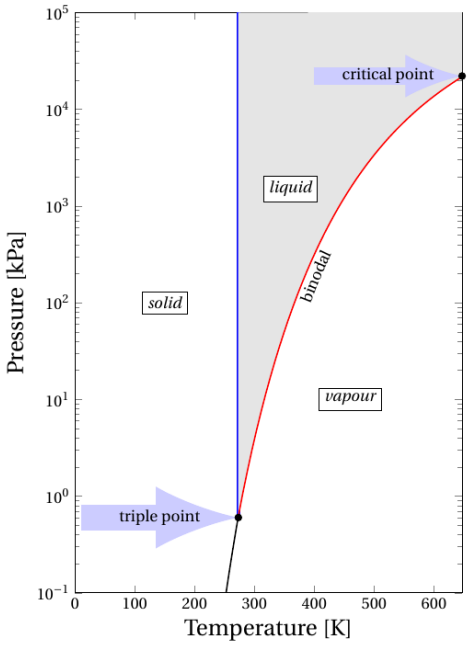

Figure 2.1: Phase diagram, after Çengel and Boles (2006)

The binodal line is approximated by Equation 2.1 (Buck 1981).

$$p_{vap} = 0.61121e^{\left(\left(18.729-\frac{T}{227.3}\right)\left(\frac{T}{257.87+T}\right)\right)} \tag{2.1}$$

2.2. Cavitation definition

There are many definitions of cavitation, but almost all of them contain two criteria in several formulations:

- cavities due to vaporization are formed in the liquid
- the forming of those cavities goes via a specific thermodynamic path.

Both criteria are well captured by Stepanoff (1948).

"The term cavitation refers to conditions within the pump where, owing to a local pressure drop, cavities filled with water vapor are formed" (note the American idiom for vapour i.e. vapor).

It is worth mentioning that sometimes this definition is narrowed by including the further development of cavitating flow, describing not only the forming of vapour but including the implosion of said vapour, Franc and Michel (2005) formulates this as follows:

"cavitation is defined as the process of formation and disappearance of the vapour phase of a liquid when it is subjected to reduced and subsequently increased pressures at constant ambient temperatures."

The addition of the subsequent increasing pressure is helpful, for it includes the total process of the forming of cavity to the implosion of it; which is typical for the process in a liquid flow. When the criteria from the definition of cavitation are met there is no guarantee that the symptoms or consequences associated with cavitation will occur.
There does not have to be a cavitation noise, the pump head does not have to be influenced nor does there have to be cavitation damage. These effects can, and typically will, occur if the cavities grow large enough and if the following implosions are violent enough.

The definition by Franc and Michel (2005) will be adopted here. One of the big differences between a cavity being formed due to a temperature rise (boiling) and a cavity formed due to a pressure decrease (cavitation) is that a change in pressure can occur almost instantaneous whereas a temperature change takes time. This closely relates to the definition of vapour, which is a gas below the critical temperature, meaning that an increase in pressure can convert it to the liquid state i.e. the process is reversible.

The cavitation process is schematically shown in Figure 2.2.

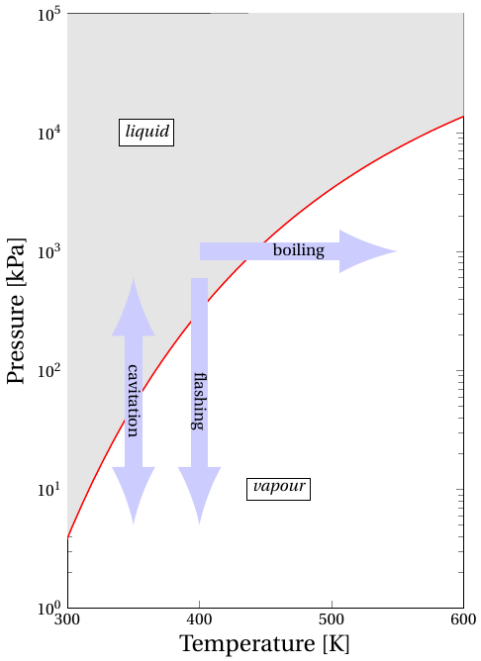

Figure 2.2: cavitation, flashing and boiling

Flashing and boiling are also shown in figure 2.2, the definitions of which are:

- flashing: *in flashing a liquid forms vapour due to a pressure decrease, there is however no subsequent pressure increase, so the vapour does not transition back into liquid.*

- boiling: *in boiling the formation of vapour occurs due to a temperature increase*

Figure 2.2 shows a part of the phase diagram of water. It shows the operating range for pumps, the line separating the vapour and liquid phase is called the binodal and can be described by the Clausius-Clapeyron relation (Velasco et al. 2009).
For completeness sake it should be added that the phase of a substance not only depends on the pressure and the temperature but also on the specific volume (the reciprocal of the density). This parameter is for now assumed to be fully determined by temperature and pressure.

2.2.1. Head loss

The main symptom of cavitation is the loss of head of the pump as shown in Figure 1.4, if the amount of vapour increases, the force that the impeller can exert on the fluid is limited, with a loss of pump head as a consequence.
This effect can be quite simply explained, if one follows a path along the pressure side of an impeller blade from the inlet to the outlet during operation. The pressure along the blade will increase due to the force it exerts on the liquid. However, if a vapour zone occurs due to cavitation the pressure in that zone is constant, around p_{vap}.

In Figure 2.3 this is shown in two different graphs, both with a qualitative representation of the pressure build up along the impeller.

(a) non cavitating pressure distribution

(b) cavitating pressure distribution

Figure 2.3: blade pressure distributions

The length of the part of the blade covered with a cavity is the cavity length (l_{cav}), this is not a typical length but initially has a more linear relation with the cavity volume. This length scales also with the length of the blade being damaged by cavitation, if cavitation damage occurs.

2.2.2. Cavitation damage

Cavitation is a violent process, this is mainly due to the implosion of a vapour bubble. In such an implosion energy is released in a short amount of time.
This can have damaging effects on the pump impeller in the long run (Lawless et al. 2017). An example of which is shown in Figure 2.4. The exact process is not a part of this research, damage can be caused by acoustic pressure waves and energy released during the bubble implosion (Terwisga 2009).

Figure 2.4: Cavitation damage, source: https://www.empoweringpumps.com

2.2.3. Cavitation development

The onset of cavitation (incipient cavitation) can reasonably be predicted by CFD calculations (Schiavello and Visser 2009), this is done by determining when the local pressure drops below the vapour pressure.
This is possible because during the process of lowering the pressure towards the vapour pressure the medium remains in the liquid phase. Once vapour has formed the medium becomes multi-phase making the CFD calculations much more complicated. That is even ignoring the hysteresis effect where the forming of vapour happens at another pressure than the implosion of the cavities (Güllich 2010).

The steps in the development of cavitation in a pump are identified by observation of the phase change and later on by the effects it has on the head of the pump, see the list below:

- $NPSH_i$: the $NPSH$ of incipient cavitation when the first small cavities form. These cavities almost immediately implode after forming and do not influence the pump performance.
- $NPSH_0$: the moment when the head of the pump starts to drop, specific case of $NPSH_x$ see next point.
- $NPSH_x$: the moment when the efficiency of the pump drops with $x\%$. The value for x is often

chosen to be 3% or 5% and is essentially arbitrary, although the head loss must be well above the value of the full cavitation value (see below and Figure 2.5b). Because the $NPSH_r$ value for (for example) 20% head drop and 25% head drop could be equal.

- $NPSH_{FC}$: The moment the pump is fully cavitating and the minimum inlet pressure is reached.

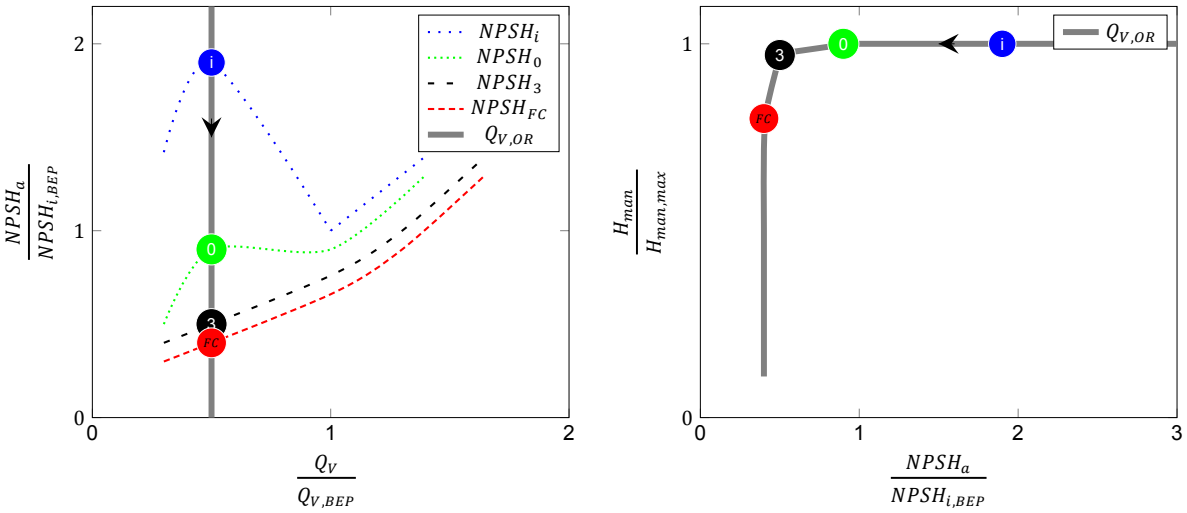

(a)Different $NPSH$ curves adapted from Güllich 2010

(b) typical $NPSH_r$ curve

Figure 2.5: typical $NPSH_r$ measurements, for a constant speed

In figure 2.5(a) those $NPSH$ types are qualitatively plotted. First thing to notice is that the shape of $NPSH_3$ differs a lot from $NPSH_i$, making it hard to relate relate the two. The thick line indicates the onset of re-circulation (indicated with subscript: OR), for flow below this line recirculation occurs at the inlet. This re-circulation is described by Güllich (2010) and is due to the low flow rate through the pump while the impeller is causing movement of the liquid. This re-circulation decreases the incidence with the impeller blade and thus decreases the value for $NPSH_i$ according to Güllich (2010). This recirculation is visualized in Figure 2.6.

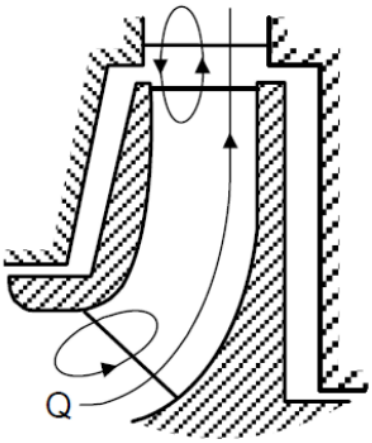

Figure 2.6: recirculation example (Güllich 2010)

Moving from a higher to a lower flow this re-circulation strongly influences the flow profile. It must be noted however that the shape of the incipient curve is strongly influenced by the pump design.
Consider in Figure 2.5 a flow kept constant at the onset of re-circulation ($Q_{V,OR}$ the thick line), if the inlet

pressure is lowered a classic $NPSH$ curve can be acquired as in figure 2.5(b) the different stages of $NPSH$ are indicated in both graphs. Where the cavitation behaviour goes from no cavitation to incipient to the first drop of H_{man} to the 3 % head drop resulting in full cavitation. Note that the x-axis of Figure 2.5(b) equals the y-axis of 2.5(a).
The $NPSH$ axes are normalized with respect to the $NPSH_i$ at BEP, the same is done for the flow in Figure 2.5.
At flow below BEP cavitation inception occurs at the suction side of the impeller blades, whereas above BEP it occurs at the pressure side. This is due to the flow in the impeller itself.

An important notion for Figure 2.5 is that it is for a measurement from right to left, i.e. from a high inlet pressure to a low inlet pressure. This is of particular importance for the incipient cavitation (Muleki et al. 2015). If one has a cavitating pump and increases the pressure to the value where cavitation would fully disappear (desinent pressure), this pressure likely has a lager value than the incipient pressure. This is referred to as cavitation hysteresis (Holl and Treaster 1966). The hysteresis effect can be due to an increase in the nucleation in a closed loop, an example of which is shown in 2.7.

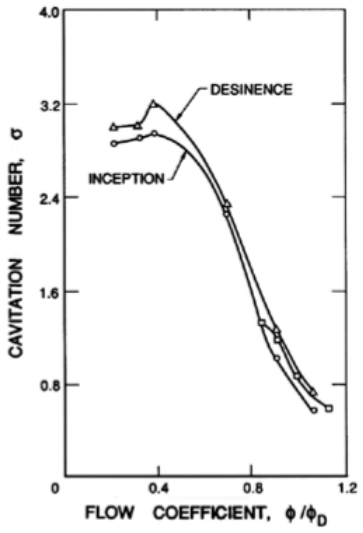

Figure 2.7: Cavitation hysterisis (Brennen 1994)

2.2.4. Water conditions

The water conditions have a great influence on the cavitation behaviour. Unfortunately it is difficult to determine the precise condition of the water but the conditions influencing it are discussed here. To illustrate the influence of the water condition reference can be made to Brennen (1995) who compared different cavitation inception experiments from several test facilities.

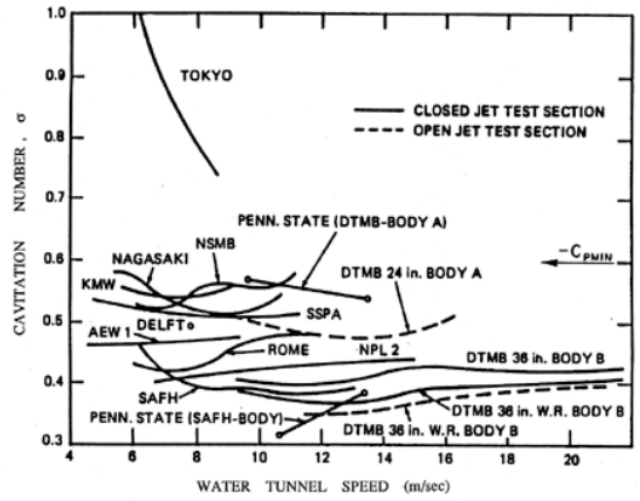

Figure 2.8: Cavitation inception tests: Brennen (1995)

Dissolved gas
Water can, and almost always will, contain dissolved gas. Dissolved gas behaves as part of the water phase. The concentration of dissolved gas is limited to the solubility of the gas in liquid, which is predicted by Henry's law (Güllich 2010):

"the solubility of a liquid is proportional to the partial pressure of the gas above the liquid level"

Or, to put it in an equation:

$$p_{par} = k_H C \tag{2.2}$$

k_H is dependent on the temperature of the liquid (Smith and Allan 2007). The dissolved gasses expand and form additional cavities resulting in loss of head. This effect typically occurs at a higher local pressure ($NPSH$). To account for this Tsai (1982) suggest an additional pressure to be added to the vapour pressure resulting in an artifical vapour pressure (p_{Avap}).

Free gas
Free gas is gas that is contained by the liquid but not dissolved in it, it is present in the form of small bubbles (Kuiper 2000), also large bubbles ($>$ 1mm) might be present in the water. Dissolved gas can, by means of lowering the pressure, also be converted into free gas. The advantage of free gas is that it is easier to remove, an open surface or a convenient obstacle in the flow can be used to "catch" the free gas.
The problem of free gas is that it directly responds to a lowering of the pressure by expansion even if the pressure is well above p_{Avap}. This behaviour can be described by the well known ideal gas law:

$$pV = nk_bT \tag{2.3}$$

The amount of dissolved air can have a significant effect on the $NPSH_r$, Lomakin and Bibik (2019) calculates a significant difference. In Table 2.1 the influence is calculated for a specific pump, at a specific flow and speed.

Table 2.1: air influence on $NPSH_r$, from Lomakin and Bibik (2019)

Dissolved air content, %	$NPSH_r$ **[m]**
0	1.8
1	2 .0
3	2.6
5	3.2

Nuclei
Nuclei are an essential ingredient for cavitation (and boiling). The binodal line shown in Figure 2.1 considers water saturated with nuclei. Which are small with diameters in the range of 10^{-3}mm to 10^{-1}mm (Güllich 2010) which are adsorbed on non-wetting particles in the fluid where the diffusion of the vapour is prevented (or delayed) by the surface tension. Kuiper (2000) also describes nuclei without such particles where the gas is contained in the micro bubble by the surface tension alone.

Pure water, without air or nuclei would start cavitating at a much lower pressure, in fact it can resist (high) tensile stresses (Temperley 1946). This is due to the fact that cavitation or vaporization occur when the cohesive forces between the water molecules are not strong enough to keep the molecules together. Nuclei in the water can be considered weak spots which will initiate cavitation, without those weak spots the forces binding the water molecules together are orders of magnitude stronger than common fluids with nuclei.

2.3. Cavitation modelling

2.3.1. Homogenous nucleation theory

In modelling the forming of cavitation the homogeneous nucleation theory is a classic starting point. It builds strongly on the fundamental work of Gibbs (1873) and is still applied.
Assume a cavity in a liquid in equilibrium situation i.e. all forces equal out. In that case three forces are at play:

- p_B, the internal bubble pressure
- p, the pressure in the liquid
- S, surface tension

The surface tension is the result of the cohesive forces between the water-film surrounding a cavity. The balance between those forces can be derived elegantly by considering the force balance of half such a sphere, as presented in Figure 2.9.

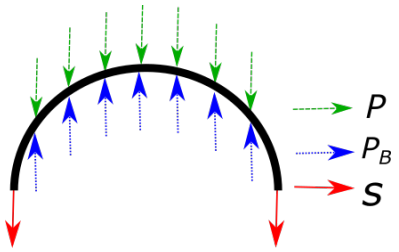

Figure 2.9: schematical presentation of forces acting on half of a bubble

$$F_{outward} = p_B * \pi r^2 \tag{2.4}$$

$$F_{inward} = p * \pi r^2 + 2\pi r * S \tag{2.5}$$

Combining this results in the Laplace's bubble law (Rapp 2017):

$$\Delta p = \frac{2 * S}{r} \tag{2.6}$$

The pressure in the bubble could exist entirely of vapour, in which case it can be assumed that $p_B = p_{vap}$ or there is a combination of vapour and a dissolved gas. In which case the partial pressure need to be taken into account using Dalton's law as in equation 2.7. Where n is the total number of gas components.

$$p_{total} = \sum_{i=1}^{N_g} p_i \tag{2.7}$$

In either case, under a given pressure a critical radius and a critical pressure differential can be defined, describing the maximum radius and corresponding pressure difference.

$$\Delta p_{crit} = \frac{2S}{r_{crit}} \tag{2.8}$$

If the pressure difference were to exceed Δp_{crit} the surface tension would not be sufficient resulting in a rupture of the bubble. Using this as a criteria one can calculate the required energy for the formation of such a bubble. The reasoning is as follows: during the formation of a bubble there is energy released and required:

- energy required: forming the water film with its surface tension costs energy, the integration of the surface tension over the surface: $4\pi r_{crit}^2 S$
- energy released by expansion, the volume times the pressure differential: $\frac{4}{3}\pi r_{crit}^3 \Delta p_{crit}$

Using the energy analysis, the energy required to form a bubble results:

$$E_{crit} = \frac{16\pi S^3}{3(\Delta p_{crit})^2} \tag{2.9}$$

It may be worth noticing that the latent heat is not taken into account in this analysis. Including this would increase the energy E_{crit}.

The above analysis is elegant, however assuming a surface tension (S) $0.073\frac{\mathrm{N}}{\mathrm{m}}$ (Passas and Pethica 1989) and taking the inter-molecular distance (around 10^{-10}m) for the r_{crit}, results in a p_{crit} in the order of $15 * 10^4$bar. Which is way above the practical experience.
This discrepancy is explained by the fact that the above calculations do not take nuclei into account, pure water however should be able to withstand such high tensions. Indeed as early as 1909 (Dixon 1909) reached a tensile strength of up to 200 bar with purified water. This is still well below the theoretical limit but also exceedingly higher than the tensile strength of everyday water.

2.3.2. Heterogeneous nucleation theory

The homogeneous nucleation theory predicts fluid tensile strength that can only be realized in a sophisticated laboratory. One of the reasons for this is that in nature water always contains contaminations, be it air or particles. The influence of particles is described by the nucleation theory.
The weakest part of an air bubble attached to a surface is the interface with the surface. This is due to the fact that the surface tension at the interface has only a component related to the contact angle that counteracts the vertical force due to the pressure difference. This angle is dependent on the surface free energies, given an angle the maximum pressure difference can be calculated as follows.

$$\Delta p_{crit} = \frac{2\sin(\theta)S}{r_{crit}} \tag{2.10}$$

It needs to be noted that r_{crit} is related to θ so a low value of $\sin(\theta)$ does not necessarily result in a low Δp_{crit}.

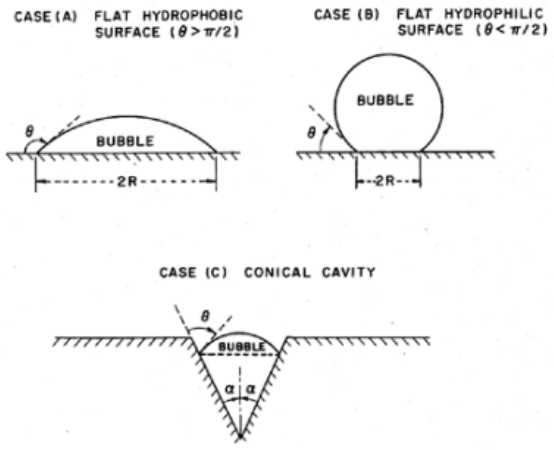

Figure 2.10: example of heterogenous nucleation after Brennen (1995)

Case C in Figure 2.10 is of extra interest. For it shows a realistic scenario for air bubbles that wil rupture at low pressures. An detailed knowledge of the surface is needed, a simple wall roughness might not suffice, especially a relative wall roughness might be misleading for it does not represent the exact dimensions of any crevices present in the wall.

2.3.3. Bubble development

Given the inception of a bubble, the subsequent development is often modelled by the Rayleigh-Plesset equation:

$$\begin{aligned} &\frac{p_{bub}(t) - p_{\infty}(t)}{\rho_{liq}} + \frac{p_{vap}(T_{bub}) - p_{vap}(T_{\infty})}{\rho_{liq}} + \frac{p_G}{\rho_{liq}}\left(\frac{r_0}{r}\right)\left(\frac{T_{bub}}{T_{\infty}}\right)^{3k} \\ &= r\frac{d^2r}{dt^2} + \frac{3}{2}\left(\frac{dr}{dt}\right)^2 + \frac{4\nu_{liq}}{r}\frac{dr}{dt} + \frac{2S}{\rho_{liq}r} \end{aligned} \tag{2.11}$$

Equation 2.11 is a rewritten form from a more condensed version, this to distinguish different physical processes:

- $\frac{p_{bub}(t) - p_{\infty}(t)}{\rho_{liq}}$: this term gives the influence of the environment. Thermal effects are not taken into account.

- $\frac{p_{vap}(T_{bub}) - p_{vap}(T_{\infty})}{\rho_{liq}}$: This term describes thermal effects and has a large influence on the bubble behaviour (Brennen 1995).

- $\frac{p_G}{\rho_{liq}}\left(\frac{T_{bub}}{T_{\infty}}\right)\left(\frac{T_{bub}}{T_{\infty}}\right)^{3k}$: This term describes the development of the initial gas content of the bubble, polytropic index (k) is used to describe the thermodynamic behaviour. k is assumed to be constant. Thus limiting the thermodynamic behaviour somewhat, a typical value for k is 1 assuming a constant temperature.

- $r\frac{d^2r}{dt^2} + \frac{3}{2}\left(\frac{dr}{dt}\right)^2$: inertia effects

- $\frac{4\nu_{liq}}{r}\frac{dr}{dt}$: viscous effects

- $\frac{2S}{\rho_{liq}r}$: Surface tension influence

2.3.4. Bubble collapse

Though the bubble collapse is not the main focus, a small description will be given. If a sufficient number of nucleation sites is assumed the Rayleigh-Plesset equation can be used to identify the environmental pressure below which the bubble growth is uncontrolled and will result in rupture and bubble collapse. This is referred to as Blake's threshold pressure as described by Harkin A. et al (1998).

$$p_{\infty,crit} = p_{vap} - \frac{4S}{3}\sqrt{\frac{8\pi S}{9knRT_{bub}}} \tag{2.12}$$

This equation assumes that the amount of gas in the bubble is known and constant, also the temperature in the bubble is assumed to be constant. Note that if those assumptions are correct but the amount of gas is unknown (which is likely) the relation still provides information on the behavior of Blake's threshold.

2.3.5. Cavitation types

The preceding theory describes the forming of a single bubble and it's development. A bubble however is seldom formed on its own. In fact, the development of combined cavitation bubbles can be classified by how it progresses along the flow.
Below some of those types are listed

- **bubble** cavitation, the cavitation bubbles maintain separate from on another. The bubbles can be surface bound but also move along with the flow. These bubbles are typically associated with high damage due to the energy stored in large bubbles.
- **sheet cavitation** in sheet cavitation the bubbles remain attached to the surface but do flow along it and are combined in the process. Forming a 'sheet' of gas along the surface.
- **cloud cavitation** cloud cavitation follows if sheet cavitation becomes unstable, due to a lowering in the cavitation number as a result of lowering the inlet pressure. As described by Mullin (2011).

- **vortex cavitation** this process is specifically well known for ship propellers (Kuiper 2010), it is caused by low local pressure due to vortices. Since high Reynolds numbers indicate the occurrence of vortices it is closely related to Reynolds numbers.

Related to vortex cavitation is the tip clearance a, see Xu et al. (2017). The tip clearance not only influence the head of the pump and the efficiency, it can also induce additional cavitation and as a consequence a higher value of the $NPSH_r$.

2.3.6. Roughness

Roughness is important for it can be a source for nucleation as discussed in Section 2.3.2. It also is an important parameter in flow systems for it strongly influences the pressure drop due to friction between a moving fluid and a surface. Be it a pipeline, an orifice or an impeller. A more generic parameter is de relative surface roughness (Takacs 2015):

$$\kappa = \frac{\epsilon}{D_{pipe}} \tag{2.13}$$

with ϵ being the absolute roughness and D_{pipe} being the pipe diameter. The absolute roughness is initially based on a surface that is optimally packed with sand particles that have ϵ as diameter, this is also referred to as the *sand roughness* due to it's similarity with sand paper Schlichting and Gersten (2017).

It may be obvious that the relative roughness of an impeller is harder to define because its flow surface is not as easily defined.

In thinking about this, the coastline paradox comes to mind (Mandelbrot 1982) where the fractal nature of the coastline is discussed. Showing that when one measures the length of a coast line it is at first glance quite straight forward. But if one zooms in (i.e. increased precision) the length will increase because more details will appear. If one zooms in further the length will increase even more, and so forth and so on.

To determine the absolute roughness it is therefore import to know the resolution of the scanning device, often determined by the wavelength. Which is exactly what is specified in ISO (2007). Also the shape has influence on the roughness, in surface measurement this is incorporated by measuring a slope. Another parameter influencing the hydraulic effect of roughness is the distribution as described by Miller 2014 a random distribution of roughness elements is assumed while by mechanically smoothed pipes the remaining and dominating elements can be evenly distributed.

In order to deal with these nuances the effective roughness is used. In fact, roughness is often determined by the hydraulic effect of (the pressure drop over) a pipeline. This results in the Darcy-Weisbach friction factor (White 2011) f:

$$f = \frac{\Delta p}{l} \frac{2D_{pipe}}{\rho \vec{v}^2} \tag{2.14}$$

The friction factor depends on the wall relative wall roughness and the Reynolds number, this is the true Reynolds number that was alluded to when describing equation 1.22 where the impeller diameter was used whereas here it is the pipe diameter, this means that the pump Reynolds number relates to the scaling of the flow through the pump as a whole. Whereas the true Reynolds number describes flow through a pipe:

$$Re = \frac{Q_V}{\nu D_{pipe}} \tag{2.15}$$

The relation between relative wall roughness, the Reynolds number and pressure drop over a pipeline is represented by the Moody diagram:

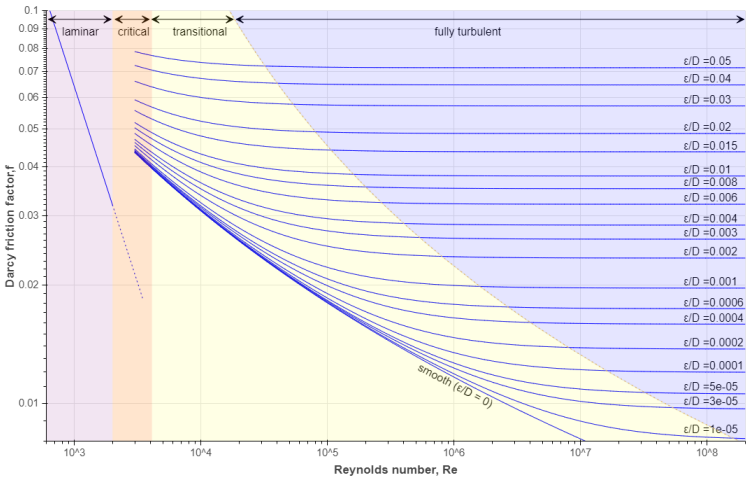

Figure 2.11: Moody diagram, adapted from D. G. Hyams

Looking at figure 2.11 from left to right:

- **laminar**, the particles flow smoothly in non-mixing layers
- **critical** with increasing Reynolds number turbulence can start occurring, the exact conditions vary but lie in the critical band.
- **transitional** the flow is turbulent and becoming more turbulent as the Reynolds number increases.
- **fully turbulent** an increase in Reynolds number has no further influence on the friction factor.

Notice that for high enough Reynolds numbers all the values of relative roughness higher than 0 enter the fully turbulent regime, here only the relative roughness determines the friction factor. This regime is also referred to as *fully rough*.

2.4. Cavitation prediction

2.4.1. $NPSH_r$ scaling

The scaling laws as derived in Section 1.7 have been around for years and are very reliable. They work because the fluid behaves as a continuum and the n_s and Q_s are easy to reproduce.
The other dimensionless parameter 1.22 is assumed to be typically high, so the effects of a change are negligible. As mentioned in Section 2.3.5 ship impellers can develop vortex cavitation specifically at high Reynolds numbers.
The scaling of cavitation however is more difficult, the inception of caviation is assumed not to be scalable (Güllich 2010). Since it depends on absolute pressure difference $\Delta p = p_{abs} - p_{vap}$. The natural starting point for deriving scaling laws for $NPSH_r$ is to compare for comparable flow profiles, i.e. identical specific capacity or identical ϕ.

Güllich (2010) combines use of the ϕ with an Euler like number and defines a variant of the cavitation number:

$$\sigma_{NPSH} = \frac{2gNPSH_r}{u^2} \tag{2.16}$$

Where u is the peripheral velocity of the impeller tip:

$$u = \frac{\omega D_{imp}}{2} \tag{2.17}$$

Expanding this results in a first estimate, see Equation 2.18.

$$NPSH_r = NPSH_{rM}\left(\frac{\omega D}{\omega_M D_M}\right)^2 \tag{2.18}$$

The subscript M in Equation 2.18 stands for model: This relation is suggested in several papers and is also applied as an ISO norm see ISO (2012).

Recalling the specific capacity:

$$Q_s = \frac{Q_V}{\omega D_{imp}^3}$$

Rewriting this to express D_{imp}^2 gives the following

$$D_{imp}^2 = \left(\frac{Q_V}{Q_s \omega}\right)^{2/3} \tag{2.19}$$

Eliminating the constant Q_s gives:

$$D_{imp}^2 \propto \left(\frac{Q_V}{\omega}\right)^{2/3} \tag{2.20}$$

Combining with equation 2.18 and 2.20 and realizing the model parameters are determined constants results in the following relation, as also given by (Tuzson 2000).

$$NPSH_r \propto \omega^{4/3} {Q_V}^{2/3} \tag{2.21}$$

Combining equation 2.21 with equation 1.13 will result in the quadratic relationship.

$$NPSH_r \propto \omega^{4/3} {Q_V}^{2/3} \rightarrow NPSH_r \propto \omega^{4/3}\left(\omega D^3\right)^{2/3} \rightarrow NPSH_r \propto \omega^2 D^2 \tag{2.22}$$

Specific Pressure
The $NPSH_r$ consists of a pressure component and a flow velocity component, as defined in Equation 1.12. If scaling is done with quadratic diameter and quadratic speed as in Equation 2.18, the flow velocity or a given Q_s will by definition scale quadratically (see also Equation 1.20). Therefore a new parameter is introduced here, the specific pressure (P_s). This parameter excludes the flow velocity component and is able to give a more precise idea of the influence of a change in inlet pressure at a given Q_s.

$$P_s = \frac{p_{in,abs} - p_{vap}}{\rho \left(\omega D_{imp}\right)^2} \tag{2.23}$$

Cavity length
In addition a relation between the cavity length (the length along the blade covered with vapour due to cavitation, see Figure 2.3) and the pump dimension is suggested Güllich 2010:

$$\frac{l_{cav}}{D} = f(\sigma_{NPSH}, \phi) \tag{2.24}$$

Implying that the cavity length for situations with identical σ_{NPSH} and ϕ scales linearly with pump size. Note that this is no $NPSH_r$ scaling , because it scales the development of length not $NPSH_r$ conditions. This scaling does have some similarities with the reasoning behind the pressure drop as described in Section 2.2.1. Where the size of the part of the blade that is covered with vapour directly relates to the drop in head.

Some observations given by Güllich (2010) about scaling pumps are listed below:

- *blade roughness and blade profile sensitivity* The incipient cavitation is highly sensitive for changes in wall roughness and blade profile. However, the $NPSH_r$ is not sensitive to those factors. This can be explained by the fact that at incipient cavitation the water particles touches the pump and all small deviations influence it. Once a cavity has started to develop a small gas film is formed creating a comparable geometry for the liquid flow profile. This is particularly convenient since the wall roughness of the blades is hard to determine as discussed in Section 2.3.6.
- *small impellers (inlet diameter below 100 - 140-* mm*)* The $NPSH_r$ increases due to blockage. For blockage there is head loss due to the fact that the space between two impeller blades is fully 'blocked' by vapour, this is another effect than loss of effective blade length due to vapour. The impellers used by the cavitation experiments referenced by Güllich (2010) are in the 6 to 8 blades range. Also the risk of blockage decreases with a decreasing number of blades. This is due to the fact that the distance between the blades increases and will therefore be not blocked that quickly.
  Blockage therefore is still something to be on the lookout for, however with a typical blade number of 3 or 4 and an inlet diameter of 100 mm the risk of blockage is limited.
- *Reynolds* At low Reynolds number there is a small boundary layer. Meaning that irregularities can be of the same order of magnitude. Which can result in tiny vortices, increasing $NPSH_i$. But leaving $NPSH_r$ unaffected.
- *nuclei* If there is no nuclei saturation the nuclei spectrum dominates the $NPSH_r$ making it unpredictable.
- *air separation* Where cavitation vapour is not reabsorbed in the water, the resulting multiphase flow upstream can disturb results.

- Since air separation mostly dominates at low $NPSH_r$ it is sometimes suggested to apply scaling laws mainly for higher speeds (for example above a certain speed for a given pump)

Concluding, it can be said that scaling to a small inlet diameter, the main challenges are repeatable water conditions, preventing air separation at low speeds and blockage.

A specific method for scaling down is suggested by Güllich (2010), in order to be on the safe side:

$$\begin{aligned} x &= 2\left(\frac{NPSH_r}{NPSH_{Ref}}\right)^{0.3} \\ NPSH_a &= NPSH_m\left(\frac{\omega D}{\omega_m D_m}\right)^x \\ NPSH_{Ref} &= 20\text{m} \end{aligned} \tag{2.25}$$

This method is based on limited data and is just designed not to over-predict. Also the scaling factor x only depends on the reference values of the pump measurement not on the predicted speed or diameter. The notion that it is only for scaling down implies its limited predictive application.
As can be seen in Figure 2.12 this equation acts purely as a lower limit not as a model.

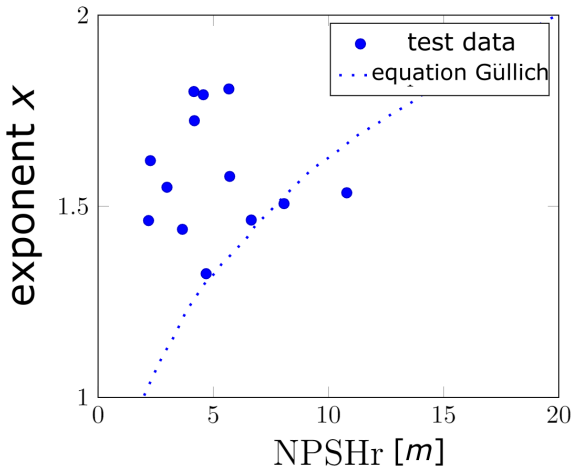

Figure 2.12: Exponent according to equation 2.25, based on manufacuter data. From Güllich (2010)

A more simplistic approach is given by Schiavello and Visser (2009) where only the speed is considered:

$$\frac{NPSH_r}{\omega^\alpha} = constant \tag{2.26}$$

The factor α varies between 1 (conservative) and 2. The chosen value is left up to the user.

2.4.2. Tenot scaling

Stepanoff (1948) (among others) uses the called Tenot scaling, the first step of which is to derive the change in $NPSH_r$ of the reference pump if the speed is changed.

$$\sigma_T{}^* = \frac{NPSH_{rm1} - NPSH_{rm2}}{H_{m1}\left(1 - \left(\frac{\omega_{m1}}{\omega_{m2}}\right)^2\right)} \tag{2.27}$$

The $NPSH$ at other speeds can then be calculated as follows:

$$NPSH_r = NPSH_{rm} - \sigma_T{}^* H_m \left(1 - \left(\frac{\omega}{\omega_m}\right)^2\right) \tag{2.28}$$

Though more elaborate, this method also assumes a quadratic relation between cavitation and speed, there is however a correction applied by using multiple reference points. The broader the range of reference points, the better this method will work.

2.4.3. Variable suction specific speed

The suction specific speed (n_{ss}) is not much discussed here but is historically widely used to compare suction capabilities. The n_{ss} as mentioned in Section 1.7 it reads:

$$n_{ss} = \omega \frac{\sqrt{Q_V}}{NPSH_3{}^{0.75}} \tag{2.29}$$

It is derived by symmetry considerations (Wislecenus 1942) much like the affinity laws. Its scalability however is disputed by Yedidiah (2012). Based on a relatively large data set he provides the following relation of the n_{ss}:

$$\frac{n_{ss}}{n_{ssm}} = \left(\frac{D}{D_m}\right)^{0.546} \left(\frac{\omega}{\omega_m}\right)^{0.432} \tag{2.30}$$

For the $NPSH_r$ the direct relation between speed and diameter is no longer used, instead a specific power is provided:

$$\frac{NPSH_r}{NPSH_{rm}} = \left(\frac{D}{D_m}\right)^{1.272} \left(\frac{\omega}{\omega_m}\right)^{1.424} \tag{2.31}$$

Unfortunately the data is not fully provided but it seems to consist of a wide array of pumps plotted against their flow for 2 specific speeds. That means that the flow profile (the specific speed) might not be taken into consideration in this analysis.

2.4.4. Extrapolating flow rate at constant speed

A quadratic relation with only the flow rate is suggested by Yedidiah (1972)

$$NPSH_r = KQ_V{}^2 + L \tag{2.32}$$

Where the factors K and L are determined with $NPSH_r$ at a low and a high flow rate, calculated using Equation 2.33 and 2.34:

$$K = \frac{NPSH_{r,high} - NPSH_{r,low}}{Q_{V,high}^2 - Q_{V,low}^2} \tag{2.33}$$

$$L = \frac{NPSH_{r,low} \cdot Q_{V,high}^2 - NPSH_{r,high} \cdot Q_{V,low}^2}{Q_{V,high}^2 - Q_{V,low}^2} \tag{2.34}$$

Equation 2.33 is issued with the notion that it is not to be used at very high or low flow rates, as the writer says:

"At high flow rates the $NPSH_r$ requirements increase rapidly. At very low flow rates, particularly near shut-off, a strong interchange develops between the liquid entering the impeller inlet and the liquid in the suction pipe. This sets up unstable performance at low $NPSH_r$ values".
Also at a closed loop the low efficiency of the pump can result in rapidly warming up the water with increased $NPSH_r$ as a consequence, the same reasoning can off course be applied to high flow rates, in fact even more so since the power will also be higher.

2.4.5. Cavitation scaling on a hemispherical body

Scaling effects have been studied quite extensively on a hemispherical model, see 2.13.

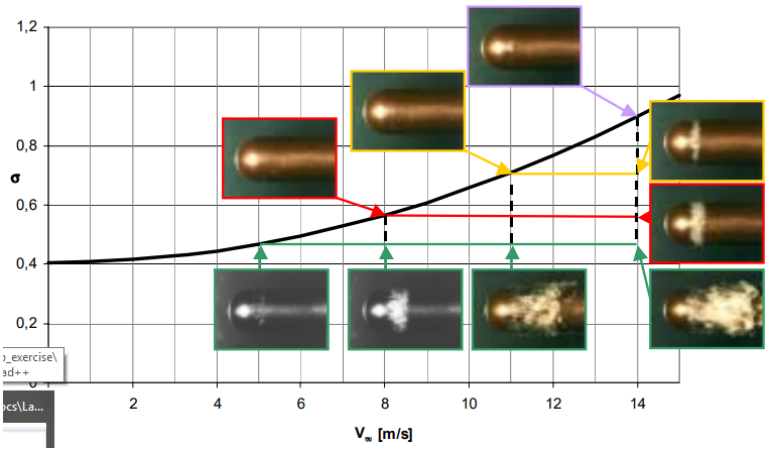

Figure 2.13: cavitation on a hemispherical object(Keller 2001)

In scaling this, empirical relations were made for the viscosity effects:

$$K\left(\frac{\nu_0}{\nu}\right)^{1/4} = constant \tag{2.35}$$

Also a turbulence effect is included:

$$K = K_0\left(1 + K_0\frac{\hat{\sigma}ff}{\hat{\sigma}ff_0}\right) \tag{2.36}$$

where K_0 is an empirical constant depending on the shape of the body. $\hat{\sigma}ff$ represents the standard deviation from the free flow velocity. The subscript 0 refers to the reference values.

Combining those factors and assuming the quadratic length scale relations, the following incipient scaling law was formulated:

$$\sigma_i = K_0\left(\frac{D}{D_0}\right)^{1/2}\left(\frac{\nu_0}{\nu}\right)^{1/4}\left(1 + \left(\frac{\vec{v}_\infty}{\vec{v}_0}\right)^2\right)\left(1 + K_0\frac{\hat{\sigma}ff}{\hat{\sigma}ff_0}\right) \tag{2.37}$$

Equation 2.37 however is overly optimistic for scaling required head in centrifugal pumps Güllich (2010). This is not surprising since it once again focuses on the incipient flow, for a stationary object.

2.4.6. CFD

CFD is known as a strong tool to calculate flows and also useful to determine incipient cavitation. However the multiphase flow resulting from cavitation is more complicated. ANSYS CFX is developed to deal with such calculations, indeed $NPSH_r$ calculations for centrifugal pumps have already been made (Salvadori and Cappelletti 2015). It is however important to note here that correction factors to the calculations were applied by using the experimental data and scaling it with the quadratic relations, or in fact the related form in equation 2.21. Since those scaling laws are the object of discussion here it is reasonable to be cautious using this method.

2.4.7. Conclusion

Almost all scaling methods revolve around the basic quadratic scaling method of the u as described by Equation 2.18. Working with that as a basis, most alternative models are developed not so much to try and predict $NPSH_r$ at for different pump sizes, but more to prevent overly optimistic predictions.
This safe approach is further shown by the warning that most adaptations are given for scaling down. The idea being that other effects come in to play.
In trying to scale the $NPSH_r$ of a pump, especially to the outer edges of the flow velocity, speed and size ranges, it seems important to either prevent or at least recognize effects (other than cavitation) influencing the head of the pump. Such effects might be air separation or air being sucked in.
CFD is an interesting method with high potential but the need for validation makes experiments a more likely first step.

2.5. Cavitation measurement

A typical $NPSH_r$ measurement is qualitatively represented in Figure 2.14 the difference in shape (more specifically the derivative of the head over the inlet pressure around $NPSH_r$) can depend on pump design, but also on flow regime. In general the shape in Figure 2.14a shows a measurement around BEP, which requires a precise measurement. This precision is needed because if the $NPSH_r$ is exceed only a little bit the head will drop significantly. So it is hard to gather multiple data points for inlet pressures below the values corresponding with the $NPSH_r$.

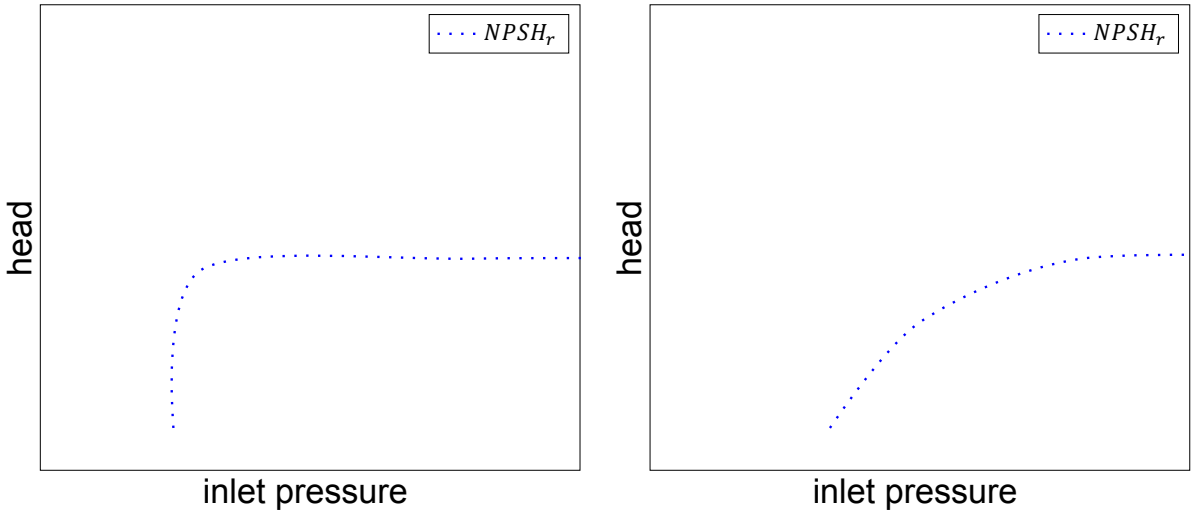

(a)typical $NPSH_r$ measurement

(b) $NPSH_r$ measurement it high Q_s (above BEP)

Figure 2.14: $NPSH_r$ examples

Many physical processes can start playing a role in the measurements but both of these can be a valid, undisturbed, $NPSH_r$ measurement. The conditions for Figure 2.14a can be chosen if optimal operation is required above a certain $NPSH_r$, this shape is often encountered if one operates near BEP. The curve of Figure 2.14(b) can be beneficial if at some part of the operation the pump has a low inlet pressure but still needs to be operational until the true working point is reached.

In Figure 2.15 an incipient cavitation effect is shown where after the onset of incipient cavitation, but before the head drop, there is an increase in head. This is often observed in flows well below BEP and is explained by looking at so called dead spaces (Yedidiah 2012) a visual interpretation of which is given in figure 2.16.

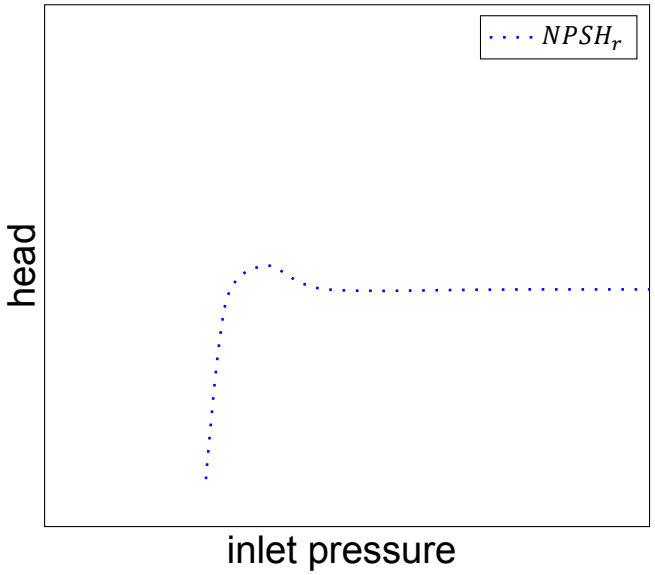

Figure 2.15: $NPSH_r$ with pre-liminary increased efficiency

The reasoning behind such a dead-zone is that it occurs due to a sub-optimal flow profile. In this dead space turbulence in the liquid causes high energy losses. Due to the sub-optimal flow profile this dead space also has a relatively low pressure so cavitation is likely to occur quickly there. If that happens the gas filled cavity can fill up the dead space thereby naturally creating the optimal flow profile around this zone and reducing losses as a consequence. This holds until the cavity extends beyond the dead space, then it will reduce efficiency.
In other words, local cavitation pockets compensate for a bad flow profile. This does remind one of the observation by Stepanoff (1948) that a small injection of air in the pump casing can reduce cavitation damage and in some cases even increase efficiency.

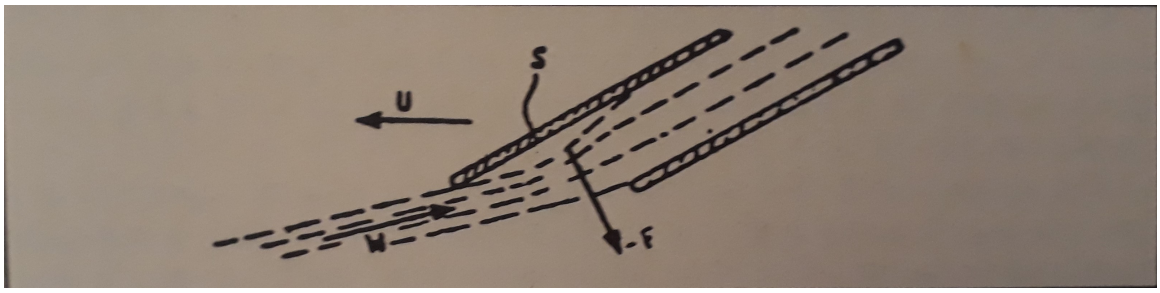

Figure 2.16: dead space in flow below BEP, (Yedidiah 2012)

2.5.1. Non scalable efficiency drop

One of the problems with cavitation measurements is that it operates on the fringe of the system operating conditions. So some effects might occur resulting in a head drop, which might be wrongly interpreted as a scalable pump cavitation problem. If this occurs it can mean either that the scaling limits are reached or that there are some other conditions which can be eliminated. Such circumstances might, among other conditions, have to do with the fluid, wrong alignment or an asymmetric impeller.

Alternating vane cavitation
In Figure 2.17 a typical $NPSH_r$ measurement for alternating vane cavitation is shown. Cavitation occurs on a limit number of blades whilst the other blades still operate at full capacity.
The onset of alternating vane cavitation results in a sudden drop in head at a certain inlet pressure, if the inlet pressure drops further the head will remain constant (the other vanes still generate head) until

full cavitation starts and the head will drop as in a regular $NPSH_r$ measurement.

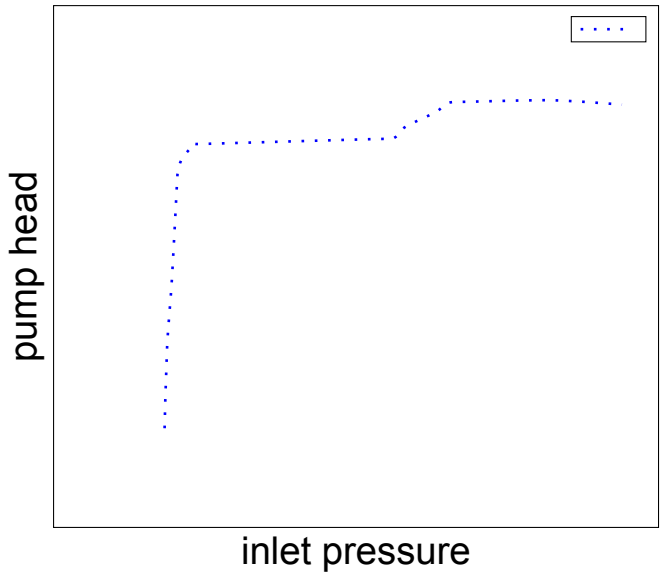

Figure 2.17: Typical alternating vane cavitation

Downstream obstruction
If the discharge pipe has too small a diameter or if there is an obstruction, cavitation could occur downstream. This can only occur further downstream or if the obstruction is really disadvantageous for flow. Otherwise the high pressure after the pump will prevent local cavitation.
If it occurs however it will not influence the pump, but it will result in an increase in hydraulic resistance with a drop in flow as a consequence, changing the operation point.

Upstream obstruction
Upstream obstructions can have even more adverse effects since it is placed in a low pressure part of the setup. If the cavitation bubbles are reabsorbed before the flow reaches the pump, the results might be limited, though an increase in resistance can still cause problems. If the cavitation bubble would reach the pump the drop in head will be immediate, also a further increase in cavity volume can occur which can cause additional problems in a closed loop.

Entrained air
Air can be sucked in or be entrained see paragraph 2.2.4. This can often visually be observed and has a detrimental effect on the pump properties. The very first step in a cavitation measurement is to remove entrained air (or dissolved air). Especially in a closed loop this is essential, because at the moment that air is entrained it can keep on circulating in the setup making a good measurement impossible.

2.6. Cavitation noise

Cavitation is well known to occur in combination with noise, Schiavello and Visser (2009) suggests that the onset of noise due to cavitation has a sharp increase right after the point of cavitation inception. That is even before a drop in head is observed. This is concluded after experiments with pumps constructed from plexiglas with a piezoelectric element registering noise, or in fact vibrations in the pump casing. Those vibrations are considered to be caused by the violent implosion of the cavitation bubbles.
Once the cavitation is further developed the noise decreases somewhat due to the increase in air pockets, this is referred to at the cushioning effect. This also happens to be an indicator for cavitation erosion, if the noise level is maximal the damage is also the highest. In Figure 2.18 such a measurement is shown, for a frequency signal at 40 kHz though the signal seemed to be independent for frequency.

In Figure 2.18 an alternative for $NPSH$ is used namely the Net Positive Suction Energy, see equation below:

$$NPSE = gNPSH \tag{2.38}$$

The same method is used for the energy rise:

$$\text{energy rise} = gH_{pump} \tag{2.39}$$

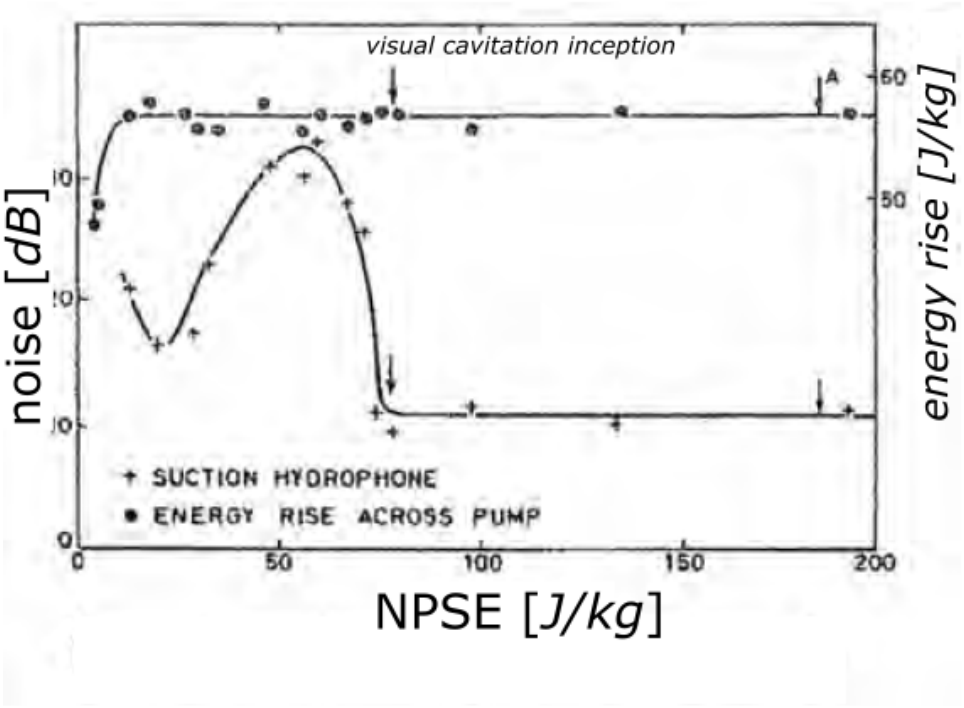

Figure 2.18: cavitation noise as a function on inlet pressure Schiavello and Visser (2009)

It is interesting that in Figure 2.18 the noise increases again once the full head start to drop, Schiavello and Visser (2009) does not speculate about the reasons for this. It seems to be that the either the cushioning effect is no longer increasing whilst the implosions do increase.

The cavitation number (as in equation 1.27) at the point of acoustic noise inception (acoustic cavitation number) if plotted against the flow normalized with respect to the BEP flow (comparable to specific capacity) is shown in Figure 2.19.

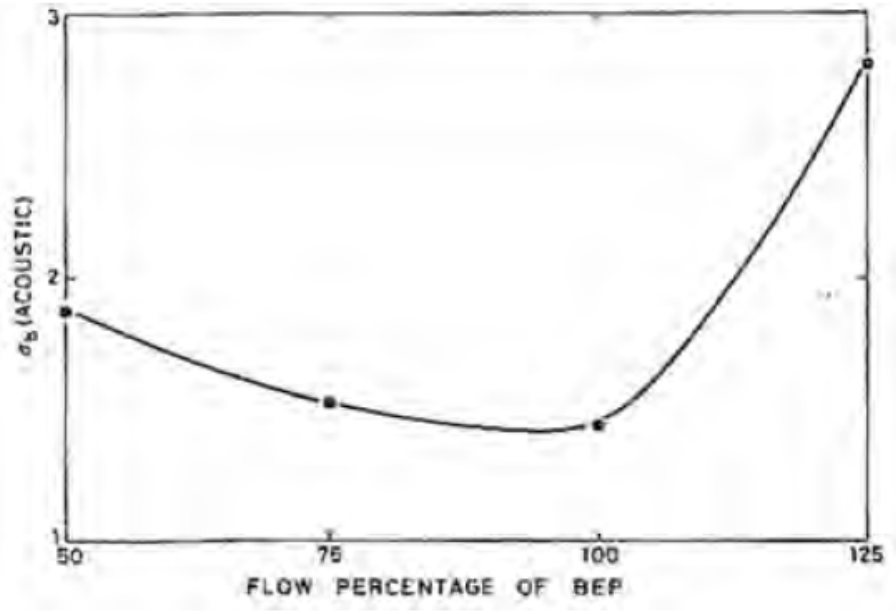

Figure 2.19: acoustic cavitation number vs flow Schiavello and Visser (2009)

2.7. Discussion of cavitation theory

Cavitation is a complex process which is hard to predict, also the sensitivity to boundary conditions such as alignment, water conditions and roughness indicate that scaling cavitation characteristics needs to be done with care. However most of those considerations apply to incipient cavitation, the further developed cavitation associated with $NPSH_r$ seems to be less sensitive.
It still remains important to be certain that one not only looks at cavitation but also at a scalable effect. If that is not the case it is essential that it is recognized, preventing those non-scalable effects and recognizing them if they occur seems to be the greatest challenge in the small scale experiments.

2.7.1. Scaling models

Turbulence is often (but not always) omitted in the cavitation scaling models, for the pump scaling it appears to be omitted always on the grounds that the turbulence is relatively high, so changes will have little effect. The most elegant scaling methods appear for stationary objects and unfortunately not rotating ones, such as a pump impeller.
It is noteworthy that several authors in their scaling models not so much try to predict the $NPSH_r$ values but focus more an a safe lower limit. The quadratic model still seems to have the strongest theoretical basis, but the experimental results suggest it needs to be treated with care.
Using CFD can be a useful tool to predict the location of the onset of the cavitation, also the further development with a multiphase capable method would provide insight. Since the variation in experimental results and the necessity for validation a scaled experiment would be needed to check the reliability of the results.

2.7.2. Approach

Experiments and CFD are powerful tools, CFD however always needs to build on validation by experiments. Also the time required to obtain the necessary insights in multi-phase CFD makes experimental research a better stating point. Therefore a small scale test setup will be employed in the current research to investigate the $NPSH_r$ behaviour along a range of specific flows at differing pump speeds. Special attention will be given to recognize head drops due to non-scalable effects. First the scale affects related to pump speed will be investigated after which the measurements will be compared with available true-size pump data.

2.8. Conclusions

- There are no definite scaling laws for $NPSH_r$. A first guess is often that the scaling is quadratic for both diameter and speed but most applied suggestions are more conservative.
- Most scaling methods aim to provide a safe operating region, not to predict the $NPSH_r$ values. With the most striking example the suggestion to use a scaling function only for scaling down to lower speeds and diameters, but not for higher speeds and diameters.
- A drop in pump head can have multiple causes, in performing the experiments other sources need to be excluded as a possible source.

II

Experiments

3

Experimental design

The goal of the experiment is to investigate the $NPSH_r$ properties of the lab scale pump. The first thing to think about here are the inlet conditions. The flow needs to be adaptable and, more difficult, the inlet pressure needs to be controlled and lowered to values well below atmospheric pressure. Also the operating conditions of the pump need to be controlled, the main parameter here is the shaft speed.
The inlet conditions of the pump are mainly influenced by the flow loop of the pump, the goal of which is to provide the relevant operating conditions for the pump: controllable inlet pressure, high enough flow range (so the minimum flow resistance needs to be low enough), controllable water conditions regarding temperature and dissolved air.
If the flow loop conforms to the requirements the pump can be investigated, the geometry needs to be identical to the on board scale. Experiments will be carried out for a range of shaft speeds, so it is essential to both control and measure this. To know the operation of the pump the inlet conditions and the pump head need to be known in addition to the speed and the flow rate. Below the setup is described, starting with the whole flow loop then zooming in on the pump itself.

All experiments are performed at the royal IHC research lab in Kinderdijk.

3.1. Flow loop

A dedicated setup for $NPSH_r$ measurements requires firstly to control the pressure in the system. Since the system is a closed loop, the pressure of each point in the loop is related to the other point. If a water particle is followed as it flows along the setup the pressure it experiences changes under influence of three factors

- **height** at the highest point there is no additional hydrostatic pressure due to a water column, below this point the height difference contributes to the pressure.
- **wall/obstacle friction** moving along the wall or obstacles such as bends or valves results in pressure loss and thus a lower pressure downstream.
- **pump head** the pump, of course add pressure to the system.

Taking this into account, the result is that if the pressure in one point in the loop can be controlled the pressure in the whole loop will depend on the pressure in this location and the three contributing factors along the loop.
The easiest way to control the pressure in one point in the loop is via hydrostatic pressure, simply add a vertical pipe to a point in the loop. If the pipe is filled the pressure increases, if the water level in the pipe is lowered the pressure decreases. In Figure 3.1 the vertical pipe is added to the pump system. The pressure changes with the height in the water column according to following equation:

$$\Delta p = \rho g \Delta h \tag{3.1}$$

If the pressure needs to be lowered below the lowest possible water level in the pipe a vacuum pump is added to the system to lower the pressure even further.

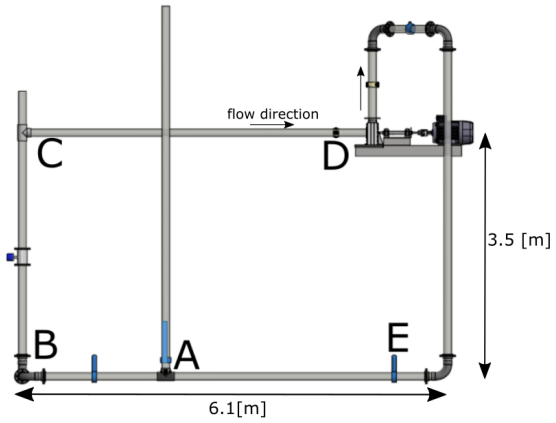

Figure 3.1: First pump setup, courtesy J. Hoebe

Some setup dimensions are listed below:

- **Inlet diameter** 100 [mm]
- **Impeller diameter** 202 [mm]
- **Pump elevation** 3.5 [m]

To visualise the effect of water column the pressure process along the system is visualized in Figure 3.2. If the pressure in the column changes while the other parameters remain identical the entire pressure line will shift, leaving the relative differences the same, unless cavitation is to occur somewhere in the loop.

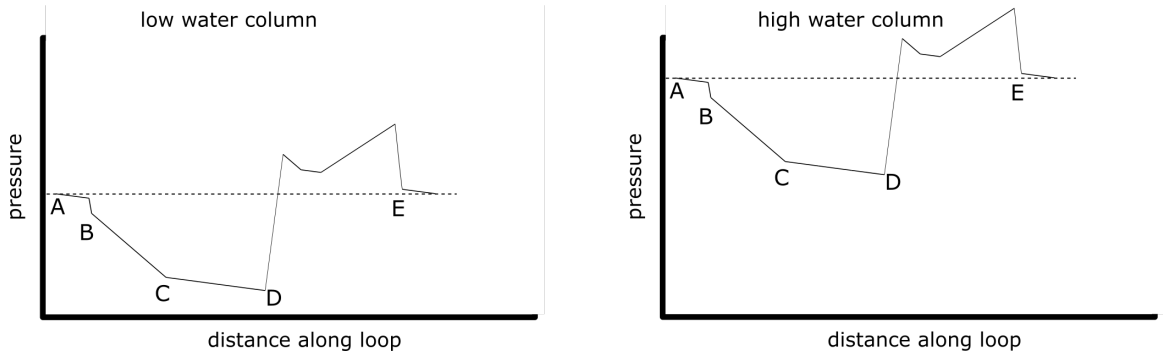

Figure 3.2: pressure along loop

3.1.1. Basic measurement and sensors

For the first measurements making a closed loop is the only requirement. In Figure 3.3 the resulting setup is shown. The sensors required are shown schematically. Also a valve is specifically mentioned. This is because the valve is used to vary the working point of the pump. Say a measurements is started with a fully opened valve, the hydraulic resistance will be minimal so the flow for the given speed will be maximal. Subsequently the valve is gradually closed creating a higher resistance, up to the point that it is fully closed. In this way one can get the pump characteristic.

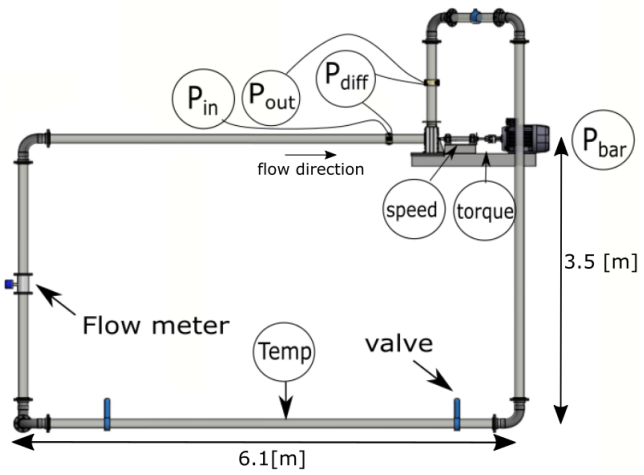

Figure 3.3: combining those sensors and making a loop for the pump to operate

3.1.2. First $NPSH_r$ experiments

The setup as in Figure 3.1 allows for an initial $NPSH_r$ test, in order to check the operation of the whole loop. Specification of the pump are described in Section 3.2. Here this is done as follows:

- set a fixed speed
- set a fixed flow velocity, by turning the valve.
- lower the system pressure by lowering the water level in the column
- if the flow starts to drop open the valve further
- once the head of the pump drops below 95% of the initial value, the $NPSH_r$ conditions are met.

The result of a few of those initial tests were for a much higher inlet pressure than anticipated. In fact in the order of 30 kPa (absolute pressure). This is a good moment to remind oneself to the fact that the drop in head is a *symptom* of cavitation. Problem with symptoms is that they can have different causes. Here the cause seems to be dissolved air, which can be seen in Figure 3.4.
The air bubbles can clearly be seen by the naked eye, the volume balance of the system was also disturbed as could be observed by the water level in the vertical column. When the vacuum pump was activated the water level in the vertical column would rise, this effect kept occurring regardless of the experiments duration. One can easily imagine that the influence of those bubble can be detrimental to the pump characteristic.
An additional problem was the heat added to the system was large relative to the heat capacity of the water, resulting in a quick temperature increase. The water temperature could rise with a rate around a degree per minute, resulting in changing conditions and quickly changing vapour pressure (the relation was shown in Figure 2.1).

Figure 3.4: recirculating air

In order to remedy this a tank was installed, in the lower part, see Figure 3.5, with a diameter of five times the pipe diameter. Which reduced the flow velocity with a factor of around 25, the advantages of this were multi-fold:

- increased water volume means an increased heat capacity and slower heating up,
- increased diameter means reduced flow velocity, this combined with chambers to ”catch” the air allowed to remove air from the system,
- the tank was placed in the lower part of the loop, meaning that the pressure is already relatively high, combining this with the lower flow velocity means even higher pressure. The valve to adapt the pressure loss in the loop was placed right before the tank. Thus reducing the risk of valve cavitation and allowing quick recuperation if it were to occur.

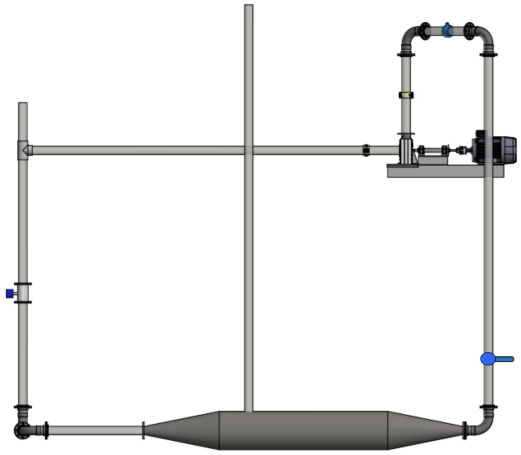

Figure 3.5: Improved pump setup, courtesy J. Hoebe

Inside the buffer tank two plates with a release valve in front of it are placed, see Figure 3.6. Gas will move up due its lower density and accumulate in front of the plates. The gas can be let out via the valves on top. This can only be done as long as the internal pressure exceeds the atmospheric pressure.

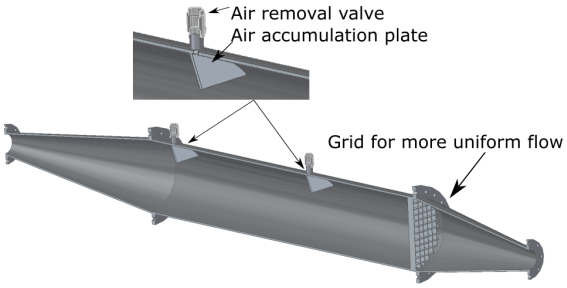

Figure 3.6: inside view watertank

Included in this buffer tank is a cooling system which has a heat exchanger coil, with tap water flowing through it in order to further reduce temperature increase.

3.1.3. Testing the setup

The adaptations immediately had a positive effect on the setup:

- air bubbles could be removed from the water, at least up to the point that they were no longer

visible. In fact the water could get so free of air and other disturbances that it was hard to see that the water was flowing through the pipes.

- the water became incompressible, for even at low pressure (-90kPa]) the water level in the water column became constant.
- the temperature increase was reduced from around $1\frac{\text{K}}{\text{minute}}$ to less than $0.1\frac{\text{K}}{\text{minute}}$

Loss coefficient components
These observations give confidence in the test setup, especially the fact that the flow into the pump seems to be free of entrained air suggest that even if some local cavitation might occur it does not influence the determination of the $NPSH_r$ characteristics. Still it is interesting to investigate what happens in the water tank. Although there are no means to look inside the tank it is possible to investigate the pressure drop over the water tank. As in equation 2.14 there is a quadratic relation between the pressure drop over a component and the flow velocity, provided the fluid is incompressible. Leading to the following equation White (2011) :

$$\Delta p = \xi \rho \frac{\vec{v}^2}{2} \tag{3.2}$$

Where ξ is the loss coefficient, viewing the water tank as a whole the corresponding loss coefficient can be determined using the flow velocity in the 100 mm pipe. The fact that the local velocities change in the water tank is of no concern since it is viewed as a whole. The loss coefficient is constant as long as no cavitation occurs. The pressure differential was measured over the water tank, though it needs to be noted the sensors had only one tapping and were located closely to a bend, see also Figure 3.7

Figure 3.7: sensors for pressure differential over water tank

With this setup the loss coefficient was determined at a variety of flow velocities, also with a cavitating pump. The loss coefficient had a value of around 5.2 for every measurement, indicating there are no phenomena disturbing the measurement occurring in the water tank, or in the valve right before it.
If this loss coefficient had changed this could be an indication that air might be sucked in or that local cavitation occurred.

3.2. Pump

The pump is powered via the electric motor, which is connected to the impeller via the shaft as is shown in Figure 3.8.

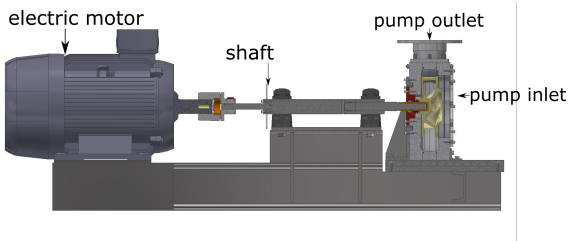

Figure 3.8: 3D printed impeller

3.2.1. Electric motor and shaft

The electric motor itself is powered by a variable frequency drive. This drive provides an alternating current, the frequency of which can be chosen by the operator. This frequency is directly related to the

rotational speed of the electric motor's shaft. Once the operating frequency is chosen the required powered can vary, as long as this power is within the range of the frequency drive the shaft will keep rotating at the chosen speed. If the required power exceeds the chosen limit, the frequency drive will shut down.

The shaft connecting the electric motor with impeller is stabilized via two bearings (as can be seen in Figure 3.9), these bearing reduce vibrations in the shaft. They do however have some friction creating a small energy loss. This influences the interpretation of the torque measurement discussed below, because a part of torque measured is exerted on the bearing and not on the impeller.

The torque is measured via shaft deformation, in order to register this a strain gauge is attached to a thin part of the shaft, deformation changes the electrical resistance, which indicates torque, in Figure 3.9 is can be seen where te strain gauge is placed.

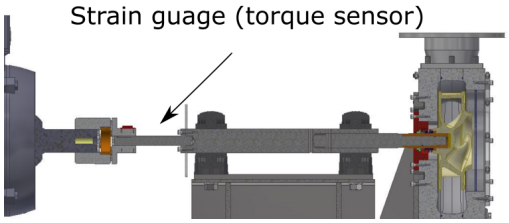

Figure 3.9: location torque sensor

3.2.2. Pump casing

The pump casing has a square as it's outer shape, this is only for easy assembly. The volute has been milled inside, as can be seen in Figure 3.10.

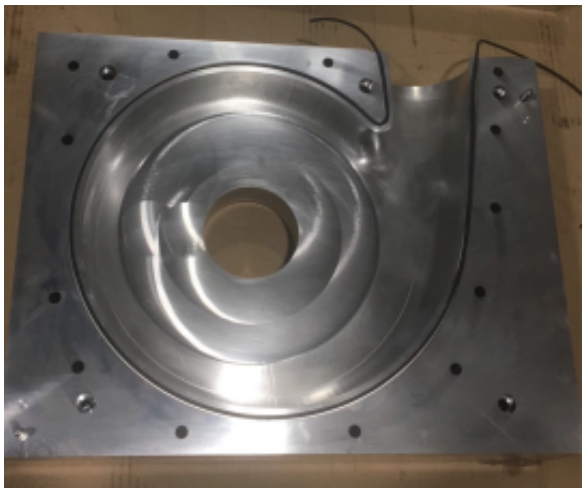

Figure 3.10: inside pump casing

3.2.3. Impeller

The impeller and the pump casing combined determine the flow profile of the pump, the impeller being the moving part that exerts the inertial force on the liquid is essential. Also one pump casing can have different impellers that are compatible with it.
Therefore the choice is made for 3d printed impellers, the benefit of which is that they are easily and quickly produced at low cost. Problem might be the roughness. However,theory suggests that roughness will influence efficiency, but the $NPSH_r$ will not be influenced by it (note that the incipient $NPSH$ ($NPSH_i$) will be affected though). An example of such an impeller is shown in Figure 3.11.

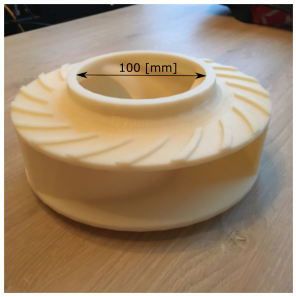

Figure 3.11: 3D printed nylon impeller

Point of attention remains the strength of the impeller connection to the shaft, since the torque on the impeller can have high values at high speeds it might be that the connection won't hold. The connection is shown in Figure 3.12, if the torque gets too high the connection fails as is shown in Figure 3.13. This can also occur if the front casing is too close to the impeller.

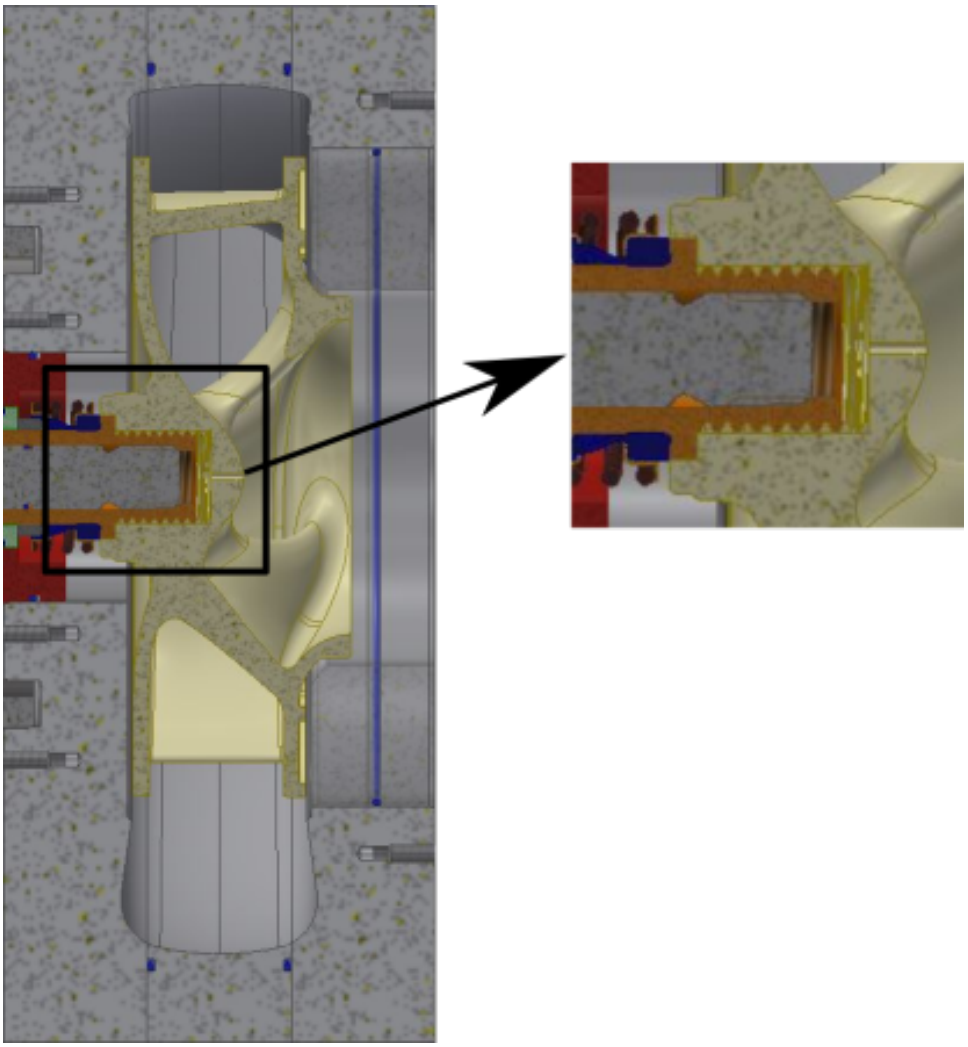

Figure 3.12: impeller connection

Figure 3.13: worn out impeller connection

Impeller variations
The pump housing is suitable for several IHC impellers, namely the ”Hoog Rendement Midden Druk” (high efficiency medium pressure) (HRMD) range:

- HRMD3B
- HRMD4B
- HRMD3B Curve
- HRMD4B Curve

Where the B stand for number of blades, and the curve is the next generation impellers with an additional curved shape in the axial direction.

Unfortunately there is limited $NPSH_r$ data for true size impellers, only the HRMD3B available data. Therefore the focus here will be on the HRMD3B impeller. Also the HRMD4B-curve impeller will be investigated, although no $NPSH_r$ data is available for the full scale HRMD4B-curve impelller.

3.2.4. Clearance

In scaling down the impeller, clearance is an important factor that is hard to scale, in Figure 3.14 this is visualized.

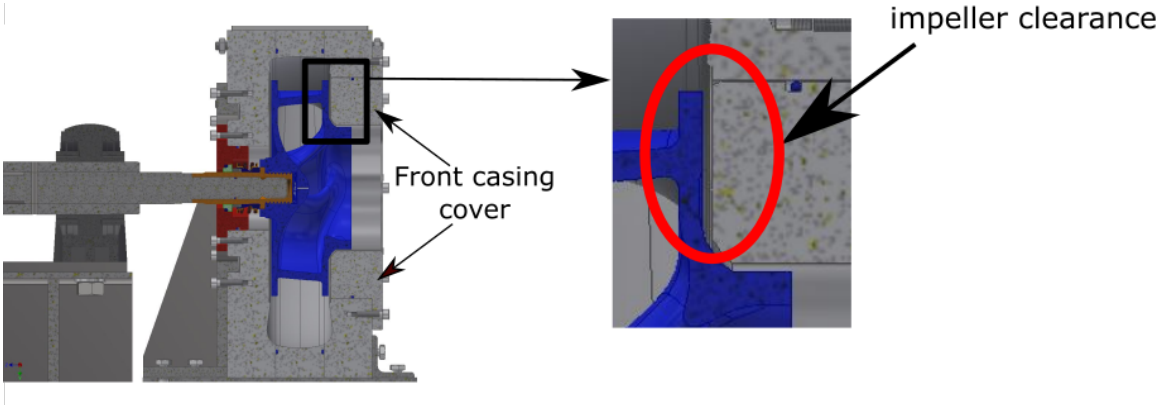

Figure 3.14: recirculating air

Backflow can occur via the impeller clearance, resulting in head loss and thus reduce efficiency, Güllich (2010). In this setup it transpired that due to the axial force, the impeller can move slightly towards the front casing cover.
In order to optimize the pump efficiency the front casing cover is adapted for each speed at the maximum flow. If the clearance is too large there will be an additional efficiency drop if it is too small however the impeller might hit the casing blocking the impeller, with a connection failure as a consequence.

Though the adjustment needs to be carried out with care, it does have a significant effect on the pump performance. In 3.15 the influence is shown.

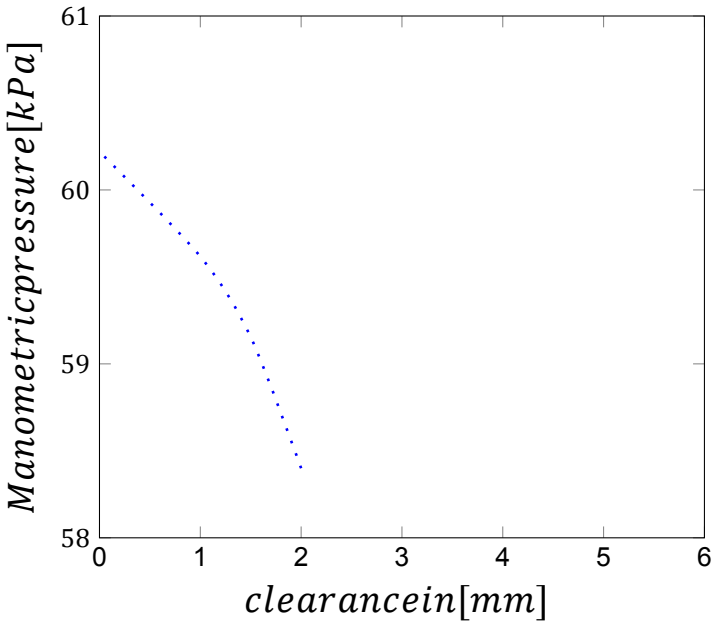

Figure 3.15: relation between clearance and manometric pressureP

This drop is not that much, however, the drop of from 60.2 to 58.4 [kPa] is 3% which for some conventions is the head drop associated with $NPSH_r$ (here it is chosen to be 5%). Variations in clearance during a measurement can disturb the results significantly.

3.3. Pump sensors

To begin the experiments, the ability to perform a good flow rate vs head measurement is the first requirement. In Figure 3.16 the pump setup is shown.

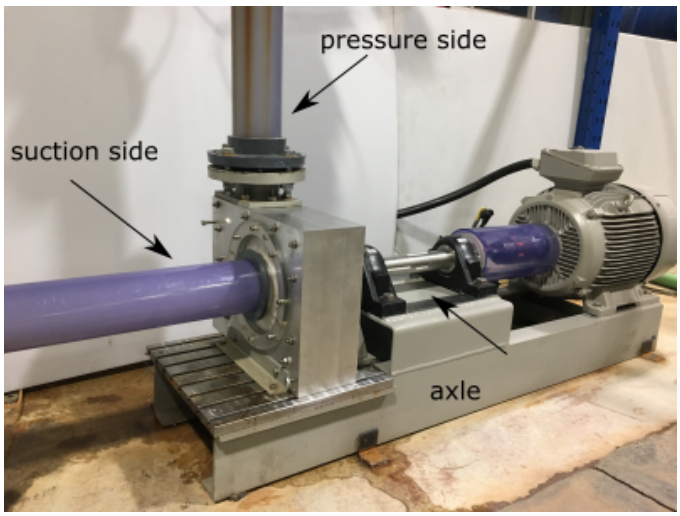

Figure 3.16: 3D printed impeller

In order determine the flow-head properties the following quantities need to be logged:

- **pressure** since a pump specifically adds pressure to a flow system, sensors measuring this are essential. Below are the used sensors listed:
  - differential pressure sensor over the pump. This sensor has a low pressure side connected

at the inlet side of the pump and a high pressure side connected to the outlet of the pump. Those connection point are installed according to ISO standards (ISO-5198 1998) meaning that they are connected to 4 points as in Figure 3.17a.

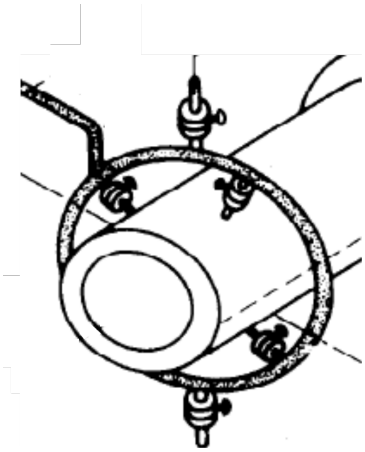

(a) point pressure sensor connection, from ISO-5198 (1998)

(b) 3d printed pressure sensor housing, courtesy J. Hoebe

Figure 3.17: Pressure sensor connections.

By connecting the four points, differences between the top and the bottom or other changes are averaged out.

The differential sensor is enough to determine the head, for validation and to know the exact inlet and outlet conditions there are three extra pressure sensors in this list.

– gauge pressure sensor at the inlet, connected to the same point as the low pressure side of the differential pressure sensor.
– gauge pressure sensor at the outlet, connected to the same point as the high pressure side of the differential pressure sensor.
– a barometer(absolute pressure sensors) is placed near the pump (specifically at the same height as it's datum). Adding the atmospheric pressure to the gauge pressures gives the absolute pressures,

The location of all sensors needs to be carefully chosen. In order to avoid mistakes with static head it is convenient to place the gauge sensors at the same height as the datum (centre of the pump). The barometer is than also placed at this height.

The location of the connection points on the pipework needs to be carefully chosen, it can not be to close because pump; instabilities and pre-rotation will influence the measurement. To far away from the pump the pressure-drop due to wall friction will become significant, though one can correct for this using the wall roughness as discussed in section 2.3.6. This correction is applied here but proves to be negligible. In order to know the full pressure conditions a barometer is mounted near the setup, at the same height as the datum of the pump. Adding the measurements of the barometer to the data of gauge pressure sensor gives the absolute pressure.

- **torque** knowing the torque and the speed gives the shaft power. Using the pressure difference and flow velocity the hydraulic power can be calculated.
  The measurement of the torque is described in Section 3.2.1.
- **temperature** the water-temperature has a large influence on the vapour pressure as was shown in figure 2.2. Knowing the vapour pressure is essential for interpreting the cavitation measurements. Since the water is pumped around in the loop the temperature will vary little over the position, it

will heat up uniformly over time. Thus the location is not that important as long as it is not in a ’dead’ zone where water is not moving.

3.4. $NPSH_r$ measurement

Once the setup is prepared the $NPSH_r$ measurement itself can start. There are multiple ways to conduct a $NPSH_r$ measurement, they all use the same criterion: the head drops a certain percentage below the head under optimal conditions. In Figure 3.18 the criterion is shown, the difference between the different methods is the path that is taken from the initial head till the head drops below the 0.97 criterion.

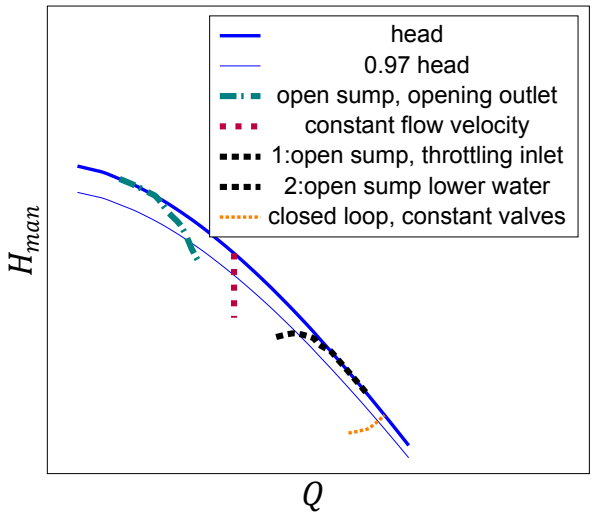

Figure 3.18: head and dropped head

In ISO (2012) a multitude of methods is qualitatively described. The development of which is shown in Figure 3.18. The starting point is chosen arbitrarily. Simplified there are three parameters:

- inlet pressure
- inlet throttle valve
- outlet throttle valve

In addition to the closed loop used in this research and shown in Figure 3.5 there is also the option of a loop with an open sump, schematically shown in Figure 3.19

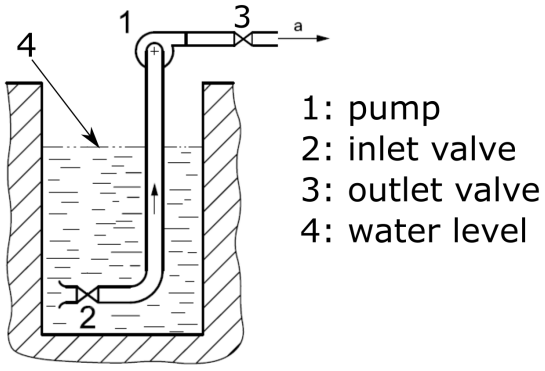

Figure 3.19: open sump setup, adapted from ISO (2012)

Below the different paths are shortly discussed.

- **open sump, opening outlet valve**
  Here the inlet conditions remain the same, the imposed static pressure is not changed nor is the position of the inlet valve. The outlet valve is slowly opened with an increase in flow velocity as a consequence. The flow velocity will increase resulting in a higher pressure drop over the inlet valve, due to which the inlet pressure drops, until cavitation sets in.

This method is often used in on board tests, with some experience the point of crossing the $NPSH_r$ threshold can be roughly predicted.

- **constant flow velocity**
  - **closed loop**
    Here the static pressure is slowly lowered, as a result the flow velocity will decrease along with the head. The flow velocity however is kept constant by adapting the outlet throttle valve. Resulting in a vertical line.
  - **open sump**
    a method as in the closed loop can be used, it can also be achieved by tuning the outlet throttle valve in combination with the inlet valve.
- **2:open sump, throttling inlet**
  The inlet valve is slowly closed, resulting in a drop in flow velocity, at first this results in an increase in head. However, as the inlet pressure drops further the head will also start to drop.
- **1:open sump, lower water level**
  The water level is lowered whilst the valves are kept constant. In lowering the water level the pressure drop due to difference in height of the water level increases. Initially corresponding gain in head results in a lowering in flow velocity along the initial flow-head line, once the cavitation starts to influence the pump performance the characteristics will drop below the initial flow-head line.
- **closed loop, constant valves**
  Tank pressure is dropped without changing the valve positions.

3.4.1. Measurement procedure

The measurements as performed here are of the constant flow in a closed loop type which follow the path of Figure 3.20:

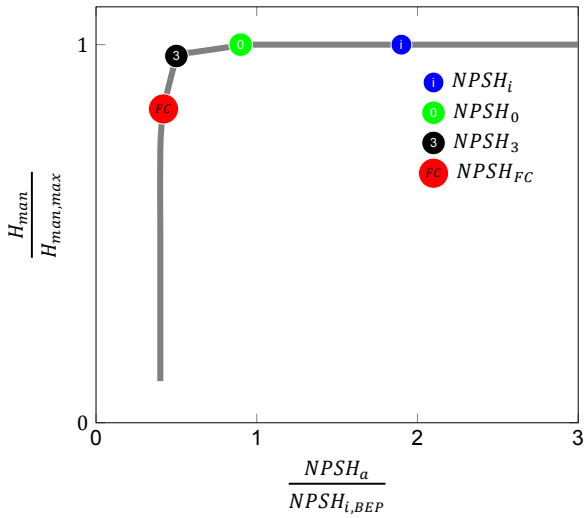

Figure 3.20: qualitative $NPSH_r$ measurement

In performing the measurement the following steps are taken:

- the pump is started at the desired speed
- the working point is set at the desired flow velocity by tuning the control valve (here expressed in specific flow to improve comparability)
- the inlet pressure is slowly lowered by lowering the height of the vertical water column

  - if the water column can't be lowered any further the vacuum pump connected to the water column is activated. At this point the entire system operates below atmospheric pressure.

- once the head start to drop (at point 0) the flow velocity will also drop, since the whole system loss coefficient will remain constant the flow will drop with a decrease in head.

- to counteract the drop in flow velocity the control valve will have to be opened.
- once the desired flow velocity is reached the inlet pressure can be lowered further, after which the desired flow velocity will be attained by opening the control valve once again.

Measurement example
One example of a $NPSH_r$ measurement done is given in Figure 3.21 where a HRMD4B curve pump is operated at a shaft speed of 25[Hz] and a flow velocity of 3 [$\frac{m}{s}$]. One can see the start at an inlet gauge pressure of -50 [kPa] where the head is stable at 100%, as the inlet pressure is lowered the head starts to drop at -80 [kPa]. As the inlet pressure is lowered further, the head drops below 95% of the initial value (the $NPSH_r$ criterion here) at an inlet pressure of -88.2 [kPa].
The inlet pressure and water temperature at the crossing with the 95% line is used to determine the $NPSH_r$ properties at the chosen operating point.

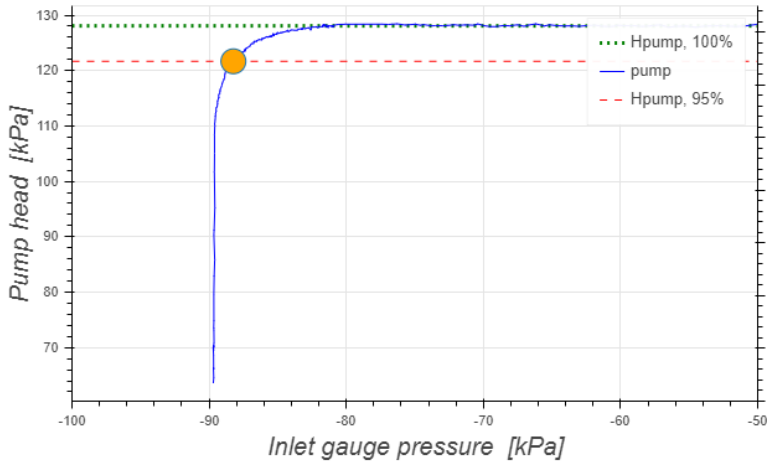

Figure 3.21: HRMD4b-curve $NPSH_r$ measurement, shaft speed 25[Hz], flow velocity 3[$\frac{m}{s}$]

3.4.2. Acoustic emission measurements

In order to gather additional confirmation that cavitation occurs an acoustic emission (Acoustic Emission (AE)) sensor was added to the test setup. Two sensors were mounted on the pump casing. Both at the back of the casing, see Figure 3.22.

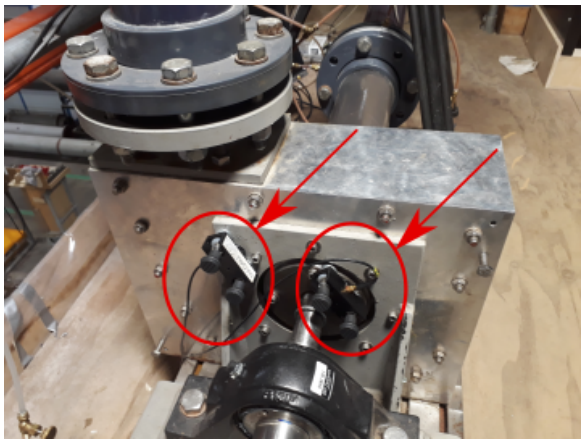

Figure 3.22: acoustic sensor locations

The sensor converts the vibrations to a voltage. In order to get a signal matching the noise registered the gain of the sensor needs to be set, the gain is the voltage amplification in dB. If the gain is too low the signal is not registered, if it's too high (as in Figure 3.23) the voltage range is saturated and the signal can not be interpreted. In Figure 3.24 a correct measurement is shown.

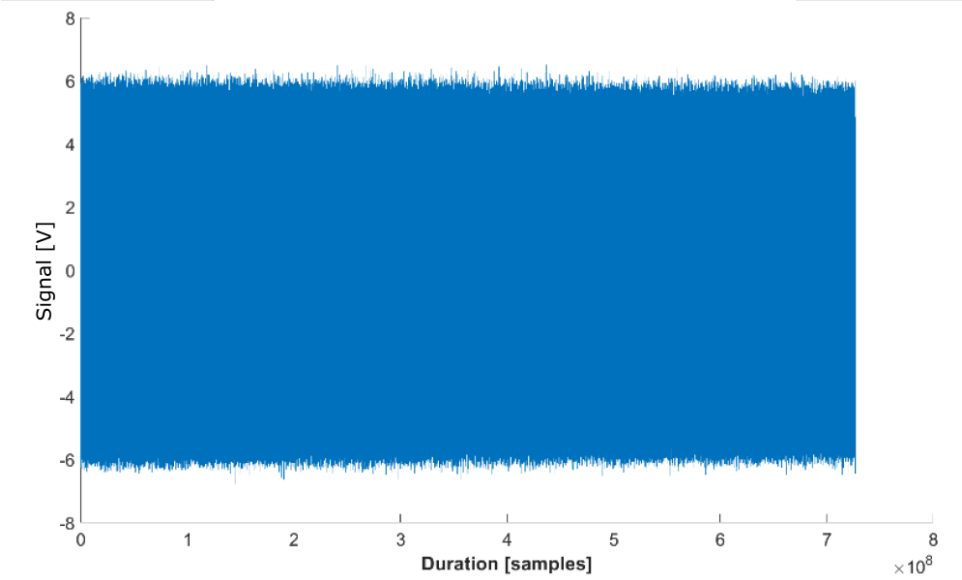

Figure 3.23: Saturated acoustic emission sensor, sample frequency 10^{-6}Hz

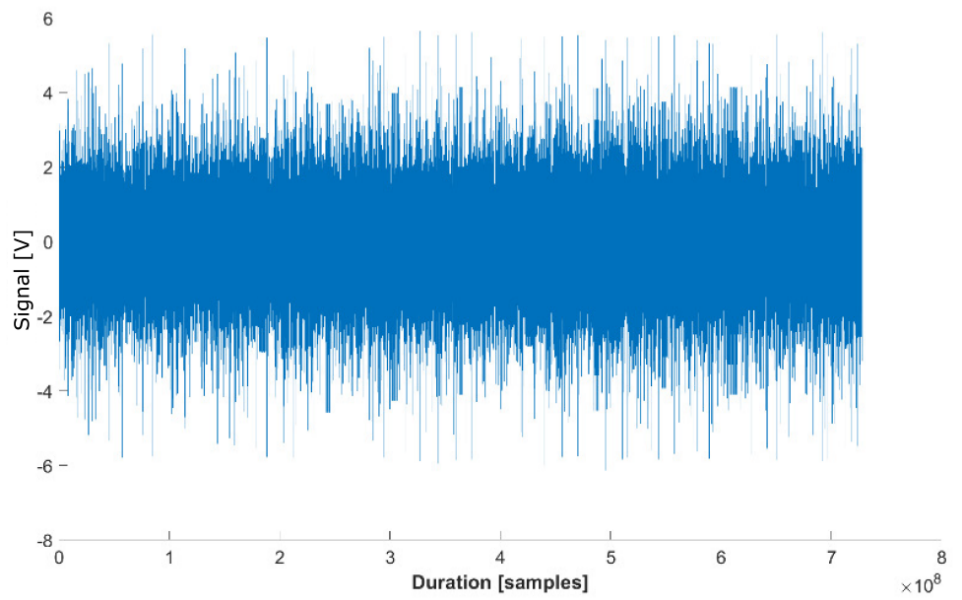

Figure 3.24: Correctly set acoustic emission sensor, sample frequency 10^{-6}Hz

The available equipment operates at a frequency of 1000 [kHz] which is probably well above the required range. The measurements did however provide usable results as shown in Figure 3.25.

In order to compare the signals the non-amplified voltage needs to be calculated using the following equation, where the output signal is called the acoustic emission (A_e):

$$A_e = U10^{-gain/20} \tag{3.3}$$

A typical measurement with acoustic emission done for this research is shown in Figure 3.25 and 3.26.

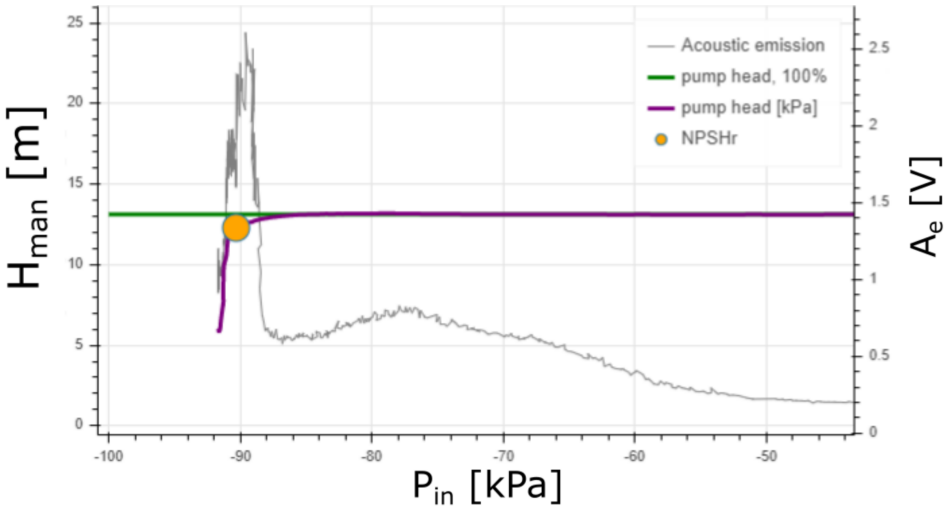

Figure 3.25: Acoustic emission measurement with local maximum

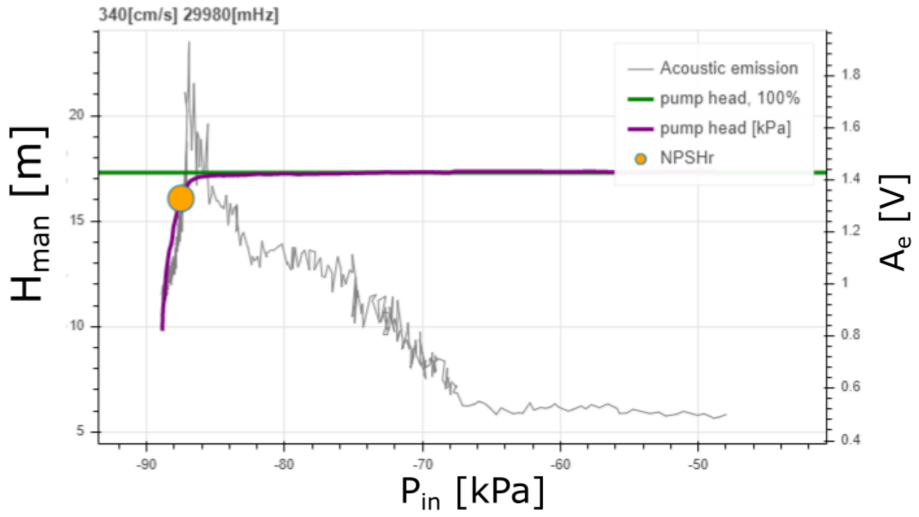

Figure 3.26: AE measurement without local maximum

Figure 3.25 is representative for the measurements done and the first part closely mimics the behaviour shown in Figure 2.18.
The AE measurements has a relatively higher peak around the $NPSH_r$ value. After this high peak the acoustic emission drops again, almost to the level of the first peak. This can be explained by the fact that in this regime the head has dropped significantly together with a decreased inlet pressure. As a result the cushioning effect will grow rapidly.

The development of the acoustic noise can differ, as can the baseline before cavitation inception. The rapid increase right before, or at the start of, the drop in head and the subsequent rapid drop in noise is universal for each successful $NPSH_r$ measurement. Therefore two points can be identified in any measurement as shown 3.27.

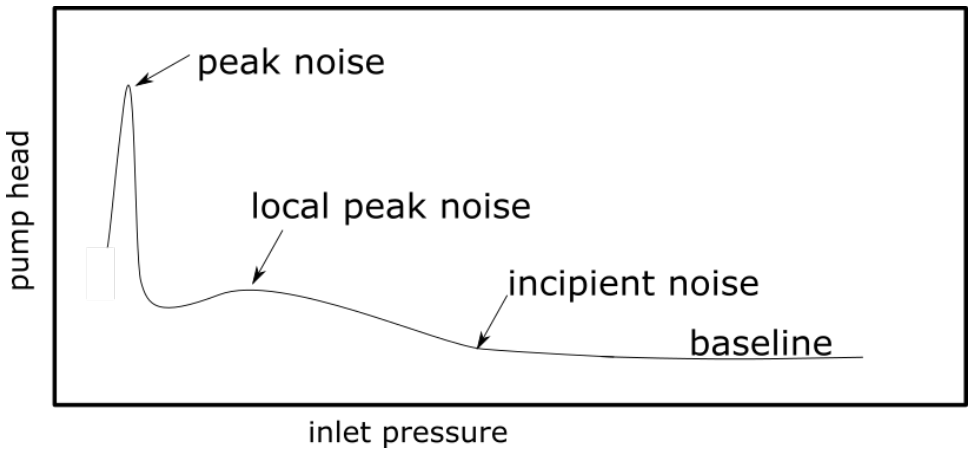

Figure 3.27: information from Acoustic Emission

Since the focus here is on the $NPSH_r$ the peak noise will be used to identify whether or not a measurement is successful. The method is as follows, if at the moment of head drop the peak has not shown the measurement is discarded.

Note that the above mentioned analysis does not provide conclusive proof of a pure cavitation measurement. The drop in cavitation noise can also be caused by air being sucked in at a low under pressure. It can however be considered as a minimum condition.

An example of a wrong measurement is given in Figure 3.28.

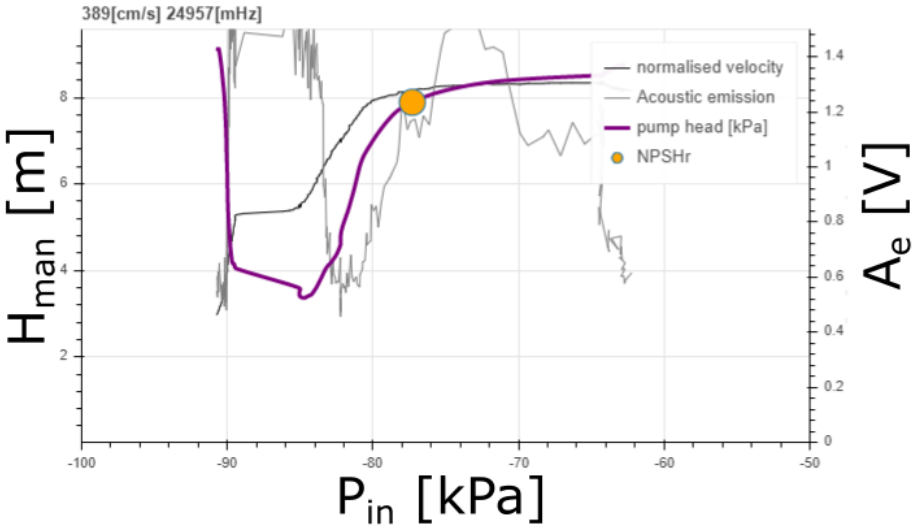

Figure 3.28: failed measurement

It is hard to determine what exactly went wrong here but it can be seen that the manometric pressure not only dropped rapidly before the true acoustic peak, but also the flow velocity dropped significantly. This change in flow velocity alone is for the $NPSH_r$ test type chosen a reason to discard the measurement. But the head drop before the start of true acoustic emission is an additional indicator.

3.5. Valve

A first step to limit influences of other components was the investigation into the local pressure drops of butterfly valves (Rodriguez and de Jonge 2018), specifically for the valves used in the IHC laboratory.

Focus was the vena contracta, which is a narrowing in a flow path causing a local acceleration of the liquid. This causes an increase in local velocity which in turn causes a local drop in pressure according to Equation 1.6.

If the flow stabilizes after the obstruction and the flow velocity has dropped the pressure will be partially restored, as is shown in Figure 3.29.

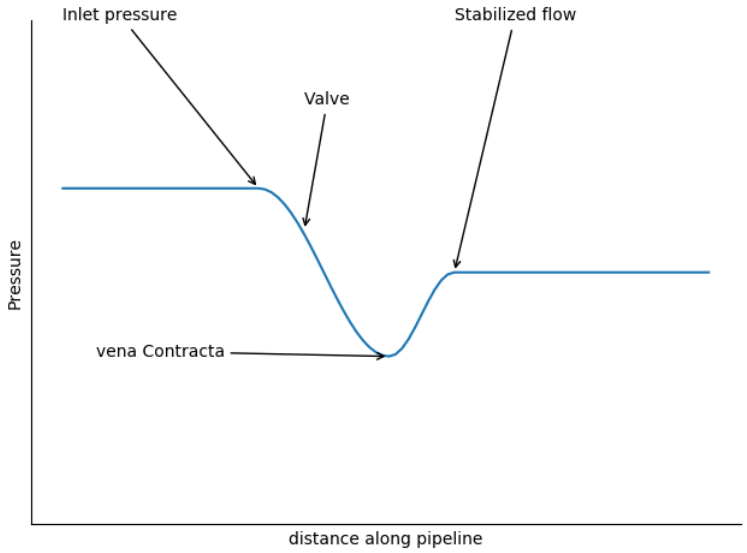

Figure 3.29: vena contracta

If the flow velocity is high enough and the pressure behind the valve low enough cavitation can also occur behind the valve, with the possible risk of efficiency drop in the pump see Section 2.5.1.

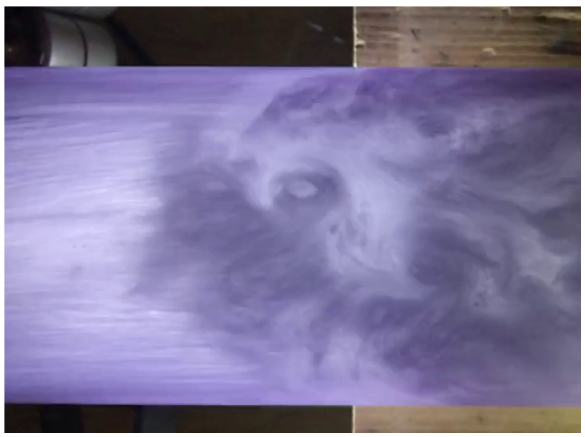

Figure 3.30: cavitating valve

In the experiment the pressure drop after the valve was measured, as was the required length for recuperation. A small increase in angle can have a significant influence on the obstacle factor. As can be seen in Figure 3.31.

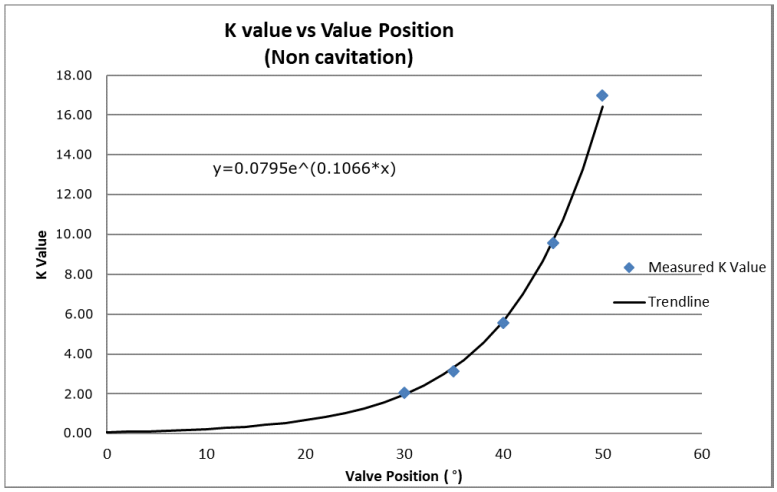

Figure 3.31: Obstacle factor in a non cavitating valve

If the angle is limited the recuperation length is also limited. This knowledge can be used to prevent a local pressure drop entering the pump and prevent too high a local pressure drop, resulting in local cavitation. In Figure 3.32 the influence of a small change in angle of the valve is shown.
An angle of 0 degree is a maximally opened butterfly valve, whereas an angle of 90 degree is a maximally closed valve.

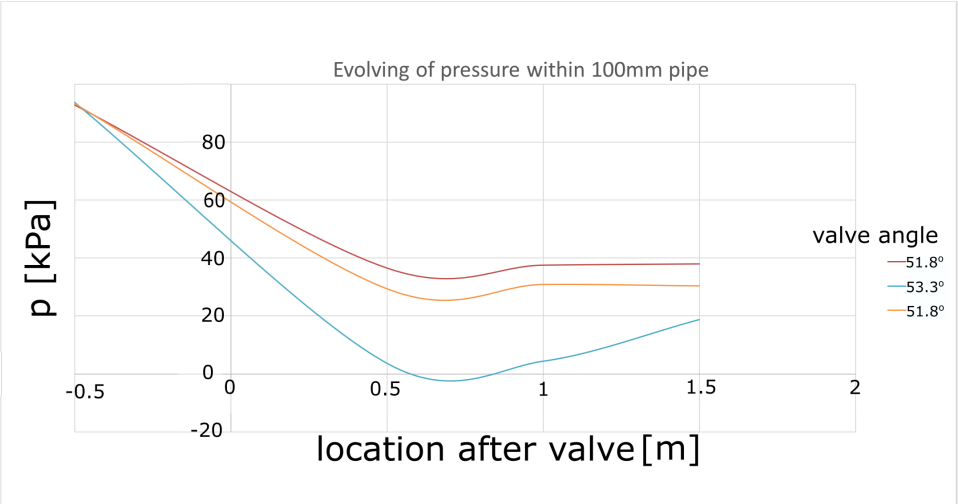

Figure 3.32: Pressure development after butterfly valve.

Figure 3.32 shows the pressure drop over the valve and the development further down the pipe. The flow velocity in the valve itself is more complex, also the lowest local pressure is likely to occur in the valve itself. If that pressure can be increased, the pressure after the valve will also be higher.
The influence of the valve position is also significant as is shown in Figure 3.31 if the angle is high, not only the pressure drop increases exponentially but the low pressure zone after the valve also extends well beyond the valve.

These specifications are especially relevant if one considers the practices in the field. For on board measurements one has to use the configuration at hand, which practically always has a non-ideal flow. The author for example has witnessed a measurement where the inlet pressure the $NPSH_r$ was -99[kPa] which is ,to put it mildly, unrealistic.
It transpired that this low inlet pressure was caused by the configuration in combination with an unfortunate valve position. Where the inlet pressure was measured after a bend where the vena contracta extended up to the location of the pressure sensor. Luckily this could be mitigated by using a valve further away from the bend.

This does however illustrate the influence of configuration and testing conditions.

3.5.1. Choked flow

If cavitation as in Figure 3.30 occurs within the valve, choked flow can occur. The reasoning behind this goes as follows, the medium in the valve becomes compressible, the vapour pressure is reached at the point of minimum pressure, the pressure downstream can't drop any lower. This makes the flow less sensitive to changes in downstream pressure (until the cavitation stops). Choking can be caused by either cavitation or flashing (Fisher 2001). In the case of flashing the downstream pressure will locally drop below the vapour pressure, if cavitation causes the drop the downstream pressure will be above the vapour pressure.

3.5.2. Globe valve

Since the lowest local pressure is very important in a flow system the right choice of valve is important. Therefore the butterfly valve is replaced for a globe valve, also this valve has a 100mm inlet diameter. The characteristics of this valve are more beneficial than the butterfly valve. The globe valve has three advantages over the butterfly valves.

- the hydraulic loss can be more precisely controlled
- the local pressure is not as low as with the butterfly valve
- the pressure after the valve is restored closer to the valve, if compared for the same friction factor.

The disadvantage is that the pressure drop over a fully opened globe valve is higher that of a butterfly valve. Still for $NPSH_r$ measurements a globe valve is preferred.
In Figure 3.33 the two valve types are schematically represented.

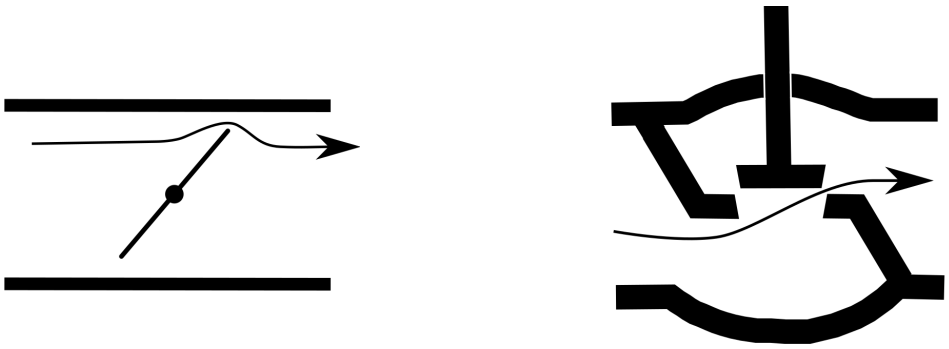

(a) schematic butterfly valve (b) schematic globe valve

Figure 3.33: schematic presentation valves

3.5.3. Measurement preparation

The above mentioned adaptations have a highly beneficial effect on the experiments. However, to ensure a qualitative measurement some steps need to be taken before a $NPSH_r$ measurement. So that the fluid is de-aired.

- fresh water
  - run loop under high pressure continuously, whilst periodically releasing air via the valves
  - once there seems to be no more air in the system; start lowering the pressure and run for several minutes at a high speed (basically a cavitation test)
  - re-pressurize system and remove air via valves, repeat in combination with the points above until no air appears
- After the steps for fresh water or at the start of a repeated test the following is important
  - Run a preliminary $NPSH_r$ measurement and check if the water level in the vertical water column stays level. If not, repeat the steps for fresh water. Note that the water level during

the test can rise, though not as much as when air is sucked in, but the critical part is that the water level will return to the initial value if the system is re-pressurized. This means that the cavities/vapour is re-adsorbed.

In addition to the steps above, there are also some routine preparations:

- remove air from the tubes connecting the pressure sensors to the setup, specifically the ones in low pressure locations.
- minimize the impeller clearance, by adjusting the position of the front casing cover.

4

$NPSH_r$ Measurements

The goal here is to determine the $NPSH_r$ properties of the lab scale pump for a range of flow velocities and a range of shaft speeds. This in order to determine the influence of the those conditions on the $NPSH_r$.
Knowing the $NPSH_r$ properties of the lab scale pump, the relation with the full scale pump will be investigated, in order to be able to make predictions for different pump sizes and different flow conditions.

Some steps are taken before determining the $NPSH_r$ properties of a pump. Those steps are listed below:

- Determine the properties of the pump, measuring the relation between the head and the flow velocity of the pump.
- Generalize the flow velocity vs head relation by expressing them in specific capacity (Q_s) and specific head (h_s) both equations are repeated below

$$Q_s = \frac{Q_V}{\omega D_{imp}^3} = \frac{Q_V}{2\pi N D_{imp}^3}$$

$$h_s = \frac{gH}{\left(\omega D_{imp}\right)^2}$$

- Determine the relation between the efficiency and the flow velocity of the pump by expressing the flow velocity in specific capacity.
- Create a test-matrix, giving the speed and flow velocity for which the $NPSH_r$ measurements are to be performed.
- Perform the $NPSH_r$ measurements by the methodology described in Section 3.4.1.

For those experiments the following parameters need to be monitored.

- inlet pressure
- outlet pressure
- differential pressure sensor (in addition to the inlet and outlet sensor)
- flow velocity
- shaft speed
- torque (on shaft)
- water temperature

- atmospheric pressure

In Figure 4.1 the setup with sensors is shown.

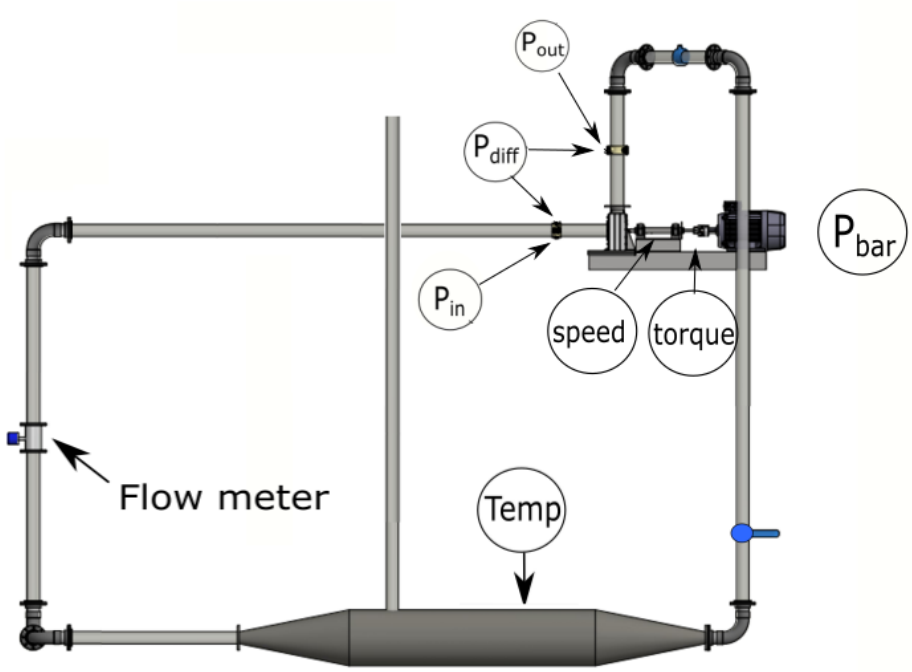

Figure 4.1: test setup, with sensors

The pressure sensors and flow velocity sensor can be used to determine the relation between pump head and flow rate. Determining this is the first step. Once the flow velocity vs head relation is known the Best Efficiency Point (BEP) can be determined by calculating the efficiency with use of the torque.

4.1. Analysis

The analysis will consist of scaling and linearisation. The scaling focuses on predicting the $NPSH_r$ for specific flow conditions (Q_s), so to use scaling one must have data points for each Q_s under consideration.
Linearisation on the other hand is used to determine the $NPSH_r$ properties as a function of Q_s.

Note also that the goal is to scale, and predict, the $NPSH_r$ as defined in Section 1.4. This is the $NPSH_a$ at the moment the head at a given Q_s has dropped with a pre-determined percentage (here 5%). The equation for $NPSH_a$ is repeated below:

$$NPSH_a = \frac{p_{suc} + p_{amb} - p_{vap}}{\rho g} + \frac{\vec{v}_s^2}{2g} \tag{4.1}$$

In the search for a scaling parameter and the linearisation other parameters than $NPSH_r$ will be investigated. The reason for this is that they might be easier to scale or that they have a more direct physical interpretation. All those parameters however have to include the absolute inlet pressure above the vapour pressure ($p_{suc} + p_{amb} - p_{vap}$), the flow velocity component might be included but that is not essential due to the fact the flow velocity will be known by definition for a given Q_s. So to know the full inlet conditions only the ambient pressure, gauge inlet pressure and vapour pressure need to be known in addition to the flow rate.

4.1.1. scaling
The main point of interest in the analysis is the scaling: how can the $NPSH_r$ properties from one pump be predicted via the $NPSH_r$ properties of a geometrically identical pump?
Since the flow conditions are very well captured by the Q_s this scaling will focus on investigating parameters defining the inlet conditions (such as the σ (cavitation number) for the chosen range of Q_s. If some of those parameters only depend on Q_s but not on the size of the pump, the flow velocity or the speed, then such a parameter is likely to be useful for scaling. Note that the combination of speed, size and flow velocity need to give the Q_s under consideration according to Equation 1.20.

4.1.2. linearisation
Linearisation investigates, by means of linear regression, if some of the parameters have a linear relation with Q_s. If this is the case one can by means of interpolation (or by deriving a linear function) predict inlet properties within a broader range of flow velocities, note that this must not exceed the investigated range of flow velocities.

There might be other relations to predict the $NPSH_r$ properties as a function of Q_s than linearisation, such as a quadratic relation or other functions. Linearisation however is a strong and easy first step, where the quality of the linearisation can be determined by the method described in Appendix A.1.

4.2. Test plan
The $NPSH_r$ measurements are performed for two impeller types, the *HRMD3B* and the *HRMD4B curve*. The shaft speeds in which the measurements are performed ranges from 20 to 35 Hz for both impellers. This is based on scaled design parameters, where the impeller tip velocity remains identical. The temperatures are withing a range of 10 to 20 °C, resulting in a vapour pressure variation ranging from 1.2 to 2.4 kPa (by using Equation 2.1).
The flow velocities are chosen in relation to the BEP, taking the limitations of the setup into account. The flow velocity has an upper limit determined by the flow resistance of the setup, the flow velocity must be achievable under $NPSH_r$ conditions. The lower limit is determined by the capacity of achieving the required inlet pressure for the $NPSH_r$ conditions. In order to determine the flow velocities needed one can express the chosen range relative to BEP, calculate the corresponding specific capacity and subsequently calculate the flow velocity for each shaft speed.

4.2.1. HRMD3 pump properties
In Figure 4.2a the flow velocity-head curve is shown, the dimensionless version (Q_s vs h_s) is plotted in Figure 4.2b.

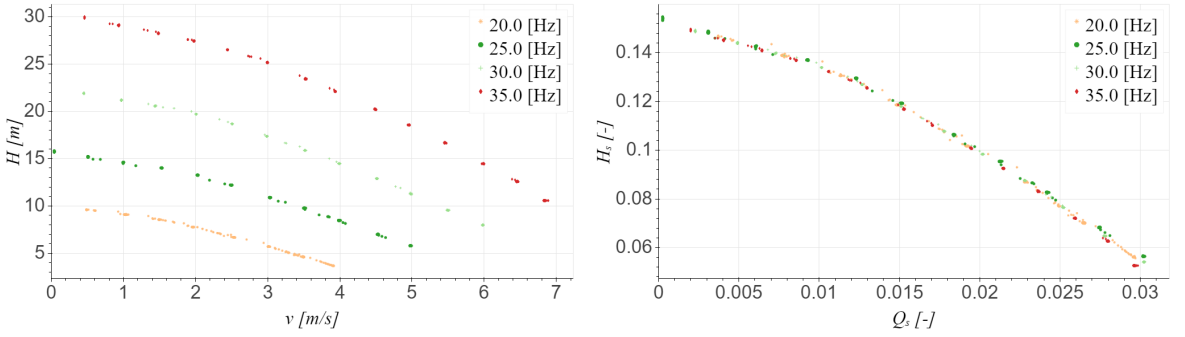

(a) flow velocity vs head for different shaft speeds

(b) dimensionless flow velocity vs specific head for different shaft speeds

Figure 4.2: head vs flow velocity and specific head vs specific capacity of a HRMD3B impeller. Measurements performed in this research.

In Figure 4.3a multiple efficiency vs flow velocity measurements are shown. In Figure 4.3b the efficiency

is plotted against the specific capacity. One can easily determine that the HRMD3B impeller has its BEP at a Q_s of 0.017 [-].

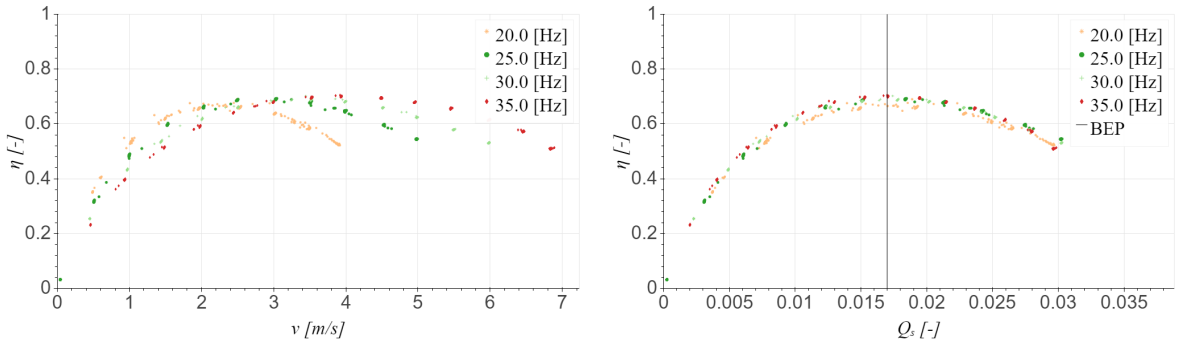

(a) flow velocity vs efficiency for different shaft speeds

(b) dimensionless flow velocity vs efficiency for different shaft speeds

Figure 4.3: efficiency vs flow velocity and specific capacity of a HRMD3B impeller. Measurements performed in this research.

In the table below the test matrix for the HRMD3B is shown:

$Q_V/Q_{V\,BEP}$	N [Hz] / Q_s [-]	20	25	30	35
0.6	0.01	1.3	1.7	2.0	2.4
0.8	0.014	1.8	2.2	2.7	3.1
1.0	0.017	2.2	2.8	3.4	3.9
1.2	0.020	2.7	3.4	4.0	4.7
1.4	0.024	3.1	3.9	4.7	5.5
1.6	0.027	3.6	4.5	5.4	

Table 4.1: Test matrix HRMD3B, flow velocity in $\frac{m}{s}$

The maximum flow ($Q_V/Q_{V\,BEP}$ of 1.4 and 1.6) at 35 Hz was too high, and is therefore excluded from the matrix. In addition to the matrix extra measurements were performed.

4.2.2. HRMD4B-curve test matrix

The same procedure as used for the HRMD3B matrix is used for the HRMD4B-curve matrix. First the flow velocity vs head characteristics are determined, see Figure 4.4. For BEP see Figure 4.5a and b, showing a BEP at a Q_s of 0.020 [-].

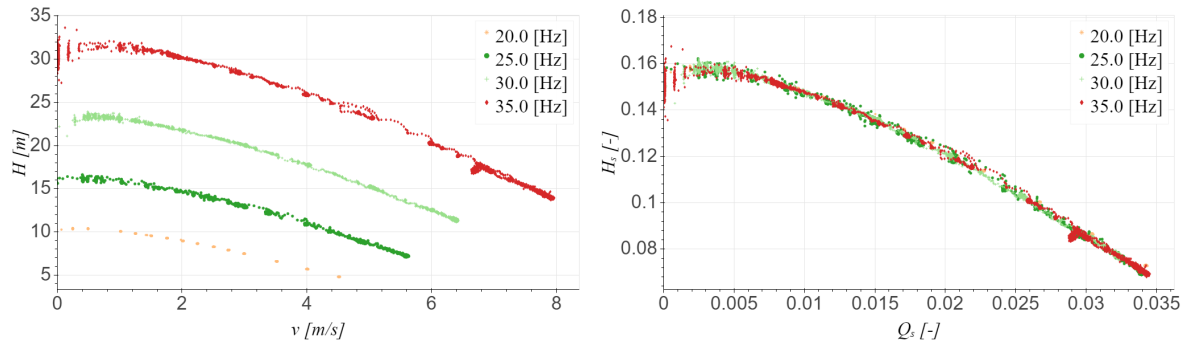

(a) flow velocity vs head for different shaft speeds

(b) dimensionless flow vs specific head for different shaft speeds

Figure 4.4: head vs flow velocity and specific head vs specific capacity of a HRMD4B-curve impeller. Measurements performed in this research.

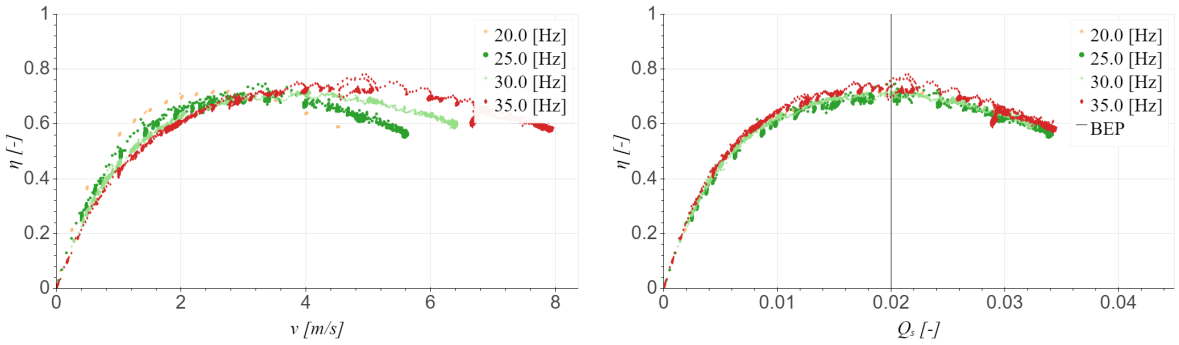

(a) flow velocity vs efficiency for different shaft speeds

(b) dimensionless flow vs efficiency for different shaft speeds

Figure 4.5: efficiency vs flow velocity and specific capacity of a HRMD4B-curve impeller. Measurements performed in this research.

In the table below the test matrix for the HRMD4B-curve is shown:

$Q_V/Q_{V\,BEP}$	speed [Hz] / Q_s [-]	20	25	30	35
0.6	0.02	1.58	1.98	2.37	2.77
0.8	0.016	2.11	2.64	3.17	3.69
1.0	0.02	2.64	3.30	3.96	4.62
1.2	0.024	3.17	3.96	4.75	5.54
1.4	0.028	3.69	4.62	5.54	
1.6	0.032	4.22	5.28		

Table 4.2: Test matrix HRMD3B, flow velocity in $\frac{m}{s}$

4.3. Influence of centripetal force of pre-rotation

The pre-rotation as described in Section 1.1.2 is not only related to a drop in efficiency (the medium rotates to optimize flow at the inlet because the flow is not optimal). It also influences the pressure measured at the inlet of the pump. In Figure 4.7 the inlet pressure of a flow velocity vs head measurement for a given speed of 35 Hz is shown. It can be seen that the inlet pressure is lowered linearly with ${Q_s}^2$ which means that the pre-rotation does not influence the measurement of the inlet pressure. This is due to the fact that the pressure at the vertical column, as seen in Figure 3.6, is kept constant. The resulting pressure at the inlet of the pump is entirely due to the friction pressure drop of the components in between, according to equation 2.14. Which gives a quadratic relation with the flow velocity (or a linear relation with the flow velocity squared). Since this relation is shown it can be concluded that pre-rotation does not influence the measurement. It is worth noting that this behaviour is observed for all speeds, and all impellers used.

If one looks closely to the inlet pressure at zero flow a local peak in inlet pressure can be seen, this is assumed to be due to pre-rotation. This is however irrelevant for the $NPSH_r$ measurements since those require at least a small flow velocity.

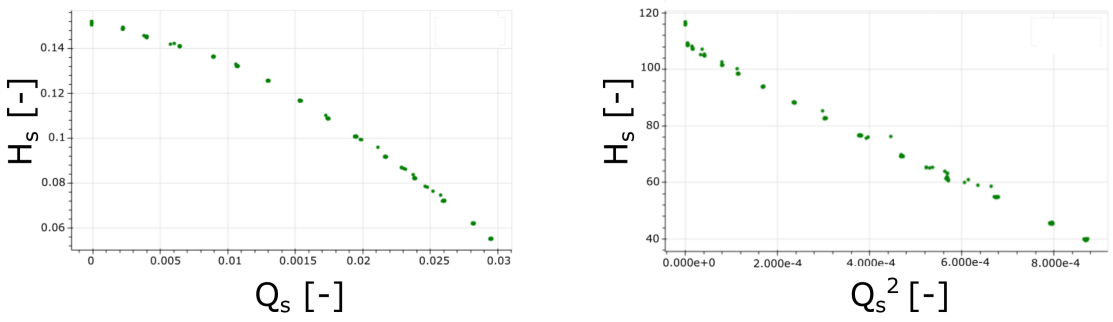

(a) specific capacity vs specific head

(b) absolute inlet pressure vs the specific capacity squared

Figure 4.7: HRMD3b at 35Hz

4.4. Results HRMD3B

First the results of the HRMD3B pump are discussed, here more methods of scaling are discussed. The most promising methods will also be applied on the HRMD4B-curve pump.

4.4.1. $NPSH_r$ vs inlet pressure

The subject of this research is to relate the $NPSH_r$ properties of identical pumps under different conditions. The definition of $NPSH_r$, and the classic way of scaling this, are given in the equations below:

$$NPSH_a = \frac{p_{suc} + p_{amb} - p_{vap}}{\rho g} + \frac{\vec{v}^2}{2g} \tag{4.2}$$

$$NPSH_r = NPSH_{rM}\left(\frac{\omega D}{\omega_M D_M}\right)^2 \tag{4.3}$$

Making a scaling parameter from this and keeping it dimensionless gives the Specific $NPSH_r$:

$$NPSH_{rs} = \frac{gNPSH_r}{(\omega\ D)^2} \tag{4.4}$$

It is interesting to set this parameter against the specific capacity:

$$Q_s = \frac{Q_V}{\omega D_{imp}^3} \tag{4.5}$$

Using the HRMD3B data and setting $NPSH_{rs}$ against Q_s results in a good fit, as is shown in Figure 4.8.

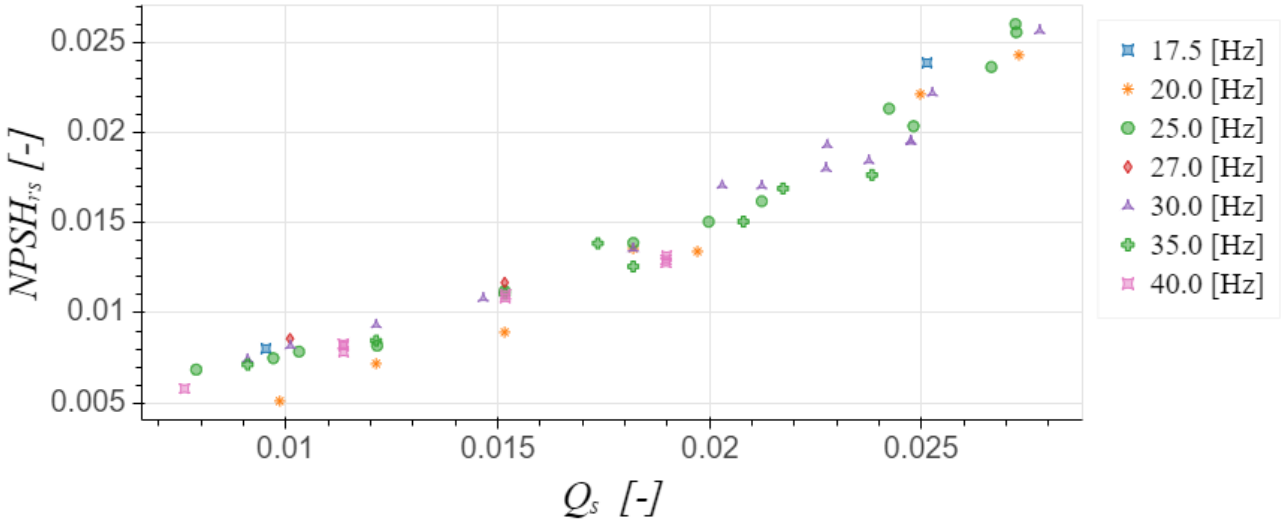

Figure 4.8: Specific NPSHr for D=0.45 m and 0.1 m inlet diameter for different shaft speeds

The fit in Figure 4.8 looks promising, however the flow velocity component makes the fit look better than it might be. To show this effect the flow velocity component is investigated, see the following equation:

$$NPSH_{rs(velocity)} = \frac{\vec{v}^2}{2\,(\omega\ D)^2} \tag{4.6}$$

If one plots only the flow velocity component of the $NPSH_r$ according to Equation 4.6, a full scale 450 mm pump data fits the 100 mm measurement data by definition as is shown below:

$$Q_s{}^2 = \left(\frac{Q_V}{\omega D_{imp}^3}\right)^2 \propto \left(\frac{\vec{v}}{\omega D_{imp}}\right)^2 \propto \frac{\vec{v}^2}{2\,(\omega\ D)^2} = NPSH_{rs(velocity)}^2 \tag{4.7}$$

Since the $NPSH_r$ is a simple superposition of the pressure component and the flow velocity component, the perfect fit for the flow velocity means that this provides no additional information for the inlet pressure. It only obscures the variations in specific inlet pressure. Because the relative error will decrease.

4.4.2. Comparing different parameters

As described above, the flow velocity component influences the value of the $NPSH_r$ because it is exactly defined by the flow velocity. Therefore it can be interesting to investigate only the inlet pressure. Below the results for the HRMD3B impeller are shown, with the absolute pressure at $NPSH_r$ on the y-axis:

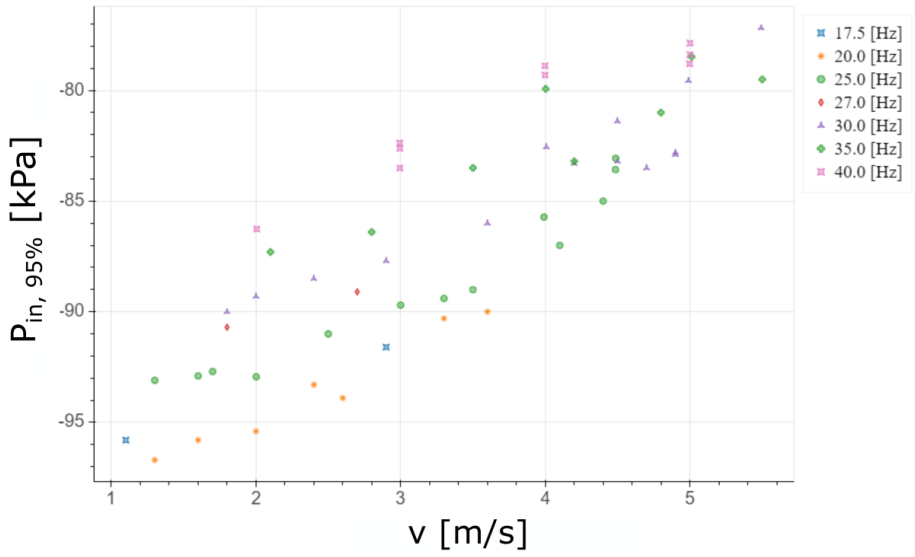

Figure 4.9: Absolute inlet pressure vs flow velocity for HRMD3B at different shaft speeds

For an improved comparison a first start is to convert from flow velocity to specific capacity, see Figure 4.10.

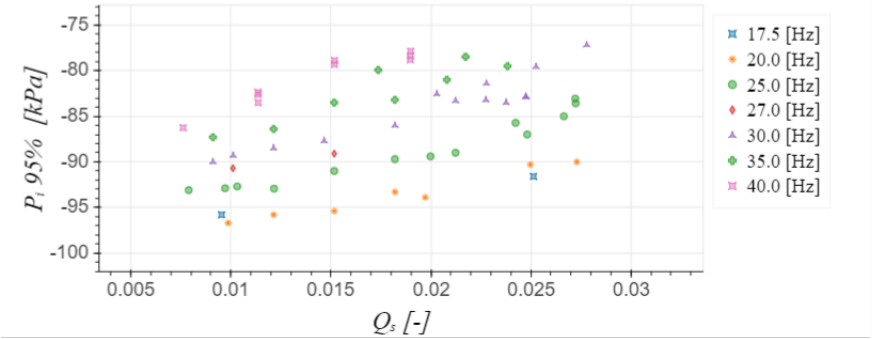

Figure 4.10: Absolute inlet pressure vs specific capacity for HRMD3B at different shaft speeds

The influence of the speed becomes more clear here, the higher the speed the higher the inlet pressure. So the next step is to look at the specific pressure as given in Equation 2.23 which is repeated below:

$$P_s = \frac{p_{in,abs} - p_{vap}}{\rho \left(\omega D_{imp}\right)^2}$$

The results of which are shown in Figure 4.11

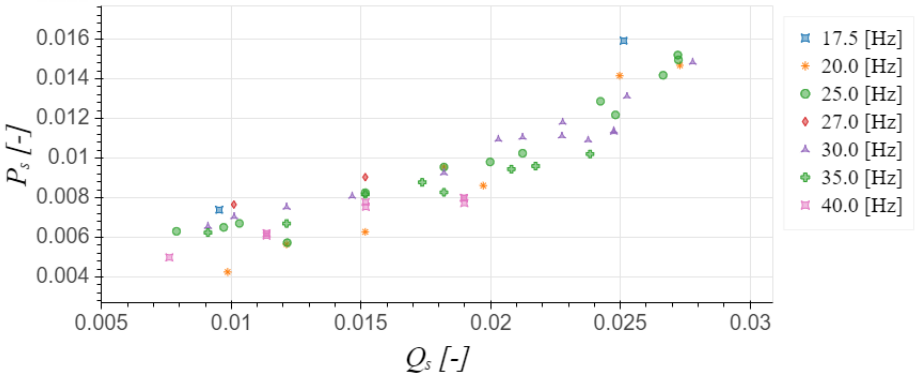

Figure 4.11: Specific inlet pressure vs specific capacity for HRMD3B at different shaft speeds

One interesting parameter is the cavitation number from equation 1.27, repeated below:

$$\sigma = \frac{p_{in,abs} - p_{vap}}{\frac{1}{2}\rho_{liq}\vec{v}^2}$$

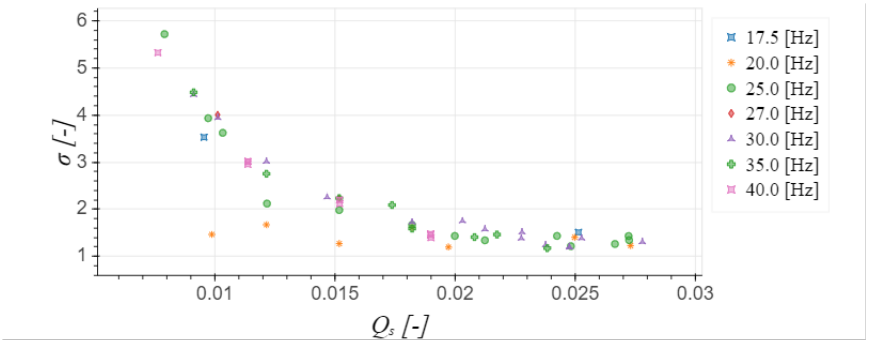

Figure 4.12: Cavitation number vs specific capacity for HRMD3B at different shaft speeds

The shape reminds one of an hyperbolic curve, making the reciprocal interesting to investigate:

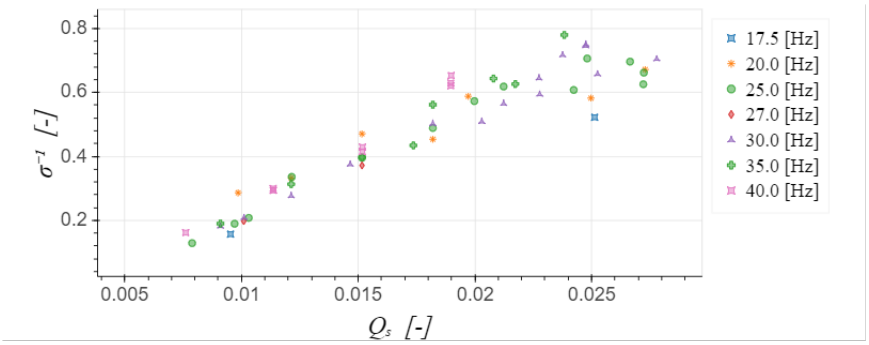

Figure 4.13: reciprocal of cavitation number vs specific capacity for HRMD3B at different shaft speeds

This last presentation has an almost linear shape, this might however be due to the dominating effect of the flow velocity component in the equation. Therefore one additional graph is shown below where the pressure components are removed. There the relevance of the pressure is clearly seen:

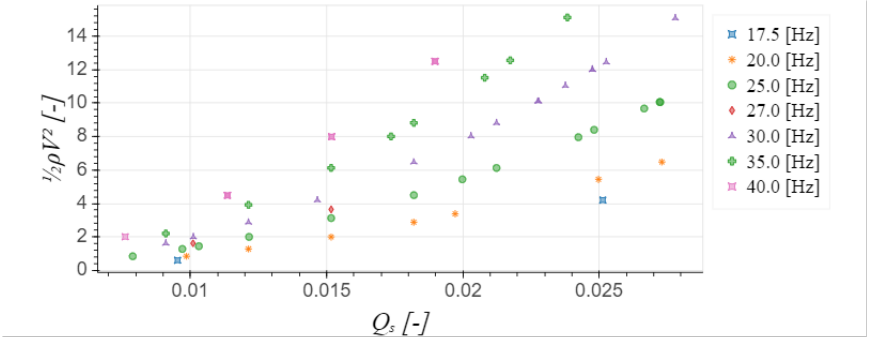

Figure 4.14: flow velocity squared vs specific capacity for HRMD3B at different shaft speeds

In the analysis below (see Figures 4.11 and 4.13) two parameters have a near linear relation with the specific capacity:

$$\sigma^{-1} = \frac{\frac{1}{2}\rho_{liq}\vec{v}^2}{p_{in,abs} - p_{vap}}$$

$$P_s = \frac{p_{in,abs} - p_{vap}}{\rho\left(\omega D_{imp}\right)^2}$$

Looking at the linear relation between σ^{-1} and Q_s and assuming a constant density, the relation can be rewritten to express the inlet pressure in flow velocity, speed and diameter.

$$\sigma^{-1} = \frac{\frac{1}{2}\rho_{liq}\vec{v}^2}{p_{in,abs} - p_{vap}} \propto Q_s = \frac{Q_V}{\omega D_{imp}^3} \propto \frac{\vec{v}}{\omega D_{imp}} \rightarrow \tag{4.8}$$

$$p_{in,abs} - p_{vap} \propto \vec{v}\omega D_{imp} \tag{4.9}$$

This relation can be rewritten into a proportional relation between specific pressure and specific capacity

$$p_{in,abs} - p_{vap} \propto \vec{v}\omega D_{imp} \rightarrow \tag{4.10}$$

$$\frac{p_{in,abs} - p_{vap}}{\rho\left(\omega D_{imp}\right)^2} \propto \frac{\vec{v}}{\omega D_{imp}} \propto \frac{Q_V}{\omega D_{imp}^3} = Q_s \rightarrow \tag{4.11}$$

$$P_s = \frac{p_{in,abs} - p_{vap}}{\rho\left(\omega D_{imp}\right)^2} \propto Q_s \tag{4.12}$$

Both Equation 4.10 and 4.8 can be rewritten to the same linear relationship. Note that this only holds if the initial assumption of a linear relation between the specific capacity and the reciprocal of the cavitation number is valid. In Figure 4.15 the relation between the inlet pressure and the product of the flow velocity, speed and diameter is shown to compare with Equation 4.8.

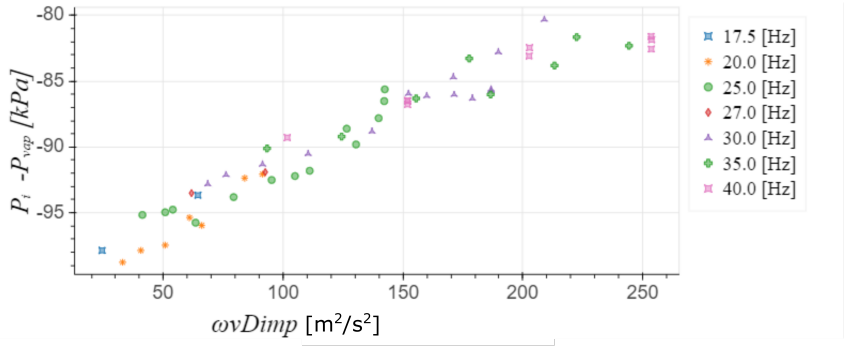

Figure 4.15: Inlet pressure minus vapour pressure vs flow velocity*speed*diameter for HRMD3B at different shaft speeds

The shape in Figure 4.15 seems slightly more linear than the other relations. The emphasis however will lie on the P_S from Equation 2.23 (plotted in Figure 4.11) for it relates to the classic scaling method from Equation 2.18, in which the impeller tip flow velocity (ωD_{imp})is governing.

4.4.3. Comparison with true size data

For the HRMD3B pump full scale data is available (courtesy royal IHC). In Figure 4.16 the Q_s vs the h_s is plotted. It can be seen that the shape is almost identical but that the full scale pump slightly outperforms the lab scale. One of the explanations for this is the higher efficiency of the full scale pump, see also Figure 4.17.

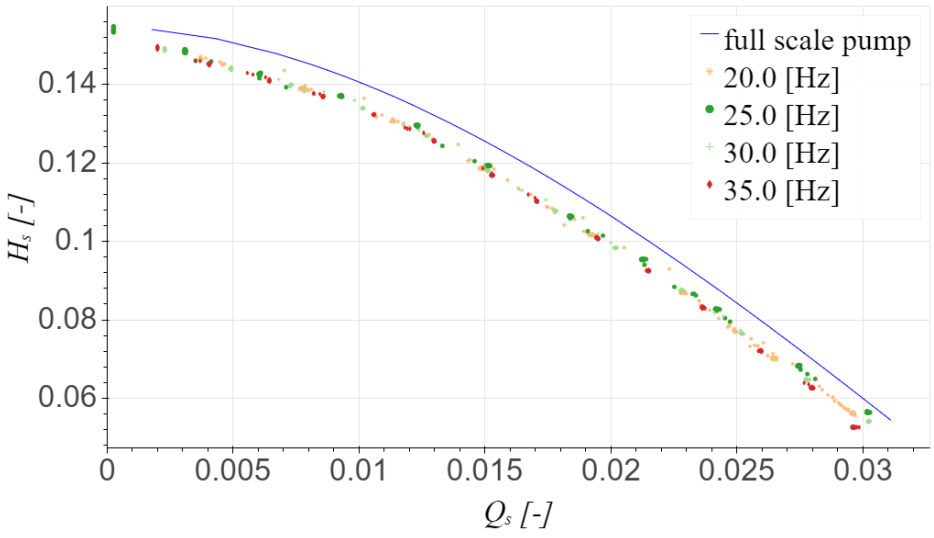

Figure 4.16: Q_s vs h_s for the 0.1 [m] HRMD3B pump at different shaft speeds and the full scale pump (0.45 [m])

In Figure 4.17 the efficiency of the full scale pump and the 100 [mm] pump is plotted. Note that the BEP is at the same Q_s. The value of the efficiency of the pump itself is significantly higher. One explanation for this is that the relative roughness of the impeller is significantly higher for the 100[mm] than for the full scale pump. Also the relative clearance of the 100[mm] pump is higher.

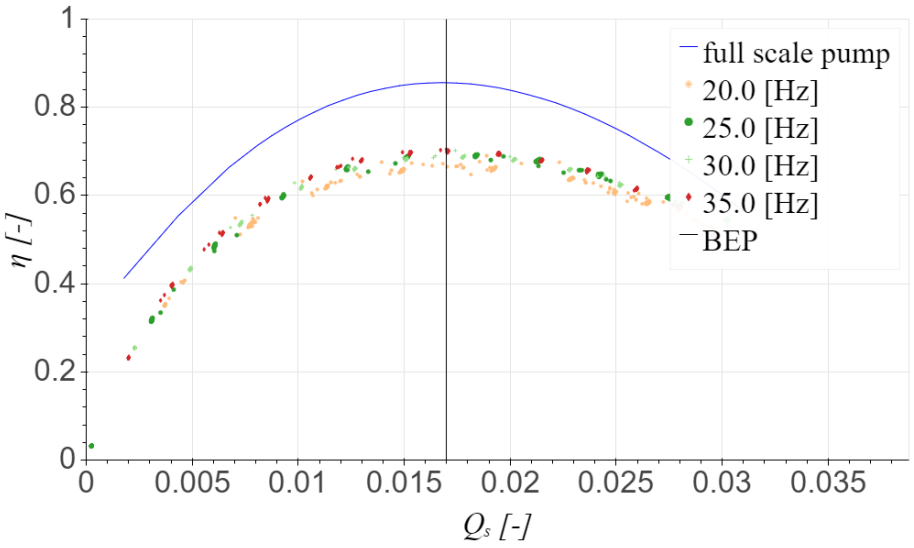

Figure 4.17: η vs h_s for the 0.1 [m] HRMD3B pump at different shaft speeds and the full scale pump (0.45 [m])

Based on the scaling methods discussed before the full scale data will be compared with the lab scale for the following relations

- σ^{-1} vs Q_s
- P_s vs Q_s
- $NPSH_{r,s}$ vs Q_s

In Figure 4.18 the HRMD3B data is shown for the 100 mm inlet diameter pump and a HRMD3B on board pump with an inlet diameter of 450[mm]. The on board pump data consists of a fit based on multiple measurements.

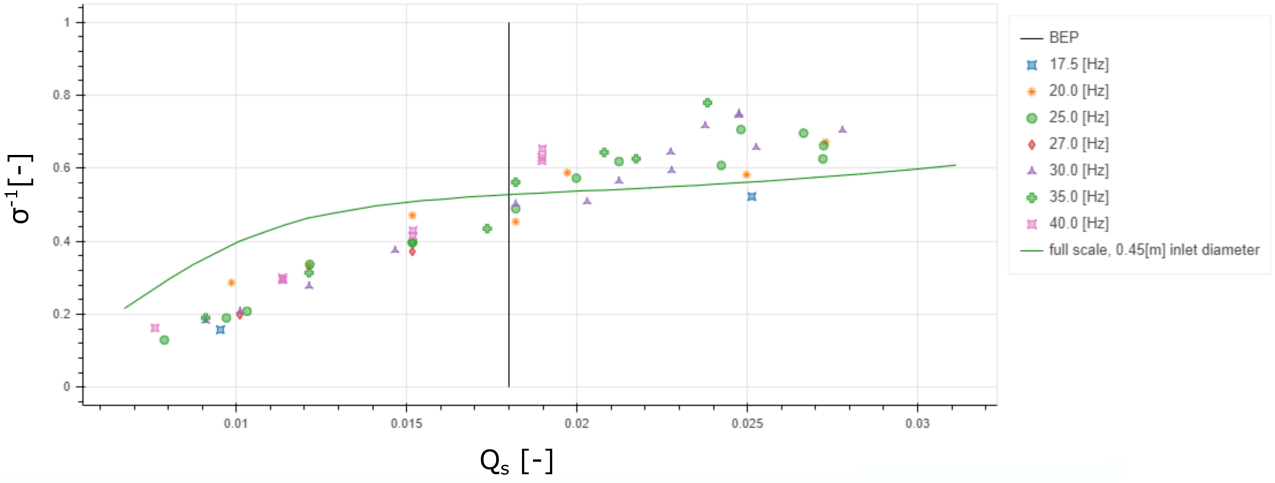

Figure 4.18: σ^{-1} for 0.1 m inlet diameter at different shaft speeds and 0.45 m inlet diameter

The order of magnitude is in the same range, the shape however differs greatly. This might be explained by the fact that the data is based on a higher order polynomial through a larger set of $NPSH_r$ data. This can result in a subtle change in shape, specifically after rewriting the data into σ^{-1}. Recalling Equations 4.8 to 4.12 the specific pressure can be used as an alternative for σ^{-1}.
The specific pressure is better suited since the pump mostly operates at a fixed speed. Also the interpretation is more intuitive since the inlet pressure is in the numerator, meaning a higher value entails a (relatively) higher inlet pressure.

The resulting graph is shown below:

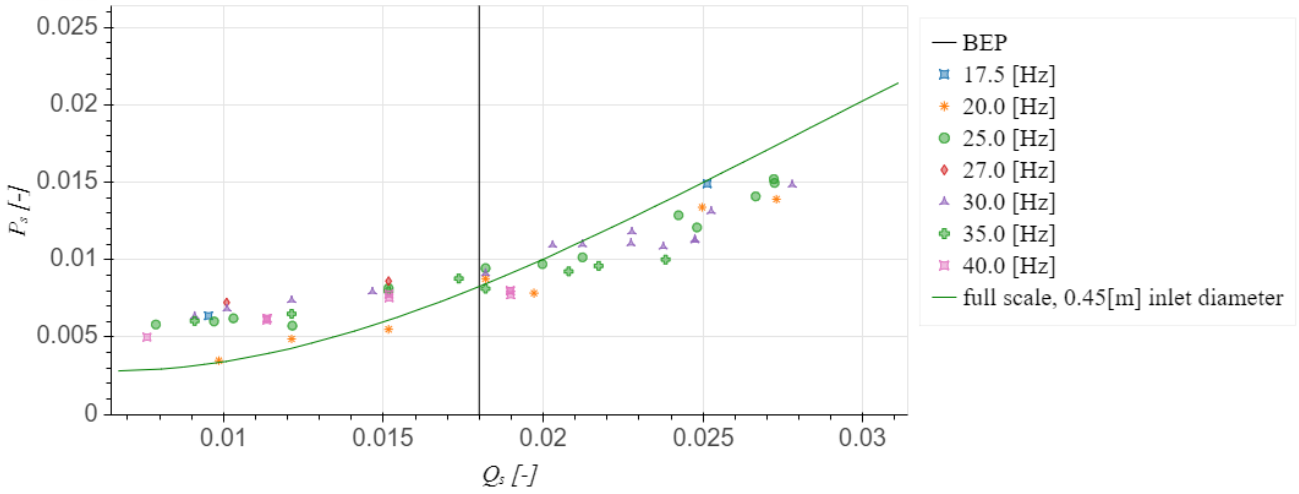

Figure 4.19: Specific inlet pressure for 0.1 m inlet diameter at different shaft speeds and 0.45 m inlet diameter

Looking at Figure 4.19 one can conclude that the 100 mm data fits the full data, especially around BEP.

4.4.4. True $NPSH_r$ scaling

The previous analyses focussed on the inlet pressure and the flow velocity as two separate components. In the usual analysis however they are combined in the $NPSH_r$, the value of $NPSH$ where the head dropped a specific percentage (often 3 or 5%). The definition of the $NPSH$ is repeated below.

$$NPSH = \frac{p_{suc} + p_{amb} - p_{vap}}{\rho g} + \frac{\vec{v}_s^2}{2g}$$

The classic scaling method for $NPSH_r$ as in Equation 4.4 is repeated below:

$$NPSH_{rs} = \frac{gNPSH_r}{\left(\omega\, D_{imp}\right)^2} \tag{4.13}$$

If one applies this to the conducted measurements, the following results:

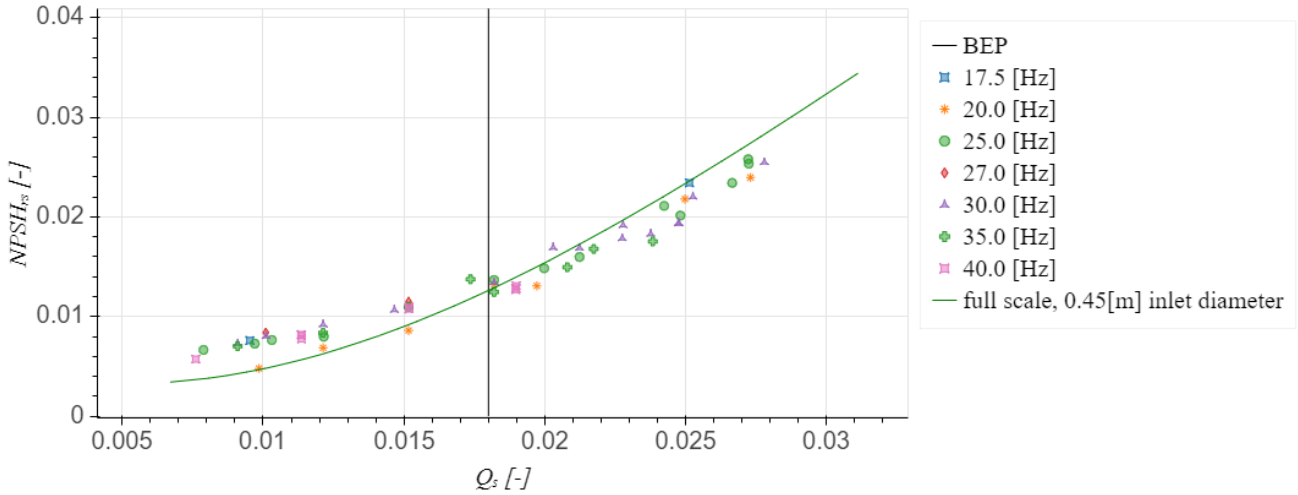

Figure 4.20: Specific NPSHr for 0.1 m inlet diameter at different shaft speeds and 0.45 m inlet diameter

Now this seems to be reasonable good fit, better than any of the others. However, the flow velocity component on the $NPSH_r$ obscures the influence of the inlet pressure. In other words, the absolute deviations are the same, but the relative deviations are smaller.

4.4.5. Linear regression

As can be seen in Section 4.4.2, there are strong indications that there is a linear relation between the specific capacity (Q_s) and the specific pressure (P_s). In order to investigate this relation an analysis of the data is made via linear regression as described in Appendix A.1.

4.4.6. Inlet pressure vs velocity and speed

Although the previous section suggested looking into the specific capacity, specific inlet pressure and the reciprocal of the cavitation number we first look at the inlet pressure, water velocity and pump speed. This is done because those are the initially measured parameters.

Below the inlet pressure is plotted against the pump rotational speed and the flow velocity. It is clear that the inlet pressure is related to both the pump rotational speed and the velocity, they do need to be combined however to make a good prediction.

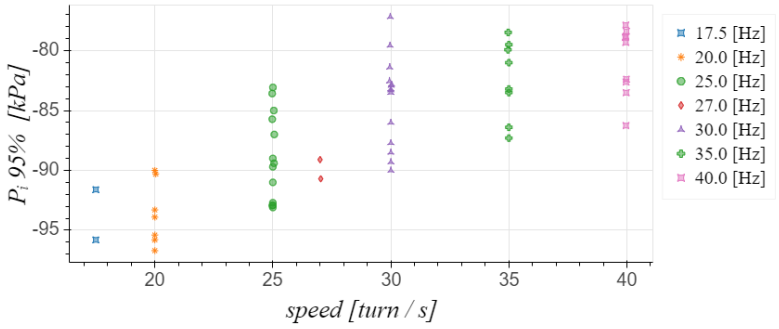

(a) inlet pressure vs pump speed at different shaft speeds

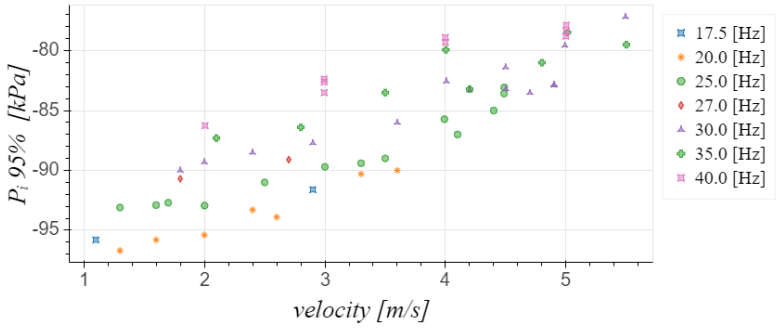

(b) inlet pressure vs pump velocity at different shaft speeds

Figure 4.21: Inlet pressure vs speed and velocity

Looking at the variance score (Equation A.4) confirms that the linear fit does not really work, seeing the value of 0.36.

4.4.7. Specific capacity and specific inlet pressure

A reasonable guess for scaling the velocity is the specific capacity given in equation 1.24. This equation is repeated below. As discussed, presenting the flow in this way shows identical flow profiles for different velocities.

$$Q_{V1} = Q_{V2} \frac{\omega_1}{\omega_2} \left(\frac{D_{imp_1}}{D_{imp_2}} \right)^3$$

Combining this with the specific pressure as in Equation 2.23, which is repeated below once more, might well provide less variance.

$$P_s = \frac{p_{in,abs} - p_{vap}}{\rho \left(\omega D_{imp} \right)^2}$$

Note that this method uses the scaling suggested in equation 2.18.

Linear fit

In Figure 4.22 it can be seen that the specific inlet pressure does behave rather linearly, this is confirmed by the correlation factor of 0.92 and a variance score of only around 0.75. See also Equations A.4 and A.2

Still this method of scaling seems reasonable since the deviations around fixed values of the specific capacity are limited. The red line in Figure 4.22 shows the 95% confidence interval according to Equation A.6

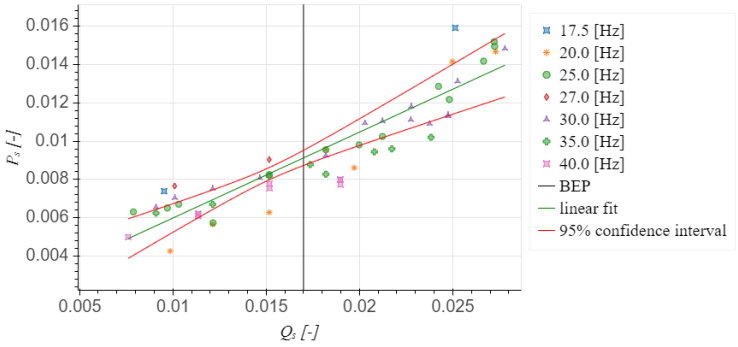

Figure 4.22: linear of specific inlet pressure and specific capacity at $NPSH_r$ for different shaft speeds

4.4.8. Reciprocal of the cavitation number vs specific capacity

As mentioned in section 4.4 the relation of Q_s with the reciprocal of the σ appears highly linear, below the equation is given.

$$\sigma^{-1} = \frac{\frac{1}{2}\rho_{liq}\vec{v}^2}{p - p_{vap}}$$

The linearised result is shown in Figure 4.23.

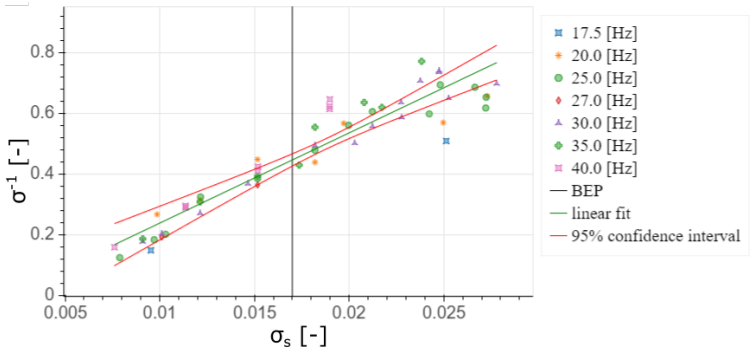

Figure 4.23: fit and confidence interval of σ^{-1}

As can be seen the linearised fit works well, this is also confirmed by the variance score of 0.93 and the correlation factor of 0.95.

4.4.9. Pin vs $\omega\vec{v}D_{imp}$

The relation between $(p_{in} - p_{vap})$ and $(\omega\vec{v}D_{imp})$ is highly linear with a correlation factor of 0.95 and a variance score of 0.89. It does however not outperform the specific pressure vs the specific capacity.

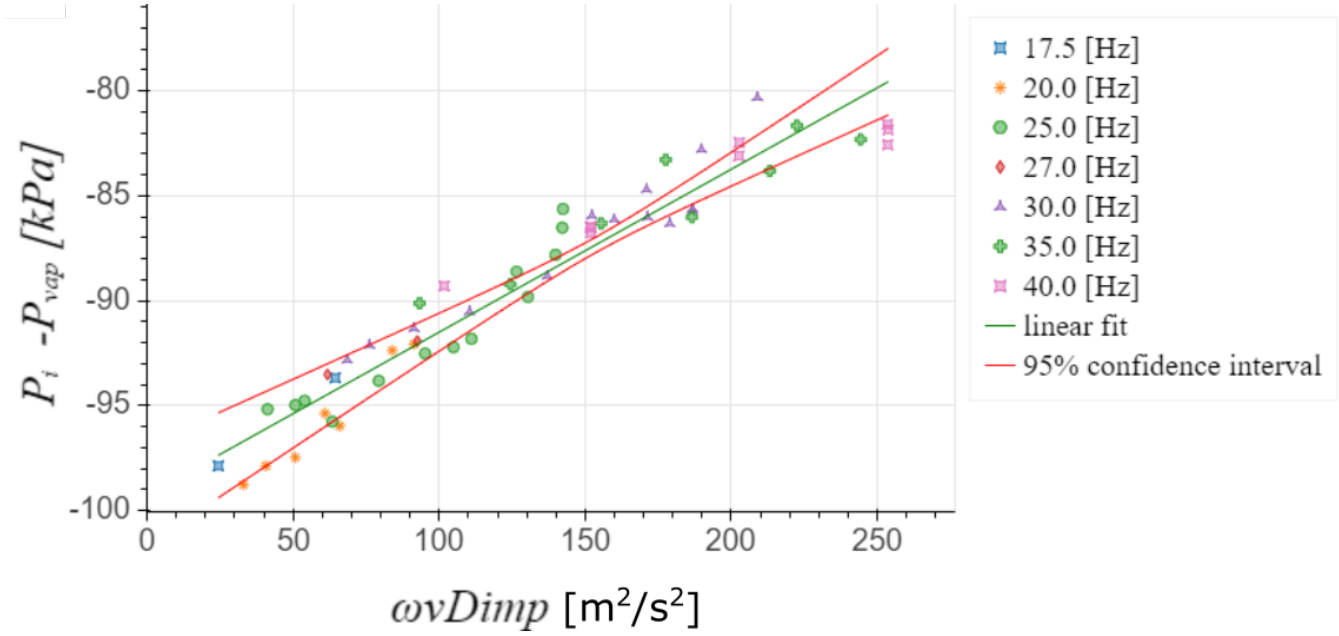

Figure 4.24: inlet pressure vs $\omega\vec{v}D_{imp}$

4.5. Results HRMD4B-curve

Repeating the analysis above used for the HRMD3B results in the following results.

4.5.1. Specific pressure vs specific capacity

In Figure 4.25 a highly linear result is seen for the specific pressure vs the specific capacity. With a variance score of 0.90 and a correlation factor of 0.94 this score very high (see also Equation A.4 and A.2).

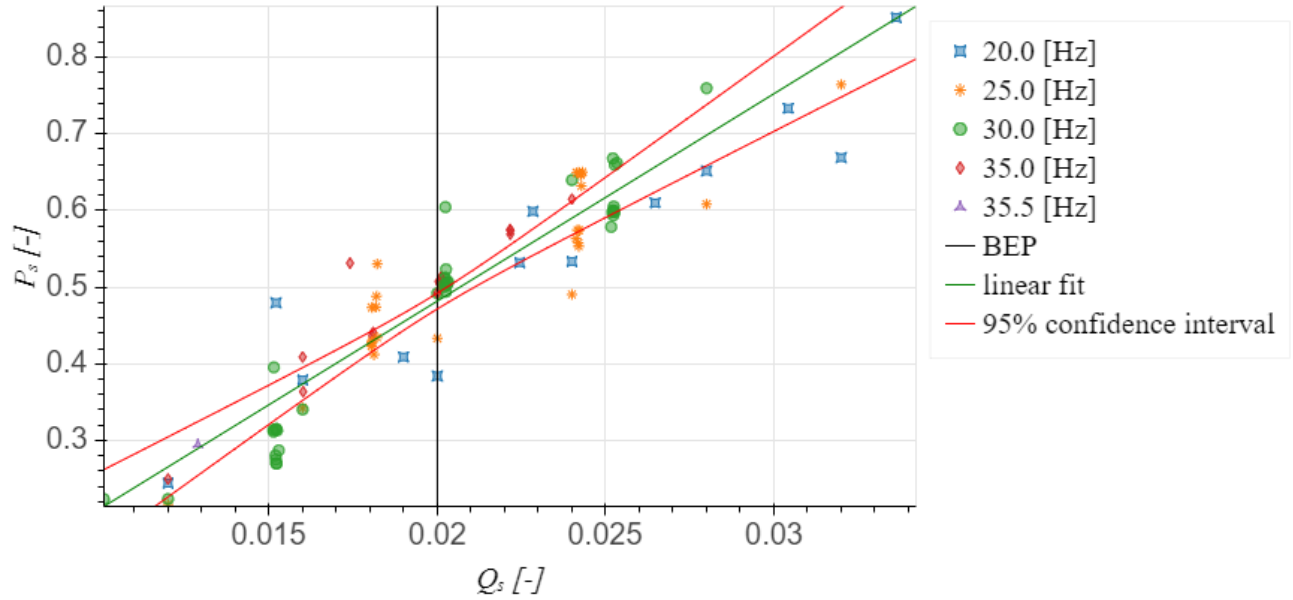

Figure 4.25: Specific pressure vs specifc capacity for HRMD4B-curve

Unfortunately there is no reliable larger scale data available to compare those results with.

4.5.2. Pin vs specific capacity

The relation between $(p_{in} - p_{vap})$ and $(\omega \vec{v} D_{imp})$ can be derived from the specific capacity vs the specific pressure. However, since its behaviour is very linear it will be added here.
With a correlation factor of 0.96 and a variance score of 0.91 it scores very high. The comparison with other sizes is more complicated since the x-axis is longer expressed in specific capacity.

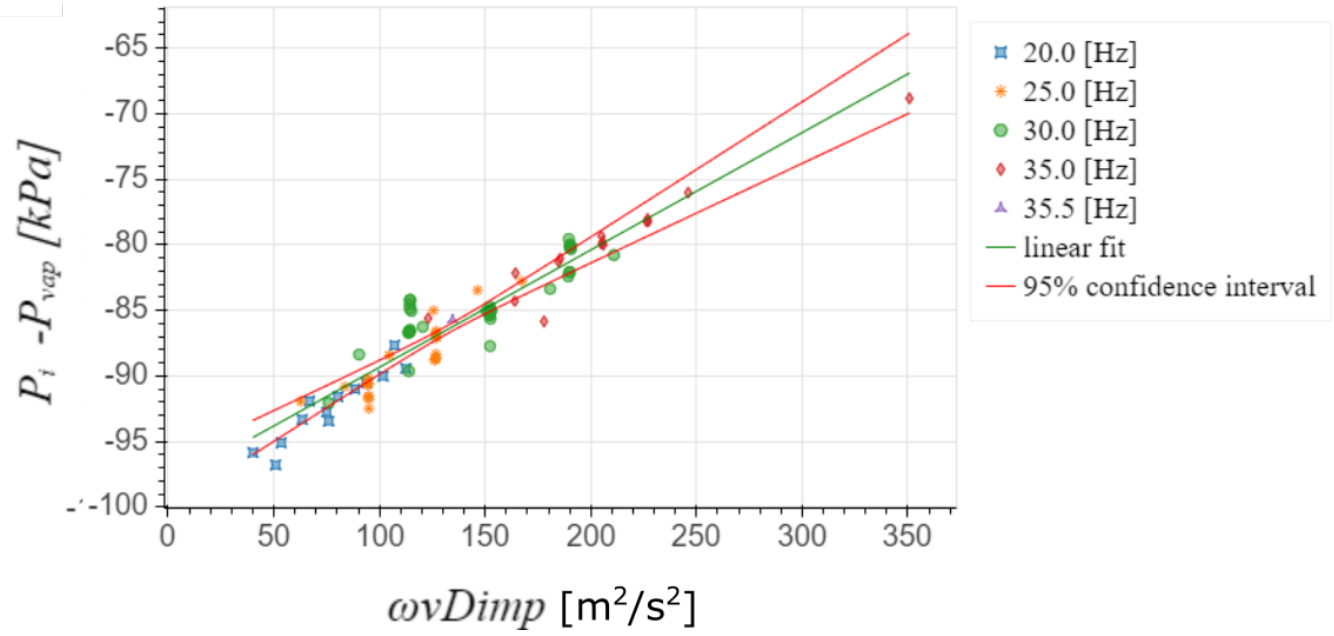

Figure 4.26: inlet pressure vs $\omega \vec{v} D_{imp}$

4.6. Conclusions of Measurements

The main challenge in creating the test-setup was to control the water conditions:

- limit temperature increase
- remove entrained air
- prevent air being sucked in

Once those conditions were met it was possible to generate repeatable experiments and conduct $NPSH_r$ values. Unfortunately the maximum speed of the setup could not be utilized due to the limitations in strength of the impeller, however a range from 20 to 35 [Hz] provides a reasonably broad range, also in relation to the available full scale data.

4.6.1. Scaling

Within the range of specific capacities used the quadratic scaling works well. The limited larger scale data available deviates slightly but is certainly in the same order of magnitude. The full scale measurements however lack the controlled conditions of a lab measurement. For an exact comparison the best method is to look at the P_s, this does not give a direct relation for the $NPSH_r$ but for the given parameters the corresponding flow velocity is known by definition, meaning that the $NPSH_r$ can easily be determined.

If one knows the P_s, the $NPSH_r$ can easily be determined by combining Equation 1.12 and 2.23

$$\left.\begin{aligned} NPSH_r &= \frac{p_{in,abs} - p_{vap}}{\rho g} + \frac{\vec{v}_s^2}{2g} \\ p_{in,abs} - p_{vap} &= P_s \cdot \rho \left(\omega D_{imp}\right)^2 \end{aligned}\right\} \qquad NPSH_r = \frac{P_s \cdot \rho \left(\omega D_{imp}\right)^2 - p_{vap}}{\rho g} + \frac{\vec{v}_s^2}{2g} \tag{4.14}$$

Note that the suggested method of scaling with Q_s is not scaling $NPSH_r$ directly. It focusses more on the prediction of the inlet pressure. Since this is the parameter being varied with scaling this seems more meaningful. Once the inlet pressure is known the $NPSH_r$ can be calculated by use of Equation 4.14.

4.6.2. Linearisation

Setting the specific pressure against the specific capacity shows a reasonably linear relation. In the investigated flow range of 0.6 up to 1.6 * Q_{BEP}. Meaning that within this range a linear fit of the P_s is justified. Some extrapolation might be possible but is not investigated. The use of a linear fit has the advantage of being more generic but is less precise than scaling for a given Q_s.

5

Conclusions and recommendations

5.1. Conclusions

5.1.1. Scaling

The lab scale $NPSH_r$ measurements done in this research and the relation with the available full scale date indicate that:
If the $NPSH_r$ is known for a given specific capacity (Q_s), the $NPSH_r$ for a geometrically identical pump operating at the same Q_s can predicted by quadratic scaling of ωD_{imp}, especially at the Best Efficiency Point (BEP), this scaling is given in equation 5.1

$$NPSH_{rs} = \frac{gNPSH_r}{\left(\omega D_{imp}\right)^2} \tag{5.1}$$

This is in contradiction to Güllich 2016 and Yedidiah 1972 who apply an exponent below 2.
The $NPSH_r$ scaling however does not provide the most clear information, a more precise comparison is to use the P_s, see Equation 5.2, which scales only the pressure conditions of the inlet.

$$P_s = \frac{p_{in,abs} - p_{vap}}{\rho\left(\omega D_{imp}\right)^2} \tag{5.2}$$

Scaling with $NPSH_r$ can overestimate the strength of the results due to the fact that the velocity component scales perfect by definition. This tends to 'hide' deviations in the scaling of the inlet pressure.
$NPSH$ is a measure for the sum of the kinetic energy and the pressure energy, interpreting this as a parameter for the conditions of cavitation is meaningless. For the velocity component tends to aggravate cavitation whereas the pressure reduces the risk of cavitation.
Still the methods of Equation 5.1 and Equation 5.2 can be compared because they are given as a function of velocity, it would however make the interpretation of the parameters more meaningful if the velocity component was not added to the pressure component.
Why the velocity component was historically included in the $NPSH_r$ is unknown to the author, one might speculate that since the velocity is needed to know the head of the pump (if the pipe diameter changes) it is also used for the $NPSH_r$. For further investigations between inlet pressure, vapour pressure, flow rate, shaft speed and pump performance it is advisable not to use $NPSH_r$ but to use the inlet pressure and flow rate separately.

5.1.2. Linearisation

The lab scale data appeared to have a strong linear relation between the the Q_s and P_s within the considered flow range of 0.6 up to 1.6 * Q_{BEP}. This linear relation was less strong in the full scale data, especially in the range below 1.0 * Q_{BEP}.

5.1.3. Acoustic emission

Acoustic emission seems a good check to see if a $NPSH_r$ measurement has been correctly executed. Unfortunately regular calibration and adaptations to operating conditions are necessary due to the sensor sensitivity. So care needs to be taken in interpreting the results.
Also the focus in using the data needs to be on recognizing not only the full cavitation and the subsequent drop in cavitation noise, but also on identifying the incipient cavitation. A drop in cavitation noise can also be caused by air being sucked in which might wrongly be interpreted as the cushioning effect due to vapour.

5.2. Recommendations

The first recommendation is naturally to extend the data with measurements at larger diameters, building up to pumps with an inlet diameter of 1 meter. A more low cost test setup with 0.2 meter and 0.3 meter inlet diameter would be a good start. This would be in addition to already available field data with an inlet diameter of 0.45 [m], in the lab however the conditions better controlled.

The number of blades used in dredging pumps and in the research is typically low, i.e. three or four. This is in order to create a large enough ball passage. A larger number would be very interesting, also to try and see if alternating vane cavitation will occur for an increased number of blades.

A broader range of pump speeds and higher flow velocities would be highly interesting, to see if the linear relation for the reciprocal of the cavitation number and if limits in the pump speed can be found where the scaling no longer applies.

In this research the exact physics of what's happening in the pump was not investigated, the study focused on the (head drop) and the conditions (inlet pressure, speed, diameter, temperature, flow velocity) for which they occurred, that the cause was cavitation could be deduced. A transparent casing (preferably with a refractive index identical or close to that of water) to study the exact location of the onset of cavitation and investigate the possible occurrence of alternating vane cavitation would be of great interest. If the impeller itself were to be transparent with a refractive index close to that of fluid under investigation- the results would be even more interesting.

A different suggestion, important to the dredging industry, is the influence of solids on the onset of cavitation and on the head characteristics of a cavitating pump.

A Appendix

A.1. Linear regression

Linear regression is a method to check how correct a linear fit is. This analysis consists of a few steps:

- Look at the histogram of the parameter being predicted, in this case the inlet pressure, if this is normally distributed it's an extra indication that linear regression is useful.
  Note that this only works if there is a large enough dataset and if the input parameters (such as speed and flow rate) are evenly distributed.
- Check the skewness, this is a measure for the symmetry of the normal distribution. If the skewness is 0 it is perfectly symmetric, if not outliers could be changing data. The skewness is defined as follows:

$$skew = \frac{\frac{1}{N}\sum_{n=1}^{N}(x[n]-\overline{x})^3}{\left(\frac{1}{N}\sum_{n=1}^{N}(x[n]-\overline{x})^2\right)^{3/2}} \tag{A.1}$$

- Investigate outliers via a box plot, outliers are removed for statistical purposes. Not because they are incorrect but because they influence the result too much.

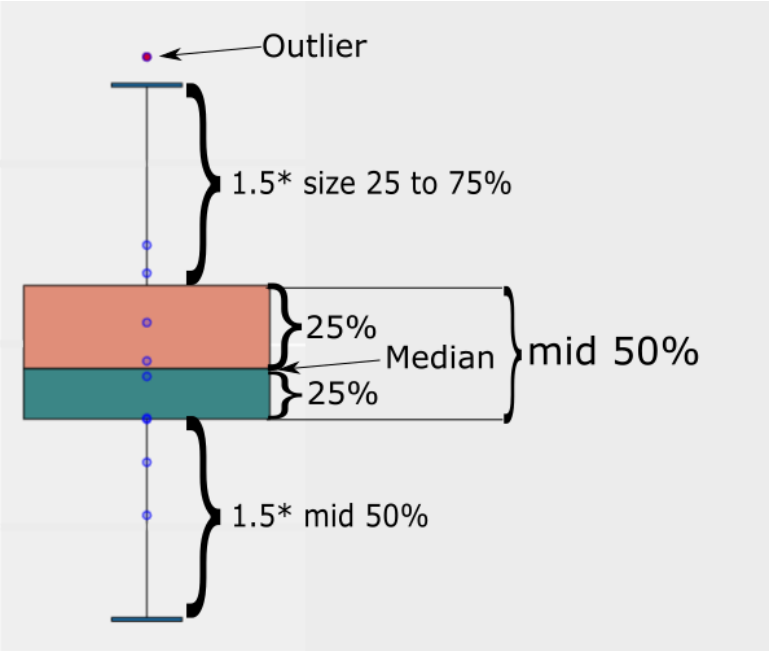

Figure A.1: box plot example

In Figure A.1 a box plot with the relevant parameters is shown.

- **Median** the median is the value between half of the data-points with the highest values and the half with the lowest values.
- **25 % above and below median** 25% of all additional data-points are expected to be in one of these two boxes. The upper box represents the values above the median, and the lower for those below the median.
- **1.5*mid 50%** the length of the range from the two combined 25% parts combined and multiplied with a factor of 1.5 and added to first 25% above and below the median.

- Make a correlation matrix determining the correlation between the parameters under investigation.
  The correlation matrix shows the relation between different parameters using the following equation:

$$r_{jk} = \frac{\sum_{i=1}^{N}(x_{ij} - \overline{x_j})(x_{ik} - \overline{x_k})}{\sqrt{\sum_{i=1}^{N}(x_{ij} - \overline{x_j})^2}\sqrt{\sum_{i=1}^{N}(x_{ik} - \overline{x_k})^2}} \tag{A.2}$$

A value of 1 means a perfect linear relation between the parameters. The lower the value the worse the match. A n example of a correlation matrix is shown below:

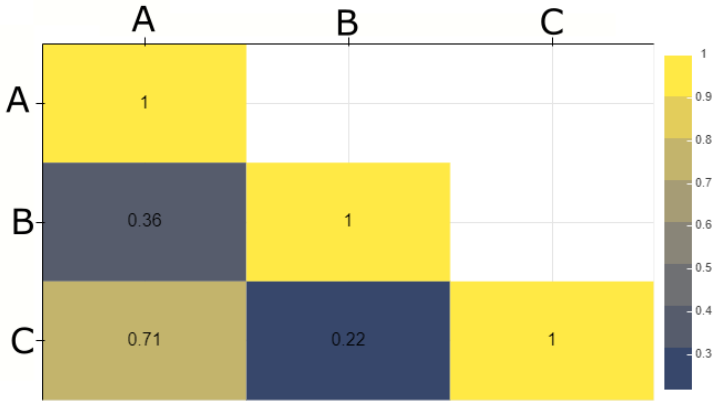

Figure A.2: correlation matrix example

Obviously parameter A correlates perfectly with itself, as for B and C. Parameter A and C have a fairly good correlation whereas the other combinations have a very low correlation.

- Apply the linear regression and check the results by means of the variance score, which uses a normalisation of the variance:.

$$Var(X) = \frac{1}{n}\sum_{i=1}^{n}(error_i)^2 \tag{A.3}$$

Normalising the variance and subtracting it from 1 gives the following equation:

$$variancescore = 1 - \frac{\frac{1}{n}\sum_{i=1}^{n}(error_i - mean(error))^2}{\frac{1}{n}\sum_{i=1}^{n}(error_i)^2} \tag{A.4}$$

meaning a value of 1 is perfect, the lower the value the worse the quality of the linear regression.

- A final check is to calculate the 95% confidence interval calculating the range within which the mean of a new set of measurements has a 95% chance to occur. This is done with respect to the linear fit chosen for the data. Although the data is checked on it's normal distribution, the confidence interval is calculated using a student's t-distribution. This is used if the number of data points is limited or if the distribution is not a true normal distribution.
  The calculation for the 95% confidence interval is conducted with the assumption of a student's t distribution. With the following parameters:

$$\hat{\sigma} = \sqrt{\sum_{i=1}^{n}\frac{(y_i - \hat{y})^2}{n-2}} \tag{A.5}$$

$$\left|\hat{\mu}_{y|x0} - \mu_{y|x0}\right| \leq T_{n-2}^{.95}\,\hat{\sigma}\sqrt{\frac{1}{n} + \frac{(x_0 - \bar{x})^2}{\sum_{i=1}^{n}(x_i - \bar{x})^2}} \tag{A.6}$$

Where $\hat{\mu}_{y|x0}$ is derived from the linear fit and $\mu_{y|x0}$ defines the confidence interval in relation to $\hat{\mu}_{y|x0}$, $T_{n-2}^{.95}$ is the x^{th} percentile of the Student's t-distribution with n−2 degrees of freedom, n is the number of observations.

An example of the resulting graph is shown in Figure A.3

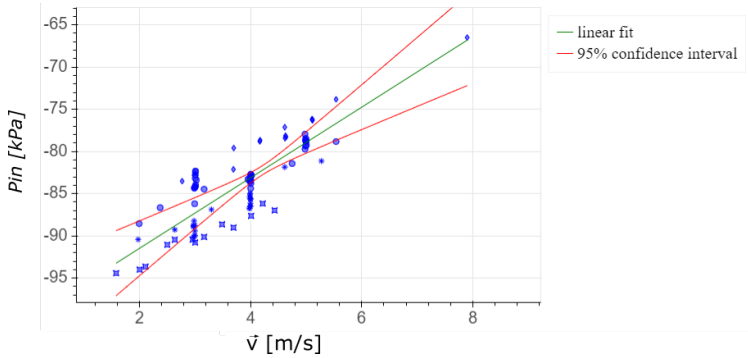

Figure A.3: axample of linear fit

A.2. Measurement data

Table A.1: HRMD3B data

speed [Hz]	**velocity** [$\frac{m}{s}$]	P_{in} [kPa]	**temperature** [deg]	P_{atm} [deg]
17.5	1.1	-95.8	18	101.5
17.5	2.9	-91.6	18	101.5
20.0	1.3	-96.7	18	101.5
20.0	1.6	-95.8	18	101.5
20.0	2.0	-95.4	18	101.5

Continued on next page

Table A.1 – continued from previous page

speed [Hz]	**velocity** [$\frac{\text{m}}{\text{s}}$]	P_{in} [kPa]	**temperature** [deg]	P_{atm} [kPa]
20.0	2.4	-93.3	18	101.5
20.0	2.6	-93.9	18	101.5
20.0	3.3	-90.3	18	101.5
20.0	3.6	-90.0	18	101.5
25.0	1.3	-93.1	18	101.5
25.0	1.6	-92.9	18	101.5
25.0	1.7	-92.7	18	101.5
25.0	2.0	-92.9	23	101.5
25.0	2.5	-91.0	23	102.1
25.0	3.0	-89.7	23	102.1
25.0	3.3	-89.4	23	102.1
25.0	3.5	-89.0	23	102.1
25.0	4.0	-85.7	23	101.5
25.1	4.1	-87.0	23	102.1
25.0	4.4	-85.0	23	102.1
25.0	4.5	-83.6	23	101.5
25.0	4.5	-83.1	21	100.9
27.0	2.7	-89.1	23	102.5
27.0	1.8	-90.7	23	102.5
30.0	1.8	-90.0	23	102.3
30.0	2.0	-89.3	23	102.3
30.0	2.4	-88.5	23	102.2
30.0	2.9	-87.7	23	102.2
30.0	3.6	-86.0	23	102.2
30.0	4.5	-81.4	25	101.7
29.9	4.0	-82.6	26	101.7
30.0	4.2	-83.3	23	102.1
30.0	4.5	-83.2	23	102.1
30.0	4.7	-83.5	23	102.1
30.0	4.9	-82.9	23	102.1
30.0	4.9	-82.8	23	102.1
30.0	5.0	-79.6	25	101.7
30.0	5.5	-77.2	24	101.7
35.0	4.0	-79.9	25	100.5
35.0	5.0	-78.5	25	100.5
35.0	2.1	-87.3	23	102.4
35.0	2.8	-86.4	23	102.4
35.0	3.5	-83.5	23	102.4
35.0	4.2	-83.2	23	102.3
35.0	4.8	-81.0	23	102.4
35.0	5.5	-79.5	23	102.4
39.9	4.0	-78.9	29	102.4
40.0	2.0	-86.3	24	102.1
40.0	3.0	-82.4	30	102.4
40.0	3.0	-83.5	23	102.4
40.0	3.0	-82.6	28	102.4
40.0	4.0	-79.3	24	102.4
40.0	5.0	-78.8	22	102.1
40.0	5.0	-78.4	26	102.4
40.0	5.0	-77.9	31	102.4

Table A.2: HRMD4B curve data

speed [Hz]	**velocity** [$\frac{\text{m}}{\text{s}}$]	P_{in} [kPa]	**temperature** [deg]	P_{atm} [deg]
20.0	1.6	-94.4	12	101.2
20.0	2.1	-93.6	12	101.8
20.0	2.6	-90.5	12	101.3
20.0	3.2	-90.1	12	101.8
20.0	3.7	-89.0	13	101.6
20.0	4.2	-86.2	13	101.9
25.0	2.0	-90.4	13	101.3
25.0	2.6	-89.3	13	101.6
25.0	3.3	-86.9	13	101.9
25.0	4.0	-83.5	13	101.1
25.0	4.6	-81.8	14	101.3
25.0	5.3	-81.1	14	101.2
30.0	2.4	-86.7	15	102.0
30.0	3.2	-84.5	15	101.7
30.0	4.0	-83.3	15	101.6
30.0	4.7	-81.4	17	101.3
30.0	5.5	-78.8	17	101.7
35.0	2.8	-83.5	18	101.8
35.0	3.7	-82.1	18	101.2
35.0	4.6	-77.1	19	101.7
35.0	5.5	-73.8	19	101.8
20.0	2.5	-91.1	19	102.2
20.0	3.0	-90.4	19	102.2
20.0	3.5	-88.6	20	102.3
20.0	4.0	-87.6	20	102.6
20.0	4.4	-87.0	20	102.2
25.0	3.0	-90.1	12	101.8
25.0	3.0	-90.0	13	101.8
25.0	3.0	-88.9	14	101.8
25.0	3.0	-88.8	15	101.7
25.0	3.0	-90.0	16	101.7
25.0	3.0	-88.8	16	101.7
25.0	3.0	-88.8	16	101.7
25.0	3.0	-88.2	17	101.7
30.0	3.0	-84.3	19	100.3
30.0	3.0	-84.4	20	100.3
30.0	3.0	-84.2	20	100.3
30.0	3.0	-84.1	21	100.3
30.0	3.0	-84.0	21	100.3
30.0	3.0	-83.4	14	99.7
30.0	3.0	-83.2	15	99.7
30.0	3.0	-82.8	15	99.7
30.0	3.0	-82.4	16	99.7
30.0	3.0	-82.3	16	99.7
35.0	3.7	-79.6	21	100.2
25.0	4.0	-86.7	17	101.7
25.0	4.0	-86.7	18	101.7
25.0	4.0	-86.5	18	101.7
25.0	4.0	-86.5	18	101.7
25.0	4.0	-86.1	19	101.7
25.1	4.0	-85.6	12	100.8
25.0	4.0	-85.6	13	100.8

Continued on next page

Table A.2 – continued from previous page

speed [Hz]	**velocity** [$\frac{\text{m}}{\text{s}}$]	P_{in} [kPa]	**temperature** [deg]	P_{atm} [deg]
25.0	4.0	-85.4	13	100.8
25.0	4.0	-85.1	13	100.8
25.0	4.0	-85.0	14	100.8
30.0	4.0	-83.4	15	100.5
30.0	4.0	-83.1	18	100.4
30.0	4.0	-82.9	18	100.4
30.0	4.0	-82.9	19	100.3
30.0	4.0	-82.7	19	100.3
35.0	4.6	-78.4	13	100.3
35.0	4.6	-78.1	14	100.3
35.0	4.6	-78.3	15	100.3
30.0	4.0	-83.6	16	100.5
30.0	4.0	-83.8	16	100.4
30.0	4.0	-83.4	16	100.4
30.0	4.0	-83.0	17	100.4
30.0	4.0	-82.7	18	100.4
30.0	5.0	-79.7	22	100.3
30.0	5.0	-79.4	22	100.3
30.0	5.0	-79.3	23	100.2
30.0	5.0	-78.8	11	99.6
30.1	5.0	-78.7	12	99.6
30.0	5.0	-78.9	12	99.6
30.0	5.0	-78.6	13	99.6
30.0	5.0	-78.4	13	99.6
30.0	5.0	-78.7	13	99.6
30.0	5.0	-77.9	14	99.6
35.0	5.1	-76.2	15	100.2
35.0	5.1	-76.3	16	100.2
34.9	5.1	-76.2	18	100.2
35.0	4.2	-78.7	20	100.2
34.9	4.2	-78.8	21	100.2
20.0	2.0	-94.0	22	101.3
30.0	2.0	-88.5	26	101.9
19.9	3.0	-90.8	22	101.5
25.0	3.0	-89.4	24	101.1
30.0	3.0	-86.2	26	101.3
35.3	3.0	-82.6	24	101.7
25.0	4.0	-85.6	24	101.7
30.0	4.0	-84.4	26	101.9
34.9	4.0	-82.9	23	101.4
35.0	7.9	-66.5	19	101.8

Bibliography

C. H. v. d. Berg. *IHC Merwede Handbook for centrifugal Pumps and Slurry Transportation*. IHC, 2013. ISBN 9789082154818.

C. Brennen. *Hydrodynamics of pumps*. Oxford science publications. Concepts ETI and Oxford University Press, Norwich Vt. USA and Oxford and New York, 1994. ISBN 0198564422. URL http://www.loc.gov/catdir/enhancements/fy0635/94035442-t.html.

C. Brennen. *Cavitation and Bubble Dynamics*. Oxford engineering science series. Oxford University Press, 1995. ISBN 9780195094091. URL https://books.google.nl/books?id=vYiUO0RlC4UC.

A. L. Buck. New Equations for Computing Vapor Pressure and Enhancement Factor. *Journal of Applied Meteorology*, 20:1527–1532, 1981. doi: 10.1175/1520-0450(1981)020<1527:NEFCVP>2.0.CO;2. URL /brokenurl#10.1175/1520-0450(1981)020<1527:NEFCVP>2.0.CO;2.

Y. A. Çengel and M. A. Boles. *Thermodynamics: an engineering approach*. McGraw-Hill series in mechanical engineering. McGraw-Hill Higher Education, 2006. ISBN 9780072884951. URL https://books.google.nl/books?id=5-hSAAAAMAAJ.

H. Dixon. note on the tensile strength of water. *the Scientific proceedings of the Royal Dublin Society*, 6, 1909.

Fisher. Control valve handbook. *Emerson*, 2001.

J. Franc and J. Michel. *Fundamentals of Cavitation*, volume 76 of *Fluid Mechanics and Its Applications*. Springer Science + Business Media Inc, Dordrecht, 2005. ISBN 9781402022326. doi: 10.1007/1-4020-2233-6. URL http://dx.doi.org/10.1007/1-4020-2233-6.

J. Gibbs. a method of geometrical representation of the thermodynamic properties of substances by means of surfaces. *Engineering*, 7(2), 1873.

J. Güllich. *Centrifugal Pumps*. Springer Berlin Heidelberg, Berlin, Heidelberg, 2010. ISBN 978-3-642-12823-3. doi: 10.1007/978-3-642-12824-0.

J. Güllich. *Centrifugal Pumps*. Springer Berlin Heidelberg, 2016. ISBN 9783662518281. URL https://books.google.nl/books?id=6QsvvgAACAAJ.

Harkin A. et al. On acoustic cavitation of slightly subcritical bubbles. *physics of fluids*, 11, 1998.

M. Hirschberger and I. James, editors. *A REVIEW OF NSS LIMITATIONS—NEW OPPORTUNITIES*, 2009. International Pump Users Symposium (25th : 2009).

J. W. Holl and A. L. Treaster. Cavitation hysteresis. *Journal of Basic Engineering*, 88(1):199–211, 1966. ISSN 0021-9223. doi: 10.1115/1.3645802.

ISO. 6765_iso 4287_2007 en fr -nen-en: Geometrical product specifications (gps). 2007.

ISO. Nen-en-iso 9906: Rotodynamic pumps - hydraulic performance acceptance tests. 2012.

ISO-5198. 6377 iso 5198 1998 en -nen-en: Centrifugaalpompen, schroefcentrifugaalpompen en schroefpompen - code voor de hydraulische beproevingen. 1998.

P. Keller. Cavitation scale effects: Empirically found relations and the correlation of cavitation number and hydrodynamic coefficients. *Fourth International Symposium on Cavitation*, 2001.

G. Kuiper. Developments in the design of propulsors and propulsion systems. *Delft University of Technology*, 2000.

G. Kuiper. *Cavitation on ship propellors*. Delft University of Technology, 2010.

W. Lawless, Q. Mittu, D. Sofge, and S. Russell, editors. *Cavitation instabilities and rotordynamic effects in turbopumps and hydroturbines: Turbopump and inducer cavitation experiments and design*. Springer, Cham, 2017. ISBN 9783319497195.

V. Lomakin and O. Bibik. Numerical prediction of the gas content effect on the cavitation characteristics of the pump using the simplified rayleigh-plesset equation. *IOP Conference Series: Materials Science and Engineering*, 492:012037, 2019. ISSN 0742-4795. doi: 10.1088/1757-899X/492/1/012037.

B. Mandelbrot. *The fractal geometry of nature*. Freeman, 1982. URL https://cds.cern.ch/record/98509.

D. Miller. *Internal flow systems*. Mentor Graphics, 3 edition, 2014. ISBN 978-0-9931378-0-8.

P. Muleki, S., C. Desjouy, J.-J. Béra, and C. Inserra. Hysteresis of inertial cavitation activity induced by fluctuating bubble size distribution. *Ultrasonics sonochemistry*, 27:262–267, 2015. doi: 10.1016/j.ultsonch.2015.05.036.

T. Mullin. Experimental studies of transition to turbulence in a pipe. *Annual Review of Fluid Mechanics*, 43(1):1–24, 2011. doi: 10.1146/annurev-fluid-122109-160652.

N. Passas and B. Pethica. The surface tension of water. *Colloids and Surfaces*, 36:3, 1989.

J. Paugh. How to compute net positive suction head for centrifugal pumps. *Warren Pumps*, 1996.

C. G. Porwall. High specific speed in circulating water pump can cause caviation, noise and vibration. *17th International Conference on Fluid Mechanics and Thermodynamics*, 2015. URL https://publications.waset.org/.

B. Predel, M. Hoch, and M. J. Pool. *Phase Diagrams and Heterogeneous Equilibria: A Practical Introduction*. Engineering Materials and Processes. Springer Berlin Heidelberg, 2004. ISBN 9783540140115. URL https://books.google.nl/books?id=MnaFQgAACAAJ.

A. Predin and I. Biluš. Influence of additional inlet flow on the prerotation and performance of centrifugal impellers. *Journal of Hydraulic Research*, 41(2):207–216, 2003. doi: 10.1080/00221680309499962.

B. Rapp. *Microfluids*. Elsevier, 2017. ISBN 78-1-4557-3141-1.

J. Rodriguez and M. de Jonge. Valve cavitation, 2018.

S. Salvadori and A. Cappelletti, editors. *EXPERIMENTAL AND NUMERICAL EVALUATION OF THE NPSHR CURVE OF AN INDUSTRIAL CENTRIFUGAL PUMP*, 2015. ISBN 9789090275192.

B. Schiavello and F. Visser. pump cavitation—various npshr criteria, npsha margins, and impeller life expectancy. *Twenty-fourth International Pump Users Symposium*, 2009.

H. Schlichting and K. Gersten. *Boundary-Layer Theory*. Springer Berlin Heidelberg, Berlin, Heidelberg, 2017. ISBN 978-3-662-52917-1. doi: 10.1007/978-3-662-52919-5.

F. Smith and H. Allan. Avoid common pitfalls when using henry's law. *Avoid Common Pitfalls When Using Henry's Law*, 103,9, 2007.

A. J. Stepanoff. *Centrifugal ans Axial Flow Pumps*. Krieger, 1948. ISBN 0894647237.

G. Takacs. *sucker-Rod Pumping handbook: production Engineering Fundamentals and Long-Stroke Rod Pumping*. Gulf Professional Publishing, 2015. ISBN 978-0-12-417204-3.

H. Temperley. The behaviour of water under hydrostatic tension: II. *Proceedings of the Physical Society*, 58(4):436–443, jul 1946. doi: 10.1088/0959-5309/58/4/311. URL https://doi.org/10.1088%2F0959-5309%2F58%2F4%2F311.

T. Terwisga, editor. *Cavitation Erosion: A review of physical mechanisms and erosion risk models*, 2009. Delft University of Technology.

M. Tsai. Accounting- for-dissolved gases in pump design. *Chemical Engineering*, 89:15, 1982.

J. Tuzson. *Centrifugal pump design*. A Wiley-Interscience publication. Wiley, New York and Chichester, 2000. ISBN 0471361003.

S. Velasco, R. F. L., and W. J. A. On the clausius-clapeyron vapor pressure equation. *Journal of Chemical Education*, 86(1), 2009.

B. Went. Pump cavitation and how to avoid it. *World Pumps*, pages 34–38, 2018. doi: 10.1016/S0262-1762(18)30146-9.

F. White. *Fluid Mechanics*. Mcgraw-Hill Education - Europe, 2011. ISBN 9780071311212.

F. Wislecenus. the hydraulic problem of cavitation in pumps. *Proceedings of the second hydraulics conference*, 1942.

Y. Xu, L. Tan, Y. Liu, and S. Cao. Pressure fluctuation and flow pattern of a mixed-flow pump with different blade tip clearances under cavitation condition. *Advances in Mechanical Engineering*, 9(4): 168781401769622, 2017. ISSN 1687-8140. doi: 10.1177/1687814017696227.

S. Yedidiah. Some observations relating to suction performance of inducers and pumps. *Journal of Basic Engineering*, 94(3):567–573, 1972. ISSN 0021-9223. doi: 10.1115/1.3425489.

S. Yedidiah. *Centrifugal Pump User's Guidebook: Problems and Solutions*. Springer US, 2012. ISBN 9781461312178.